東海大学大学院平成 28 年度博士論文

Improvement of Mobility and Stability for Small Electric Vehicle: Integration of Oversteering Characteristic, Four Wheel Drive and Independent Steering

(オーバーステアリング特性、四輪駆動と独立操舵の統合による小型電気自動車の運動性と安定性の向上)

指導　山本　佳男　　教授

東海大学大学院総合理工学研究科

総合理工学専攻

MUHAMMAD IZHAR BIN ISHAK

Contents

Acknowledgments

First and foremost, praises and gratitude to God, the Almighty for His showers of blessing, providing the opportunity and granting me the ability to succeed in completing my research.

I would like to express my sincere gratitude to my supervisor Prof. Yoshio Yamamoto (山本　佳男　教授) for the continuous support of my Ph.D. study and related research, for his patience, sincerity and motivation. I would like to express my gratitude to my second supervisor Prof. Hirohiko Ogino (荻野　弘彦　教授) for introducing me to immense knowledge in mechanical engineering, guiding me since I was an undergraduate student, and who gave access to the laboratory and research facilities. I would also like to thank to my late supervisor Prof. Yasuo Oshinoya (押野谷　康雄　教授) for his encouragement and support. Their guidance helped me in all the time of research and writing of this thesis. I could not have imagined having a better advisor and mentor for my Ph.D. study. Besides my advisor, I would like to thank the rest of my thesis committee: Prof. Satoru Iwamori (岩森　暁　教授), Prof. Moriyama Hiroyuki (森山　裕幸　教授), Prof. Ochiai Masayuki (落合　成行　教授), Prof. Shinya Hasegawa (長谷川　真也　教授), and Prof. Hideaki Katou (加藤　英晃　助教), for their insightful comments and encouragement, but also for the hard question which incented me to widen my research from various perspectives.

My sincere thanks also goes to my fellow lab mates Dr. M. Heerwan Peeie, Mr. Zed Al-Habshee and Mr. M. Zharif for their stimulating suggestions and providing a fun research environment.

I would like to acknowledge the Ministry of Education Malaysia and University of Malaysia Pahang for the financial support during my Master and Ph.D. research.

Last but not the least, I would like to express my heart-felt gratitude to my family: my parents, Ishak Embam and Mahhizon Mahazan for their prayers and blessings, my wife and son, Erny Afiza Alias and Yusuf Nufayl M. Izhar for their encouragement, support and patience.

Nomenclatures

B_F	braking force (N)
b	width of the interacted tire surface, 0.1, (m)
C	regenerative brake coefficient
d_F	front tread, 0.840, (m)
d_R	rear tread, 0.815, (m)
g	gravitational acceleration, 9.81, (m/s^2)
h	center gravity of the vehicle, 0.105, (m)
I	yaw inertia moment at the center gravity point of the vehicle, 1470, (kgm^2)
I_ω	inertia moment of the tire, 2.53, (kgm^2)
K_x	the rigidness of the tire in longitudinal axis, $1.333x10^6$, (N/m^3)
K_y	the rigidness of the tire in lateral axis, $1.333x10^6$, (N/m^3)
K_f	
l	length ofrom front wheel axle to the rear wheel axle, 1.28. (m)
l_F	the length from front wheel axle to the vehicle center gravity point, 0.725, (m)
l_R	the length from rear wheel axle to the vehicle center gravity point, 0.525, (m)
l_T	length of the interacted tire surface, 0.15, (m)
m	vehicle mass, 421.61, (kg)
P	pressure (Pa)
R	radius of the brake shoe
r	wheel radius, 0.23, (m)

T	torque (Nm)
t	time (s)
u	vehicle velocity in the longitudinal direction (m/s)
v	vehicle velocity in the lateral direction (m/s)
V	vehicle velocity at the center of gravity (m/s)
W_z	wheel load (N)
X	the longitudinal force acting on the tire (N)
Y	the lateral force acting on the tire (N)
β	side slip angle of the vehicle (rad)
β*	side slip angle of the state observer (rad)
β_T	side slip angle of the tire (rad)
θ	steering angle (rad)
γ	yaw rotational speed of the vehicle (rad/s)
γ*	yaw rotational speed of the state observer (rad/s)
μ	friction coefficient
ρ	slip ratio
ω	tire angular velocity (rad/s)

Subscripts:

F	front
R	rear
FR	front right
FL	front left
RR	rear right
RL	rear left

Chapter 1

Introduction

1.1 Background

Over the 20th century, increasing carbon dioxide emission by petroleum-based transportations is one of the main contributor to global warming. Moreover, escalation of global human population has put a pressure on the amount of carbon dioxide emission especially in developing countries rather than developed countries [1-1]. A research paper from the National Academy of Sciences of the USA concluded that climate change that takes place due to the global warming is largely irreversible for 1,000 years even after emissions of carbon dioxide stop [1-2]. This environmental issues by petroleum-based transportations along with the issue of fossil fuel depletion around the world have led activist and lobbyist to pressure automotive manufacturers to redesign future vehicles.

Under the aspect of redesigning future vehicle, in the past few years, car manufacturers have reintroduced hybrid electric vehicle (HEV) and full-electric vehicle (EV). Hybrid electric vehicle is a vehicle that incorporate a smaller and generate less emission fossil-fuel engine with an electric powertrain. Downsized engine with the presence of the electric powertrain is intended to achieve higher fuel efficiency and less emissions than conventional vehicle. However, we believe hybrid electric vehicle is more of a business approach rather than as a counter-measure to address the current global issue mention before. This is due to the fact that hybrid electric vehicle still uses fossil-fuel engine as a primary propulsion. A Harvard business professor indicated that consumer will purchase things they desired [1-3]. If a person wants a fuel efficient car they will buy a hybrid without thinking about the actual efficiency of the product.

A fully-electric vehicle is an automobile that is propelled exclusively by one or more electric motors. Since electric vehicles do not have internal combustion engine, they don't use any fuel and produce zero tail emission. This means that an electric vehicle benefits the environment more than a hybrid electric vehicle. The empty space from a withdrawn combustion engine is replaced with rechargeable batteries. The number and size of the batteries determine the range an electric vehicle can travel. Additionally, electric motors are able to give the vehicle an instant torque which create fast acceleration.

Fully-electric vehicle will become prominent as a means of transportation in the future, especially in urban areas where there are limited spaces and a very high dense population. The One of the challenges of owning an electric vehicle is that they are expensive in comparison to a conventional and hybrid electric vehicles due to the price of their lithium-

ion batteries. However, the price of the battery is expected to drop by the year according to research [1-4, 5]. Nonetheless, to meet the consumer demands, some car manufacturers have obtained a way to cut the cost by developing an ultra-compact or small electric vehicle. Small electric vehicles are light-weight, compact and cheaper due to less battery and small electric motor. In compensation to the merits, they have short to medium travel distance and speed, which is very suitable for city usage and connecting nearby suburb area.

The propulsion system of a small electric vehicle such can be divided into two types. The most basic type is the central motor system, where a conventional combustion engine is replaced with an electric motor. Figure 1-1 shows the Renault 'Twizy' design and market the by Renault is an example of system on small electric vehicle. The other type is the in-wheel motor system, where the electric motors are incorporated into the hub of each wheel. Figure 1-2 shows the Toyota COMS as an example of an in-wheel small electric vehicle. Due to the drivetrain location at the wheels, this system promotes freedom of layout for various driving system (two-wheel Drive, four-wheel drive) with high-energy efficiency. The in-wheel motor can also be governed separately by a control system.

Similar to telephones and computers, new devices which was once a huge and shared-item has gotten smaller, faster and cheaper. The shrinking and personalization of technological device phenomena does not limit to computer and telephone. They have also spread to automotive. Small electric vehicle meets the consumer demand as they are practical, efficient and affordable. Moreover, Government and car manufacturer have join together to promote small electric. The reason government support small electric vehicles is because they can be used to improve the lives of people in cities. The small size electric vehicle can ease traffic congestion, and improving access to tourist areas and communities in a city

Figure 1-1 ‘TWIZY’ a small electric vehicle by Renault.
(https://en.wikipedia.org/wiki/Renault_Twizy)

Figure 1-2 ‘Toyota COMS’ a small electric vehicle by Toyota Body.
(https://commons.wikimedia.org/wiki/File:Toyota_Auto_Body,_COMS_T%E3%83%BBCOM,_Bule.jpg)

1.2 Problem Statement

Mobility within a city such as Tokyo and Osaka along with its surrounding suburbs can be difficult. The rapid development within a small concentrated area and high density population has led to construction of various narrow and complex roads. In order to drive in such roads mixed with vehicles and pedestrians, small electric vehicles nowadays have to face critical driving condition and even have bypass long roads contrary to the will of the driver [1-6].

For example, in the city when a small electric vehicle enters a narrow road and encounters with an oncoming vehicle, the driver has no other choice but to reverse. On the other hand, there is also a situation where a vehicle has to reciprocate on a narrow road, due to space limitation the driver has to either advance until a turntable space is available or make an exit at a larger road. As a result, a great detour is always required. A small electric vehicle is also use to commute from a city to neighboring suburb. Without any stability control system, driver of the vehicle has to drive under the maximum velocity and be more precautious. All of these situations are worsen when they occur on a slippery road surface during heavy rain or snow that would can be easily categories as a very dangerous state.

In addition, similar to conventional vehicle, most in-wheel small EVs that exist today are design with understeer (US) characteristic. US characteristic has no velocity limit but during cornering they require high steer input and produce low steer ability.

These situations need to be solve in order to develop a more efficient small electric vehicle. A future small electric vehicle should meet the requirements as follows:

1) Maneuver in tight narrow road at low speed
2) Can execute cornering in stable condition even at high speed
3) Can be driven even if the maximum road surface friction coefficient is small

1.3 Objective of research

Thus, the main objective of this research is to improve the mobility and stability of small electric vehicle. The emergence of steer-by-wire and drive-by-wire technologies present an opportunity for automakers to develop current small electric vehicle. In order to achieve a vehicle that fulfills the requirements mention previously, we study the possibility that a small electric vehicle with oversteer characteristic can increase the mobility of the vehicle. However, one of the disadvantage of oversteer characteristic is that the vehicle will have a stability velocity limit. In order to overcome this, the oversteer small electric vehicle is integrated with a four-wheel drive system by implementing in-wheel motor at each wheels and can be steer independently with four steering actuators. Even though we have achieved in increasing the mobility and steering performance of the small electric vehicle, the system is faulty if traction can't be managed. The regenerative brake timing control was developed as a substitute to an anti-lock brake system.

1.4 Past Research

Researches on development of future small electric have spread widely in recent years. Firstly, we have to understand that electric vehicles have the advantages as follows [1-7];

1. Electric motor has torque response faster than a normal engine
2. All wheels can be governed independently by in-wheel motor system
3. Electric motor torque can be accurately measured by the motor current.

Two major aspects of which is being research are based on battery technologies and electric vehicle motion control. The objective of studying on battery technologies is to manage energy consumption in order prolong the small electric vehicle travel distance with a single charge [1-8] ~ [1-12]. The main issue with electrical energy storage systems is their energy density. Energy density is defined as the amount of energy stored in a given system per unit mass [1-7]. The conventional lead acid battery has an energy density about 35 Wh/kg compared to a useful energy density of more than 2000 Wh/kg for gasoline [1-8]. Therefore, the electric drive range for electric vehicle is proportional to the size and mass of the energy storage system set on board.

On the other hand, there are researches on electric vehicle motion control that aim to improve stability and mobility of electric vehicle [1-13] ~ [1-28]. The motion control of these researches can also be separated into traction control methods [1-21] ~ [1-23] and motion stabilization control methods [1-24] ~ [1-28]. In the study of electric vehicle control system, there are three point that must address:

1. A vehicle must provide good controllability by responding quickly and accurately to the driver command input
2. A vehicle must provide good stability, with little change in behavior in relation to changes in driving condition
3. There must be an effective control loop between the driver and the vehicle when conveying operational inputs and the vehicle response in order to ensure that the driver can easily recognize present operating conditions and also predict vehicle behavior.

1.4.1 Oversteer and Understeer Characteristic Review

During a normal cornering, a vehicle changes from a transient state where the vehicle begins in straight line into cornering, and then change into steady state after some time where the vehicle moves at a steady circular motion. In automotive engineering, the steering characteristic of a vehicle, either oversteer or understeer, is determined by the steady state cornering test [1-29]. The term understeer means that a vehicle requires more steering input into a turn if the vehicle velocity is gently increase on a constant steer angle. Conversely, an oversteer is when a vehicle requires to lower the steering as the vehicle increases [1-30].

Most of vehicle in the market are design with understeer characteristic. R.T. Bundorf have studied the influence of vehicle design parameters on characteristic speed and understeer since 1967 [1-31]. He presented methods for predicting understeer quality in proposed vehicle designs and for measuring understeer quality in existing vehicles. The methods make possible complete and accurate quantitative descriptions of vehicle understeer. Since then, there are various researches that aim to improve the maneuverability of vehicle with understeer.

T.Goggia et. Al. have proposed a torque vectoring control in fully electric vehicle via integral sliding modes [1-32]. The integral sliding mode calculate the reference yaw moment to be actuated by the torque-vectoring system. A similar research was performed by E. Siampis et. Al where they proposed a predictive rear wheel torque vectoring control with terminal understeer mitigation using nonlinear estimation [1-33]. A linear Model Predictive Control strategy using the rear wheels' slip ratios as input which is then calculated by a sliding mode controller for the necessary motor torques according to the requested wheel slip ratios.

Due to nonlinearity of a vehicle, there are possibility that they are understeer at low speed and oversteer at high speed. In our research, we try to induce oversteer characteristic in small electric vehicle so that the vehicle will have a lower steer input at low speed with high steer ability. Due to this, we hope that it will open a broader field of research.

1.4.2 Four Wheel Steering Review

Based on the advantages of electric vehicle, four-wheel steering has been developed to improve dynamic stabilization. Steering of the front wheel with the rear wheel makes it possible to increase yaw motion and reduce the vehicle side slip angle at the center gravity. The steering characteristic of a four-wheel steering vehicle can be separated into [1-34];

1. Opposite steering
2. Parallel steering and
3. Zero-radius steering

The performance of the steering characteristic depends on the method the rear wheels are controlled in regards to vehicle speed, steering angle, and state of the system.

There are various ways to address this control issue that can be used in four-wheel steering system and the following are some of the examples:

D.Sawamura and H.Fujimoto had proposed a method of tire-workload equalization for each wheel in emergency avoidance for electric vehicle with four wheel independent driving and active front and rear steering [1-35]. In this method, the longitude and lateral force was distributed properly in order to for the vehicle to follow a certain trajectory. In the paper, we learn that they assumed the angle of each front and rear wheels' angle are small and the vehicle was modelled with linear two-wheel vehicle. In the results, we see that the rear wheels rotated in the same direction as the front wheels. M. Galvani et. Al. also did a similar research with the same objective [1-36].

El-Nashar et. Al. proposed Kalman filter algorithm to design a four-wheel steering control as an enhancement of vehicle lateral stability in crosswind [1-37]. In their work, the system used the feedback signals of lateral acceleration and front steering angle to obtain the control law. Furthermore, a theoretical investigation of four-wheel steering system was presented using a linear model to simulate the vehicle handling characteristics.

Ali Hakima et. Al. proposed a fuzzy logic controller to adjust the angle of tires in four-wheel steering vehicle [1-38]. In this research, two simulations were done to design a fuzzy controller for an experimental vehicle and a reference vehicle. The design controller was separated into high level controller and low level controller. These

controllers were used to govern the vehicle yaw behavior. The author emphasized the complexity and nonlinearity of the system equations justifies the use of Fuzzy Logic Controller for controller design strategy. However, a 2 DOF linear vehicle model was used in the mathematical modelling. A few similar research can be found by S.Wang et. Al., J. Zhanga et. Al. and J. Naranjo et. Al [1-39] ~ [1-41].

J.Tian et. Al proposed fractional order sliding model control of active four-wheel steering vehicle [1-42]. In this research, fractional sliding mode control is designed to eliminate the state error caused by the different parameters. We have to agree that the error between the state observer and vehicle should occur. This is because the researcher used an ideal front wheel steering vehicle model to represent the state and the vehicle model is a four-wheel steering with a nonlinear model. The end results were merely to associate the yaw rate steady gain and lateral acceleration gain to a conventional front wheel steering for a four-wheel steering vehicle. A few similar research can be found by M. Amodeo et. Al and Y. Ikeda [1-43] ~ [1-44].

R. C. B. Sampaio proposed an optimal H∞ controller as a control strategy for the steering system of an autonomous vehicle with four independent steering and driven wheels' configuration [1-45]. In their work, they present the synthesis and the analysis of an optimal H∞ controller based on the γ-iteration algorithm to adjust the steering angles by acting over the angular position of a motor shaft which is coupled directly to the pneumatics.

A considerable amount of researches are dedicated to stability control of four-wheel steering from prediction control, fuzzy logic, sliding mode to H∞ robust. However, every physical system in our life has nonlinearities and very little can be done to overcome them. In case of automobile, the governing differential equation of an actual vehicle is also nonlinear and complex in nature. Much of past researches adopted easy way of modelling a control system based on a vehicle which are largely oversimplified in the form of either linearized or decoupled model. Additionally, we can also find that in the research the small angle approximation to the steering angle is also utilized.

1.4.2 Regenerative Brake Control Review

When driving in a metropolitan where traffic congestions are at the highest, around one third of energy is wasted due to frequent braking [1-46]. If this energy loss due to braking can be harvest, fuel consumption of a conventional combustion engine vehicle can improve by 33% [1-47]. In electric railway transportation, regenerative braking system had been introduced since 1886 by Frank J. Spraque. In one of his inventions, the electric motors of the train are turn into electrical generators during braking. Based on this concept, major of the electrification of today's railway transportation have been modelled with such system to reduce electrical energy consumption [1-48] ~ [1-49].

In the case of automotive, the implementation of regenerative braking system onto a conventional vehicle with internal combustion engine is much harder. Additional equipment is necessary during the process of converting and storing energy. Nonetheless, in the aim of improving environmental problem and energy efficiency, manufacturer has in cooperated small internal combustion engine with electric powertrain that we call hybrid electric vehicle. Hybrid electric vehicle involves a lot of continuous interaction between mechanical part and electrical components. Thus, various researches have spread to manage the vehicle dynamic operation.

C.Sankavaram et. Al has proposed a systematic data-driven process for detecting and diagnosing faults in the regenerative braking system of hybrid electric vehicles [1-50]. The diagnostic process involves signal processing and statistical techniques for feature extraction, data reduction for implementation in memory-constrained electronic control units, and variety of fault classification methodologies to isolate faults in the regenerative braking system. J.Ko et. Al developed a brake system for an automatic transmission-based hybrid electric vehicle (HEV) and a regenerative braking cooperative control algorithm [1-51]. A simulation and a vehicle test showed that the brake system and regenerative braking with cooperative algorithm satisfied the friction braking.

M.Heerwan et. Al. have proposed a combination of ABS and regenerative brake control for improving the safety of two-wheel drive small electric vehicle that uses hydraulic-mechanical brake system [1-52]. The study was performed in a numerical simulation where the front wheels that consist of hydraulic brake system is control by an ABS and the rear wheels that consist of in-wheel motor is control by regenerative brake

with timing control. In case of regenerative brake timing method, he suggested that the regenerative brake is turned off when the slip ratio is above the upper limit and the produced current is transferred to charge the battery. When the slip ratio reduced to the lower limit, the regenerative brake is turn on.

The principle of turning on and off is understandable. However, the mechanism needs to be corrected. During braking, the rotor of the motor is force to turn by the wheel's momentum and becomes an electric generator converting kinetic energy into output of electric energy. The electrical load produced generates the braking effect. In other meaning, regenerative brake is on and the produced current is then transferred to charge the battery. In order to simply turn off the regenerative brake, the electric motor needs to be turn off, no electrical current is produced which allows the wheel to turn freely.

In our research, we re-simulated ABS and regenerative brake control on a two-wheel drive small electric vehicle in order to understand the possibility of four-wheel drive small electric vehicle that is fully dependent on regenerative braking.

1.5 Organization of Thesis

This thesis is organized into 5 chapters. A brief outline of the thesis is as follows:

Chapter 1 In this chapter, brief explanations on small EVs and the propulsion system of the small EVs are presented. The background of the study, problem statement, objectives of the study, past research and organization of the thesis are described.

Chapter 2 In this chapter, in-wheel small electric vehicle is modelled with an oversteer characteristic to increase the mobility of the vehicle. At first, a basic understanding of oversteer and understeer characteristic is described. Later, Toyota COMS EV is introduced as a sample model of electric vehicle with in-wheel motor. The specification of this vehicle was modified to produce an oversteer characteristic by simply reposition the center weight distribution to the rear end of the vehicle. A set of multiple simulations of a steady state cornering with regard to a constant front steer angle and at constant velocity was done to determine the steer characteristic of the modelled in-wheel small electric vehicle with oversteer characteristic. Even though by modelling the vehicle with an oversteer characteristic can increase the mobility, the vehicle has a stability velocity limit.

Chapter 3 In this chapter, the yaw moment control by four-wheel drive and independent steering. In chapter 2, theoretically the mobility of a small electric vehicle has increased by modelling the vehicle with an oversteer characteristic. However, when the vehicle velocity is equal to or beyond the stability velocity limit the yaw rotational speed and side slip angle of the modelled small electric vehicle with oversteer characteristic reach infinite value. In this chapter, we introduced a yaw moment control by integrating a four-wheel drive and independent steering (4WDIS) as a lateral stability system of the vehicle. With steer-by-wire technology, 4WDIS on electric vehicle is much more accomplishable. Many past researches adopt easier way of modelling a lateral control system based on vehicle model with linear characteristics. We prefer a nonlinear vehicle model which represent an actual vehicle more accurately. A linear control model was used to control the vehicle with nonlinear model. The output of yaw rotational speed for both model was compared, multiplied by high gain and feedback to linear model to produce a rectified control input. Then the input is fed back to vehicle with nonlinear model. The end result shows the 4WDIS eliminate the stability velocity limit of the OS small electric vehicle

and provide stability.

Chapter 4 is the skid control system by regenerative brake control. Even though we have achieved in increasing the mobility and steering performance of the small electric vehicle, the system is faulty if traction can't be managed. In this chapter, based on the characteristics of in-wheel motor, which are fast torque response and easiness in obtaining an accurate torque feedback, the regenerative brake timing control was developed as a substitute to an anti-lock brake system. The ABS control the slip ratio of the tire so that friction coefficient can be maximized. In case of regenerative brake control, if the slip ratio is greater than the optimum value, the regenerative brake turns off and the current produced is transferred to charge the battery. However, if the slip ratio is smaller than the optimum value, the regenerative brake is restored to regain the ideal brake force. From the simulation results, during braking on an icy road, the regenerative brake control has the same effect as an ABS. thus, for an in-wheel small electric vehicle, the regenerative brake control can be substituted to ABS and be utilized as a skid control system

Chapter 5 In this chapter, the overall conclusion of the study that has been done are discussed. The recommendations for future work for this study also presented.

Chapter 2

Modelling an In-Wheel Small Electric Vehicle with Oversteer characteristic

2.1 Introduction

In this chapter, we increased the mobility of small electric vehicle by modelling with oversteer characteristic. At first, a basic understanding of oversteer and understeer characteristic is described. Later, Toyota COMS EV is introduced as a sample model of electric vehicle with in-wheel motor. The specification of this vehicle was modified to produce an oversteer characteristic by simply reposition the center weight distribution to the rear end of the vehicle. A set of multiple simulations of a steady state cornering with regard to a constant front steer angle and at constant velocity was done to determine the steer characteristic of the modelled small electric vehicle with oversteer characteristic.

2.2 Oversteer and Understeer Characteristic

The word “Oversteer” and “understeer” have been mentioned since the early automotive engineering. Oversteer and understeer are vehicle dynamics terms used to describe the sensitivity of a vehicle when steering. According to oxford dictionary, oversteer of a vehicle occurs when a vehicle has a tendency to steer more sharply than amount intended, while understeer occurs when a vehicle have a tendency to steer less than the amount intended [2-1].

Automotive engineer determines oversteer and understeer characteristic of a vehicle based on steady-state cornering test [2-2]. Under normal conditions, a vehicle at constant speed and fixed front steer angle will make a steady circular motion with a constant radius of curvature. This is called steady-state cornering. By understanding the vehicle characteristics in steady-state cornering, the fundamental characteristics of vehicle motion can be understood.

2.2.1 Steady-state cornering test

Figure 2-1 shows the relationship of the steady state yaw rotational speed to velocity while figure 2-2 shows the relationship of steady state side slip angle to velocity between oversteer and understeer characteristics during steady state cornering at constant steer angle. Based on the figure, the OS characteristic is separated into stable region and unstable region depending on the velocity of the vehicle and stability velocity limit. The stability limit velocity can be mathematically calculate based on the following equation [2-3];

$$V_c = \sqrt{-\frac{1}{A}} \tag{2-1}$$

Where A is called the stability factor and can be written as;

$$\mathrm{A} = -\frac{m}{2l^2}\left(\frac{l_f K_f - l_r K_r}{K_f K_r}\right)$$

Where m is the mass of the vehicle, l is the wheelbase, l_f is the distance from center of gravity to the front wheel, l_r is the distance from center of gravity to the rear wheel, K_f is the cornering stiffness of front wheel and K_r is the cornering stiffness of rear wheel.

When the vehicle velocity V is below the stability limit velocity Vc, oversteer vehicle can achieve steady state cornering with a higher yaw rotational speed in comparison to vehicle with understeer characteristic. A higher yaw rotational speed should also mean that the vehicle can achieve a shorter turning radius. On the other hand, the side-slip angle becomes negative as the absolute magnitude increases with velocity. This means that when the velocity increases, the vehicle will point into the inner side of the circular path of the cornering.

However, in the case of the vehicle velocity V greater the stability limit velocity Vc, the yaw rotational speed and the side-slip angle will produce an infinite value in regards to a constant steer angle. It does not mean that the vehicle cannot be driven above this velocity but it is important to note that the vehicle motion is unstable. For this particular reason, most vehicles are manufactured with US characteristic that has no stability limit velocity as a compensation to low steering response. When the vehicle velocity increases the yaw rotational speed increase. However, the yaw rotational speed saturates at a certain

value. Similar can be said to the steady state side slip angle to increase velocity with regards to constant steer.

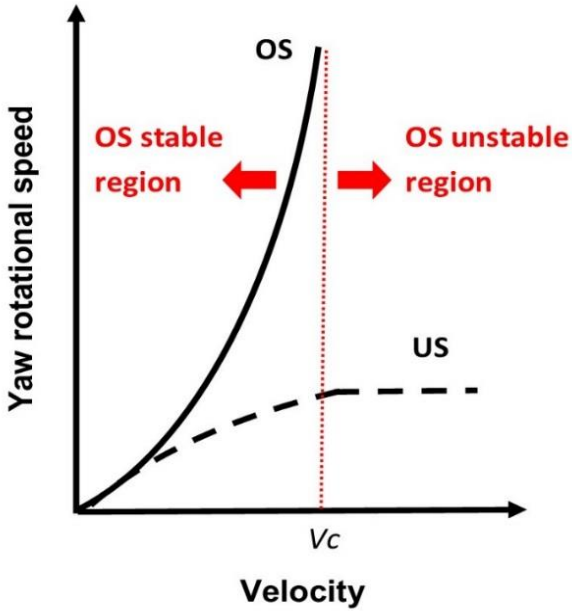

Figure 2-1 The relationship of the steady state yaw rotational speed to velocity

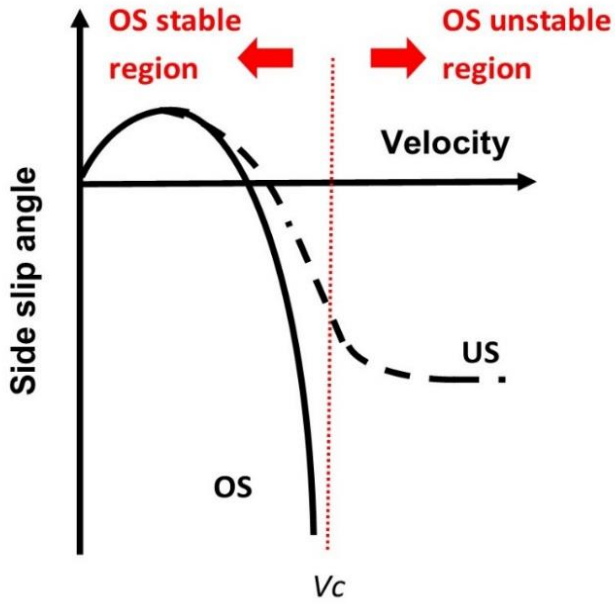

Figure 2-2 The relationship of the steady state side slip angle to velocity

2.2.2 Mathematical calculation

The vehicle steer characteristic can be calculated by utilizing the static margin equation that is shown in equation 2-2. Static margin is a dimensionless quantity of the ratio between ln and l. Figure 2-3 shows the ln which the distance of neutral steering point (NSF) from the vehicle center of gravity and l which is the wheelbase of the vehicle. The neutral steer point is the longitude location on a vehicle that gives a neutral response when lateral force is applied on the location.

$$SM = \frac{l_N}{l} = -\frac{K_f l_f - K_r l_r}{l(K_f + K_r)} \tag{2-2}$$

From the above, the quantity of $K_f l_f - K_r l_r$ determines the vehicle steer characteristics. Thus,

when $K_f l_f - K_r l_r < 0$, SM > 0,

Then the vehicle has Understeer characteristic

when $K_f l_f - K_r l_r > 0$, SM < 0,

Then the vehicle has Oversteer Characteristic

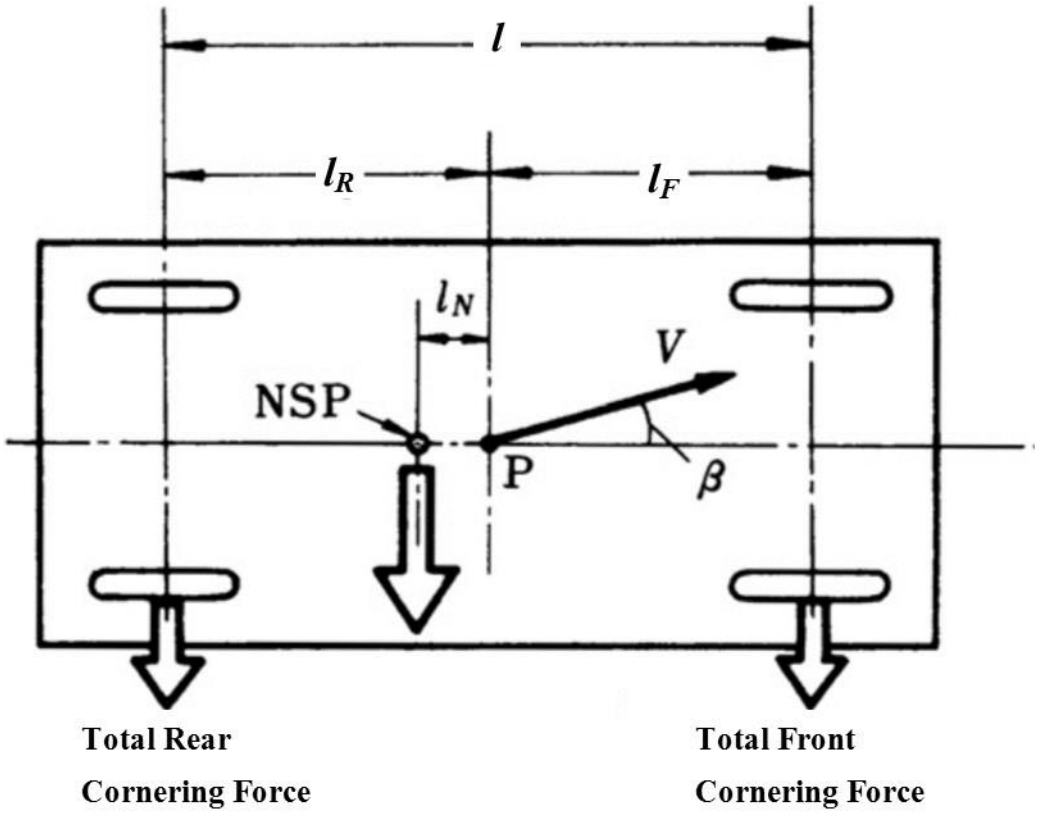

Figure 2-3 the distance of neutral steering point (NSF) from the vehicle center of gravity

2.3 Analysis Vehicle Model

2.3.1 Sample of a small electric vehicle with in-wheel motor system

Toyota COMS AK10E-PC, which is a small electric vehicle utilizing in-wheel motor system as driving propulsion, manufactured by Toyota Auto Body Co, was used as an analysis vehicle model in the simulation. Figure 2-4 shows the Toyota COMS AK10E-PC. Based on the handbook from the Toyota Auto Body Company, the main specifications of this vehicle are as in Table 2-1 [2-4]. We believe the chassis specification of the Toyota COMS to be an ideal small electric vehicle model. The important specification that are necessary to be highlighted for this study is the weight of the vehicle, maximum speed, dimension of the vehicle, braking system and steering system.

Table 2-1 Main Specifications of the Toyota COMS AK10E-PC

Vehicle Model		AK10E-PC
Weight	Vehicle Weight (kg)	270
	Vehicle Gross Weight (kg)	325
Type of fuel		Electricity
Maximum speed	Forward (km/h)	50
	Backward (km/h)	15
Mileage per 1 charge of battery (km)		80
Length (mm)		1935
Width (mm)		995
Height (mm)		1600
Wheelbase (mm)		1280
Tire (Front and rear)		90/90-12 54J
Main battery		Lead Acid Battery 12V x 42Ah x 6 pieces (72V)
Braking System		4 Wheel Drum Brake (Front : Hydraulic Braking System, Rear : Mechanical Braking System)
Driving System		Rear Wheel Drive (In-Wheel Motor)
Charging time (h)		8 Hours

Figure 2-4 The Toyota COMS AK10E-PC

2.3.2 Modelling a small electric vehicle with oversteer characteristic

We learn that when $K_f l_f - K_r l_r > 0$, the static margin produces negative value and the steer characteristic will yield an oversteer characteristic. The cornering stiffness of front and rear are equal and cannot be manipulated. However, due to in-wheel motor, a small electric vehicle can have a 'skateboard-shape' chassis where the top of the chassis can be managed freely. Thus, we can easily manipulate the distance of the center gravity of a vehicle. When the distance from center of gravity to the front wheel is larger than the distance from center of gravity to the front wheel, the static margin produces negative value.

In this study, we chose a 56.7% to 43.3% weight distribution for the small electric vehicle. Based on the specification of the Toyota COMS EV, the wheelbase of the vehicle is 1280 mm. Therefore, the distance from center of gravity to the front wheel and rear wheel can be calculated as follow;

Wheelbase, $l = l_f + l_r$ (2-3)

$$1280 = l_f + l_r$$

$$l_r = 1280 - l_f, (l_f > l_r)$$

l_f = 725mm → l_r= 555mm

If the center of the gravity is located too far at the rear end the steering of the vehicle will become too sensitive.

2.4 Vehicle Motion

2.4.1 Nonlinear dynamic equation of motion

In vehicle dynamics, the vehicle equation of motion in simple plane motion that includes longitudinal direction, lateral direction and yaw motion can be expressed by the following equation:

$$\mathrm{m}\left(\frac{du}{dt} - v\gamma\right) = \sum X_F + \sum X_R$$

$$\mathrm{m}\left(\frac{dv}{dt} + u\gamma\right) = \sum Y_F + \sum Y_R$$

$$\mathrm{I}\frac{d\gamma}{dt} = l_F \sum Y_F - l_R \sum Y_R$$

In this study, a nonlinear dynamic model was used to obtain the basic understanding of the dynamic motion for the small electric vehicle with front two-wheel steering and oversteering characteristic. The vehicle model has six degrees of freedom: three translational along the *x, y,* and *z*-axes, and three rotational about the *x, y* and *z*-axes. However, a planar motion is assumed so that a translation along the z-axis and rotations about the x and y-axes are disregarded. Figure 2-5 depicts the force vector of a vehicle with four two-wheel steering. The front steering angle that are define as θ_F was not assumed to be small. Thus, the sum of forces and yaw moment acted on each wheel can be written as follow:

$$\sum X_F = (X_{FR} + X_{FL})\cos\theta_F - (Y_{FR} + Y_{FL})\sin\theta_F$$

$$\sum X_R = X_{RR} + X_{RL}$$

$$\sum Y_F = (X_{FR} + X_{FL})\sin\theta_F + (Y_{FR} + Y_{FL})\cos\theta_F$$

$$\sum Y_R = Y_{RR} + Y_{RL}$$

$$N_z = l_F[(X_{FR} + X_{FL})\sin\theta_F + (Y_{FR} + Y_{FL})\cos\theta_F] + l_R(Y_{RR} + Y_{RL})$$

$$N_t = \frac{d_F}{2}[(X_{FR} + X_{FL})\cos\theta_F + (Y_{FR} + Y_{FL})\sin\theta_F] + \frac{d_R}{2}(X_{RR} + X_{RL})$$

Where $\sum X_F$ is the total longitude force of front right and left, $\sum X_R$ is the total longitude force of rear right and left, $\sum Y_F$ is the total lateral force of front right and left,

$\sum Y_R$ is the total lateral force of rear right and left, N_z is the yaw moment generated by the longitude force of each wheels, N_t is the yaw moment generated by the lateral force of each wheels. The subscript FR and FL represent front right and front left and the RR and RL represent rear right and rear left. The counter clockwise rotation is considered positive. These total forces and yaw moments can be substituted in the equation. The longitude, lateral and yaw dynamic equation of motion can be rewritten as follow;

$$m\left(\frac{du}{dt} - v\gamma\right) = (X_{FR} + X_{FL})\cos\theta_F - (Y_{FR} + Y_{FL})\sin\theta_F + X_{RR} + X_{RL} \quad (2\text{-}4)$$

$$m\left(\frac{dv}{dt} + u\gamma\right) = (X_{FR} + X_{FL})\sin\theta_F + (Y_{FR} + Y_{FL})\cos\theta_F + Y_{RR} + Y_{RL} \quad (2\text{-}5)$$

$$I\frac{d\gamma}{dt} = l_F[(X_{FR} + X_{FL})\sin\theta_F + (Y_{FR} + Y_{FL})\cos\theta_F] - l_R(Y_{RR} + Y_{RL})$$

$$+\frac{d_F}{2}[(X_{FR} + X_{FL})\cos\theta_F + (Y_{FR} + Y_{FL})\sin\theta_F] + \frac{d_R}{2}(X_{RR} - X_{RL}) \quad (2\text{-}6)$$

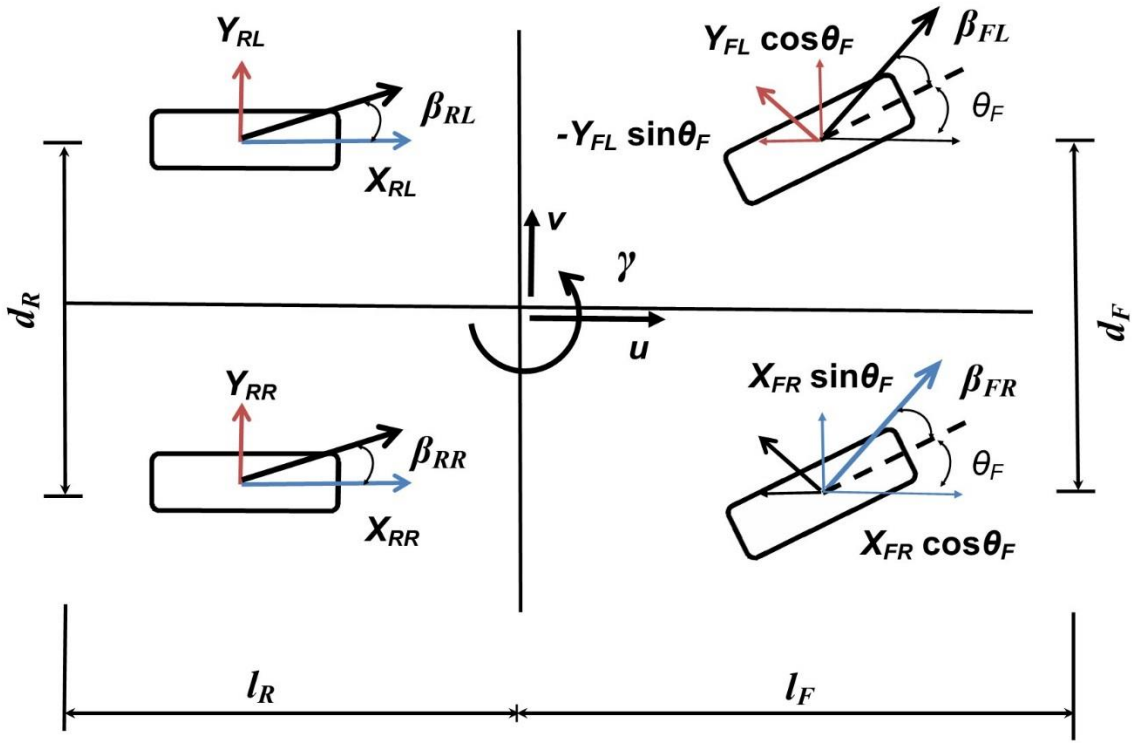

Figure 2-5 The force vector of the nonlinear vehicle model with front two-wheel steering

2.4.2 Nonlinear tire characteristic for driving condition

Fiala's Theory is fundamental theory widely and commonly use when we examine the tire characteristic [2-5]. In this theory, the tire structure is modelled as in Figure 2-6. This structure is called the brush model. The tread rubber, which is fitted to the stiff rim, is not a continuous circular body, but consists of large numbers of independent spring bodies around the tire circumference. Brush model is use to form the force equation generated by the wheel in the longitude and lateral direction. The forces are influenced by the elastic deformation of the tread rubber and the slippage of the wheel during driving, braking and cornering.

As shown in Figure 2-7, the tire is rotating with an angular velocity, u; while traveling in a direction that forms an angle of β to the rotation plane. The velocity component in the rotation plane is taken as *u*. Three forces act upon this tire, namely the longitudinal force, *Fx*, lateral force, *Fy*, and vertical force, *Fz*. When the tire longitudinal slip ratio and side slip angle are produced, tire deformation occurs. The deformation of tread rubber to the tread base at the contact surface is shown by a dimensionless variable ξ_p,

$$\xi_p = 1 - \frac{K_\rho}{3\mu W_z}\lambda$$

Where,

$$\lambda = \sqrt{\rho^2 + \left(\frac{K_\beta}{K_\rho}\right)^2 (1+\rho)^2 \tan^2\beta}$$

$$K_\rho = \frac{b{l_T}^2}{2}K_x \quad , \quad K_\beta = \frac{b{l_T}^2}{2}K_y$$

When $\xi_\rho > 0$, the contact surface comprises of adhesive and slip region. Thus, longitude force and lateral force can be written as;

$$X = -K_\rho \rho {\xi_p}^2 - 6\mu W_z \frac{\rho}{\lambda}\left(\frac{1}{6} - \frac{1}{2}{\xi_p}^2 + \frac{1}{3}{\xi_p}^3\right) \tag{2-7}$$

$$Y = -K_\beta (1+\rho)\tan\beta\, {\xi_p}^2 - 6\mu W_z \left(\frac{K_\beta \tan\beta (1+\rho)}{K_\rho \lambda}\right)\left(\frac{1}{6} - \frac{1}{2}{\xi_p}^2 + \frac{1}{3}{\xi_p}^3\right) \tag{2-8}$$

However, when $\xi_\rho \leq 0$, the contact surface only holds the slip region. Therefore, the longitude force and lateral force can be written as;

$$X = -\mu W_z \frac{\rho}{\lambda} \tag{2-9}$$

$$Y = -\mu W_z \left(\frac{K_\beta \tan\beta (1+\rho)}{K_\rho \lambda} \right) \tag{2-10}$$

Generally, when a vehicle is traveling in a straight line, the heading direction of the wheel coincides with the traveling direction. In other words, the wheel traveling direction is in line with the wheel rotational plane. However, when the vehicle has lateral motion and yaw motion, the traveling direction can be out of line with the rotational plane. Tire side slip angle is defined as the angle between the tire traveling direction and the tire heading direction or the tire rotation plane.

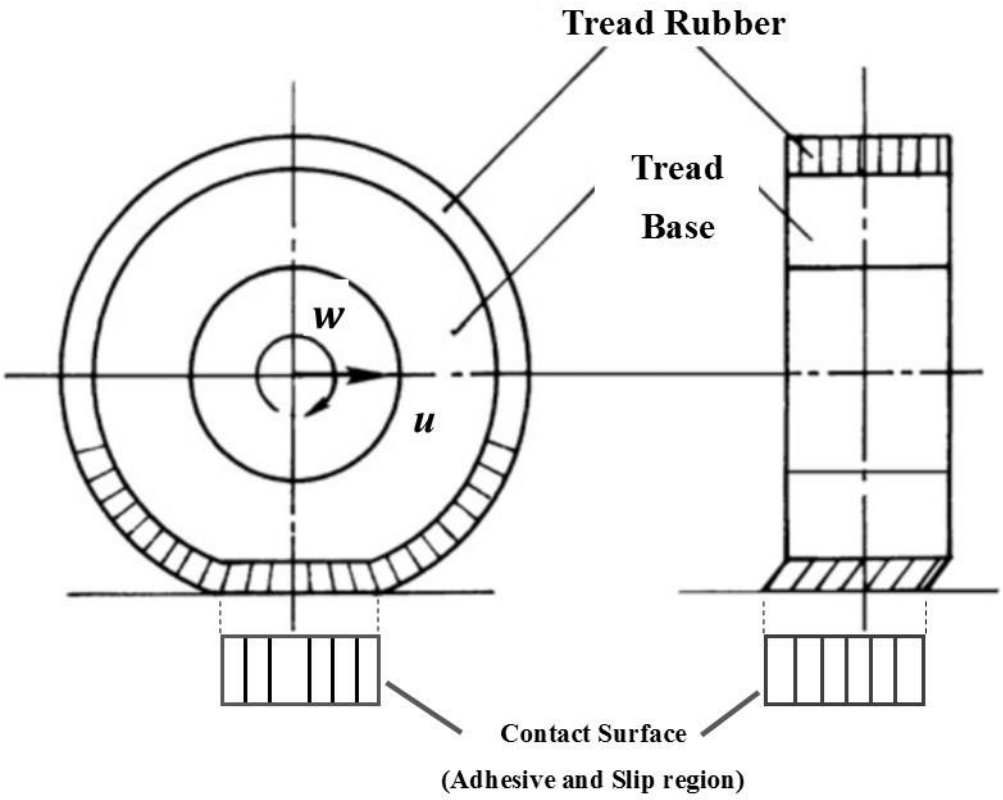

Figure 2-6 Tire structure model

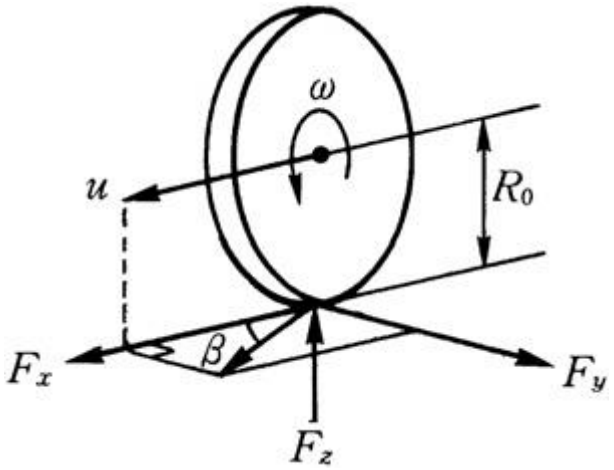

Figure 2-7 The force distribution for tire

The vehicle has a velocity component of u in the longitudinal direction, and v in the lateral direction. The vehicle also has an angular velocity of γ around the center of gravity. Consequently, each tire will have the velocity component of the center of gravity, and velocity component due to rotation around the center of gravity. The equation for side-slip angle for each tire is given as follows;

$$\beta_{FR} = \tan^{-1}\left(\frac{v + l_F\gamma}{u + d_F\gamma/2}\right) - \theta_F$$

$$\beta_{FL} = \tan^{-1}\left(\frac{v + l_F\gamma}{u - d_F\gamma/2}\right) - \theta_F$$

$$\beta_{RR} = \tan^{-1}\left(\frac{v - l_R\gamma}{u + d_R\gamma/2}\right)$$

$$\beta_{RL} = \tan^{-1}\left(\frac{v - l_R\gamma}{u - d_R\gamma/2}\right) \quad (2\text{-}11)$$

The slip ratio ρ can be represented in terms of the traction between the road and the tire surface, which is defined as

$$\rho = \frac{r\omega - u}{r\omega} \quad (2\text{-}12)$$

Then the coefficient of friction μ can be approximated by the following equation;

$$\mu = -1.10k \times (e^{35\rho} - e^{0.35\rho}) \quad (2\text{-}13)$$

where

$$\begin{cases} k = 1.0 \ \ (dry\ asphalt) \\ k = 0.2 \ \ (icy\ road) \end{cases}$$

2.5 Simulation Procedure

Based on the equation provided in previous section, numerical simulations of steady state cornering test were performed to examine the steering characteristic of the modelled small electric vehicle with oversteer characteristic. The simulation parameters are as follow:

Road Condition: Dry asphalt

Steering System: Front wheel steering

Vehicle velocity V = 0 km/h ~16km/h

Front steer angle $\theta_F = 10^0$(constant)

Steering initiate time t =10s.

In the simulation, the vehicle will accelerate until it reaches the desired velocity set initially. Then, the vehicle will maintain a constant speed. The front wheels will initiate rotation $\theta_F = 10^0$ at t =10s. The steady state yaw rotational speed and steady state side slip angle during the steady state cornering test are recorded. The process was repeated for every velocity.

2.6 Simulation Result and Discussion

Figure 2-8 and Figure 2-9 show the results of the steady state yaw rotational speed and steady state side-slip angle during cornering in regards to constant front wheel steer angle, respectively. Based on both of these graphs, in regards to constant front steer angle of 10^{o}, the steering characteristic of the modelled small electric vehicle with oversteer characteristic are as follows;

1. The stability limit velocity *Vc* = 15.5km/h.
2. The maximum steady state yaw rotational speed γ= 1.01 rad/s
3. The maximum absolute value of the steady state side-slip angle β =0.29 rad

At this velocity *Vc* = 15.5km/h, the vehicle is stable and can reach the maximum steady state yaw rotational speed of 1.01 rad/s with a maximum absolute magnitude of the steady state side-slip angle of 0.29 rad. Below the Vc, when the constant velocity increased, the longer time it took for the vehicle model to generate a constant yaw rotational speed. This is due to the increase side-slip angle to the constant velocity. When the velocity is above 15.5km/h, the yaw rotational speed and the side-slip angle will give an infinite value. However, the vehicle can still be drive but it is very unstable. Nonetheless, we believe that even in the stable region which is below the stability limit velocity, the OS small EV can be improved. The relation of the steady state yaw rotational speed to velocity is represent by the Figure 2-10 and the relation of the steady state side slip angle to velocity is represent in Figure 2-11.

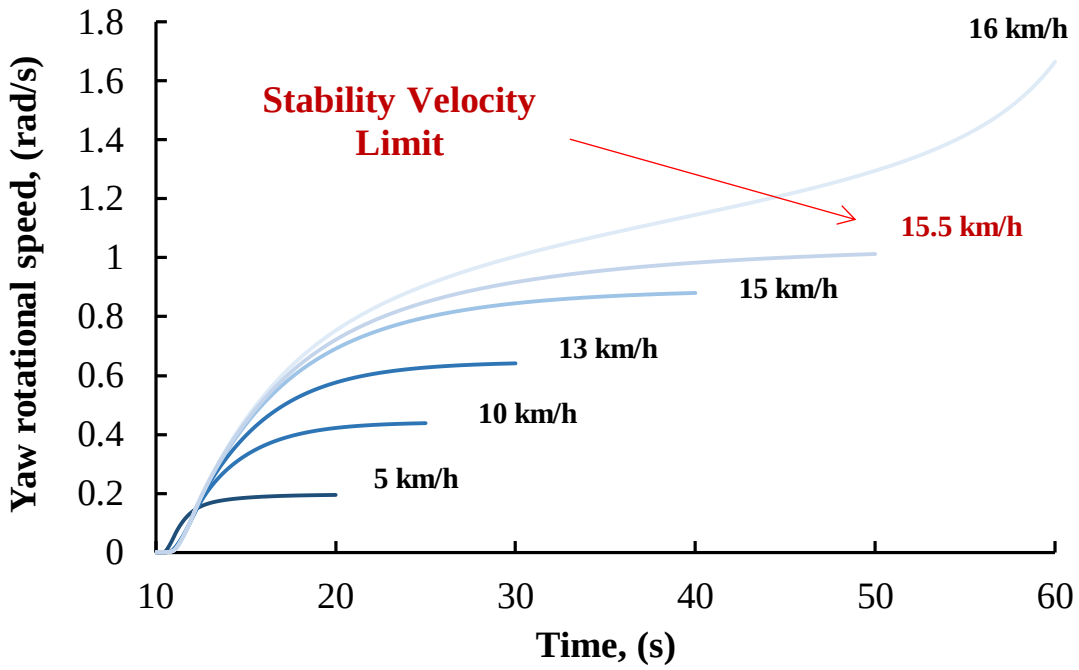

Figure 2-8 Change of time for steady state yaw rotational speed during cornering for 2WS small electric vehicle

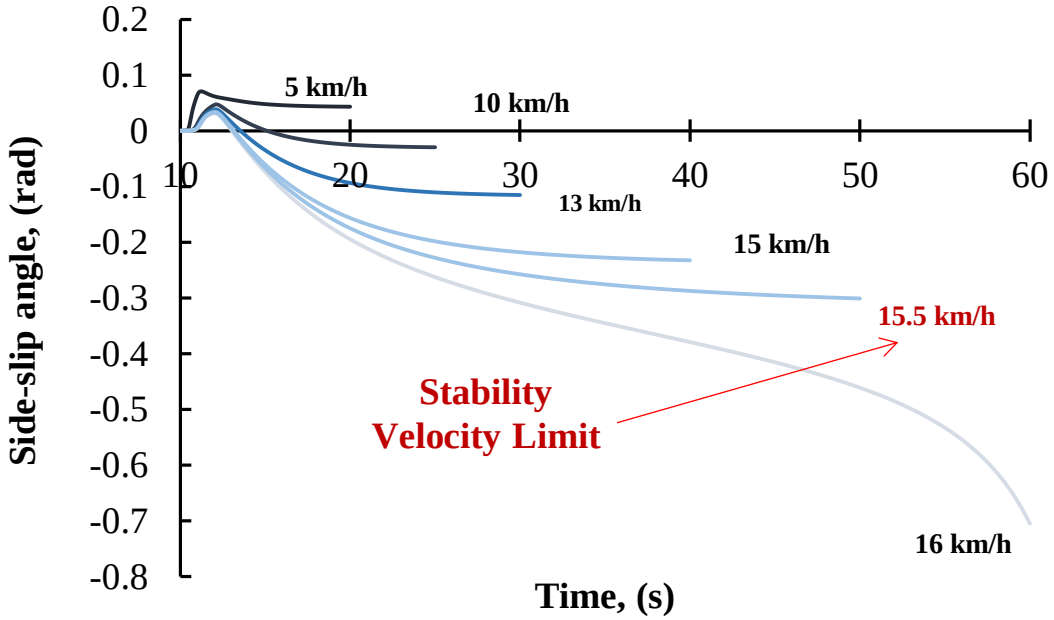

Figure 2-9 Change of time steady state side slip angle during cornering for 2WS small electric vehicle

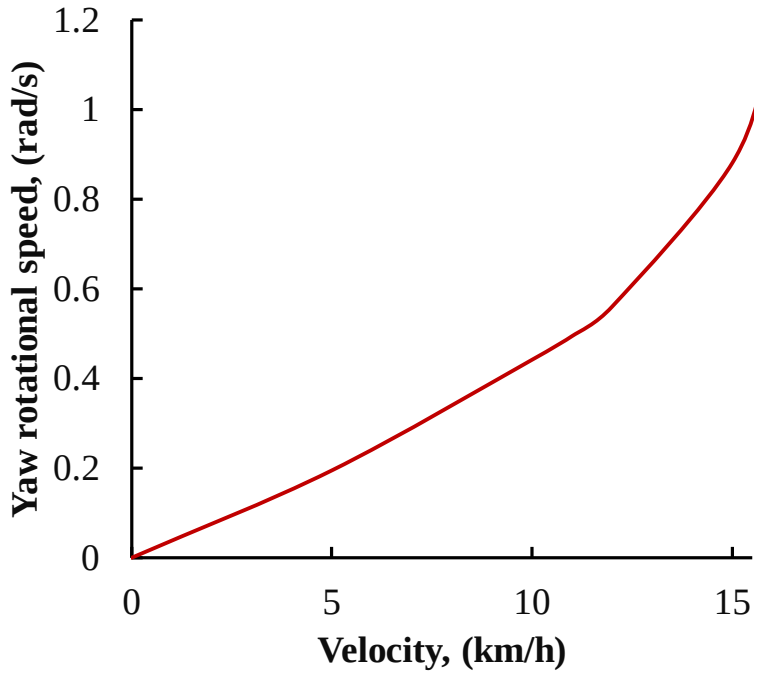

Figure 2-10 The relation of the steady state yaw rotational speed to velocity during cornering for 2WS small electric vehicle

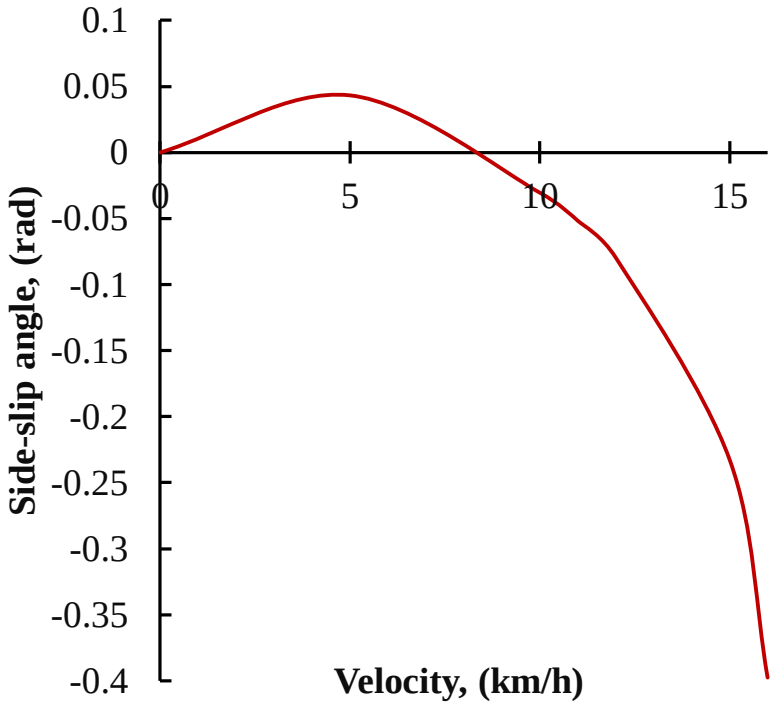

Figure 2-11 The relation of the steady state side slip angle to velocity during cornering for 2WS small electric vehicle

2.7 Summary

The steering characteristic of the OS small electric vehicle was determined by performing steady state cornering test in regards to a constant front steer angle and at constant velocity. The end results show that the modelled OS vehicle has a stability velocity limit at 15.5 km/h. Nonetheless, the vehicle can achieve high yaw rotational speed at below this velocity even with small steer angle. However, as the velocity increases, the longer time it will take for the vehicle to achieve steady state cornering.

Chapter 3

Yaw Moment Control by Four Wheel Drive and Independent Steering

3.1 Introduction

In previous chapter 2, theoretically we have successfully increased the mobility of a small electric vehicle by modelling an oversteer characteristic. However, when the vehicle velocity is equal to or beyond the stability velocity limit the yaw rotational speed and side slip angle of the modelled small electric vehicle with oversteer characteristic reach infinite value. In this chapter, we introduced a yaw moment control by integrating a four-wheel drive and independent steering (4WDIS) as a lateral stability system of the vehicle. With steer-by-wire technology, 4WDIS on electric vehicle is much more accomplishable. Many past researches adopt easier way of modelling a lateral control system based on vehicle model with linear characteristics. We prefer a nonlinear vehicle model which represent an actual vehicle more accurately. Thus, in order to redesign a yaw moment control, we have devised a few steps as follows;

Step 1: Feed Forward Control System

The output of linear feedback control is fed forward to the vehicle with a nonlinear model.

Step 2: Nonlinear Feed Back Control System

Output error between both systems are compared to form a close-loop feedback system.

Step 3: Clarification

Overall steer characteristic is examined and compared to the result in chapter 2.

3.2 Four Wheel Drive and Independent Steering Characteristic

As we have discussed in the past research section, In-wheel motor system and steer by-wire technology allows a freedom of layout for small electric vehicle [3-1]~[3-2]. Due to the in-wheel motor system located at the wheels, a small electric vehicle can have a 'skateboard-shape' chassis as shown in Figure 3-1. There will be no need of engine room nor transmission on board the chassis. For the same reason, each wheels' driving torque and braking can be governed separately [3-3]. Furthermore, by adding a steering actuator on top of each wheel, the direction of the wheels can be manipulated with certain control. Figure 3-2 (a), (b), and (c) show the different steering modes of a four-wheel drive and independent steering. We had concluded that the steering modes can be separated as follow [3-4];

a) Opposite steering

   Figure 3-2 (a) shows the diagram of opposite steering. The rear wheels will turn on the opposite direction as the front wheels. This will increase the vehicle yaw rotational speed which tighten the turning radius. The angular speed of the inside wheels is slower compared to the outer wheels.

b) Parallel steering

   Figure 3-2 (b) shows the diagram of parallel steering. The rear wheels will rotate in the same direction parallel to the front. This steering characteristic does not generate yaw motion, instead it will decrease the yaw rotational speed.

c) 'Zero-radius' steering

   Figure 3-2 (c) shows the diagram of 'Zero-radius' steering. Unlike parallel and opposite steering, the third steering characteristic allows the vehicle to rotate in stationary and has a zero turning radius. The front wheels have to be 'toe-in' position and the rear wheel in 'toe-out' position. The driving direction of the left and right is in opposite so that the vehicle can alternate.

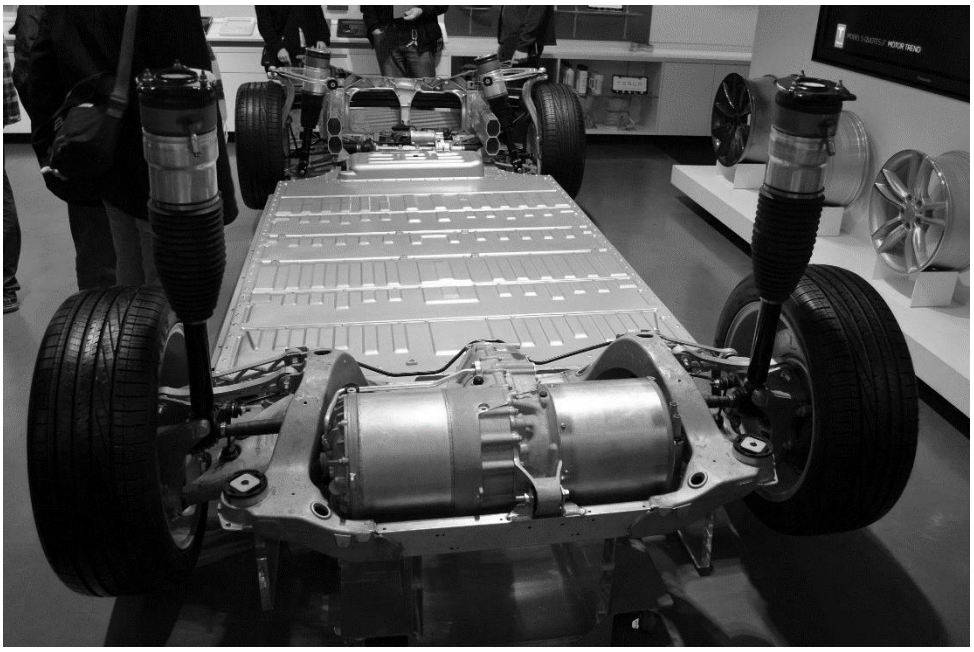

(https://upload.wikimedia.org/wikipedia/commons/f/f3/Tesla_Motors_Model_S_base.JPG)

http://img-s-msn-com.akamaized.net/tenant/amp/entitynid/AAgoTIJ.img?h=312&w=624&m=6&q=60&0=f&l=f

Figure 3-1 'Skateboard-shape' chassis of an electric vehicle

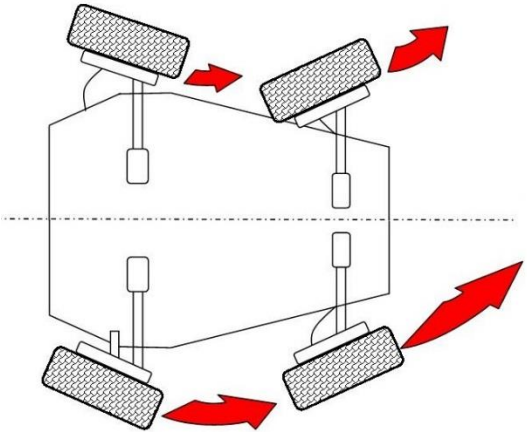

(a) Opposite steering

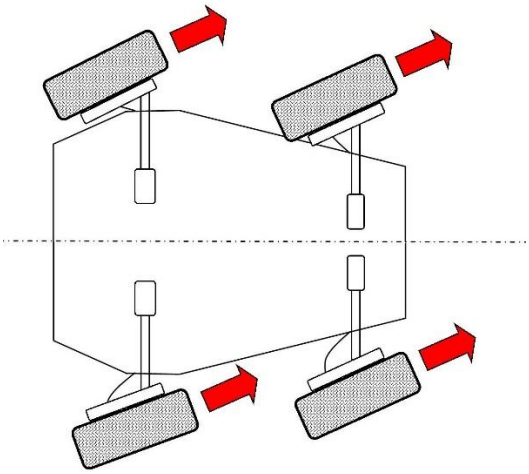

(b) Parallel steering

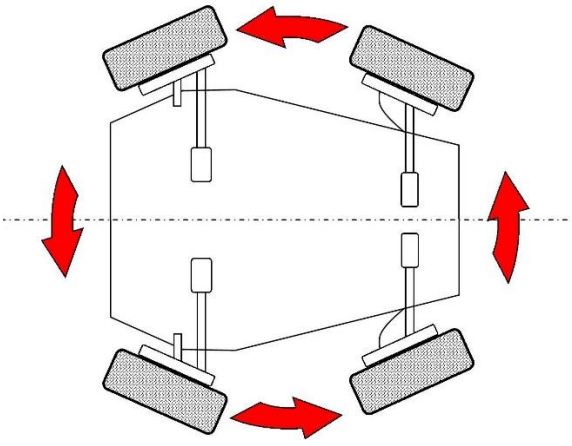

(c) ‘Zero-radius’ steering

Figure 3-2 Four-wheel drive and independent steering mode

3.3 Simplified Four Wheel Drive and Independent Steering Vehicle Motion

3.3.1 Linear dynamic equation of motion

There is an extensive researches on control method of 4WS [3-5] - [3-7]. Unfortunately, the vehicle model was design based on linear dynamic equation. From this onward, we will explain the simplification of a linear dynamic equation commonly used to represent a vehicle.

As shown in figure 3-3, "X-Y" is the fixed plane coordinates on the ground, and x–y are the fixed coordinates on the vehicle, with x in the vehicle longitudinal direction, and y in the lateral direction [3-8]. The vehicle center of gravity is P and the yaw rotational speed is taken as positive in the anti-clockwise direction. The position vector of point P, with reference to coordinate system X–Y, is defined as R. The velocity vector $\dot{R}$ can be written as:

$$\dot{R} = ui + vj \tag{3-1}$$

Where, i and j are the respective unit vectors in x and y directions, while u and v are the longitudinal and lateral velocity of point P in the x and y directions. Then, the acceleration of the vector R can be written as below.

$$\ddot{R} = \dot{u}i + ui + \dot{v}j + vj \tag{3-2}$$

Figure 3-4 shows the i and j swing by yaw motion from its position at $t=t_0$ to a new position at $t = t_0+\Delta t$. the change in the position can be written as;

$$\Delta i = \gamma \Delta t j$$

$$\Delta j = -\gamma \Delta t i$$

Thus, in the limit $\Delta t \rightarrow 0$,

$$i = \lim_{\Delta t \rightarrow 0} \frac{\Delta i}{\Delta t} = \gamma j$$

$$\acute{j} = \lim_{\Delta t \rightarrow 0} \frac{\Delta j}{\Delta t} = -\gamma i$$

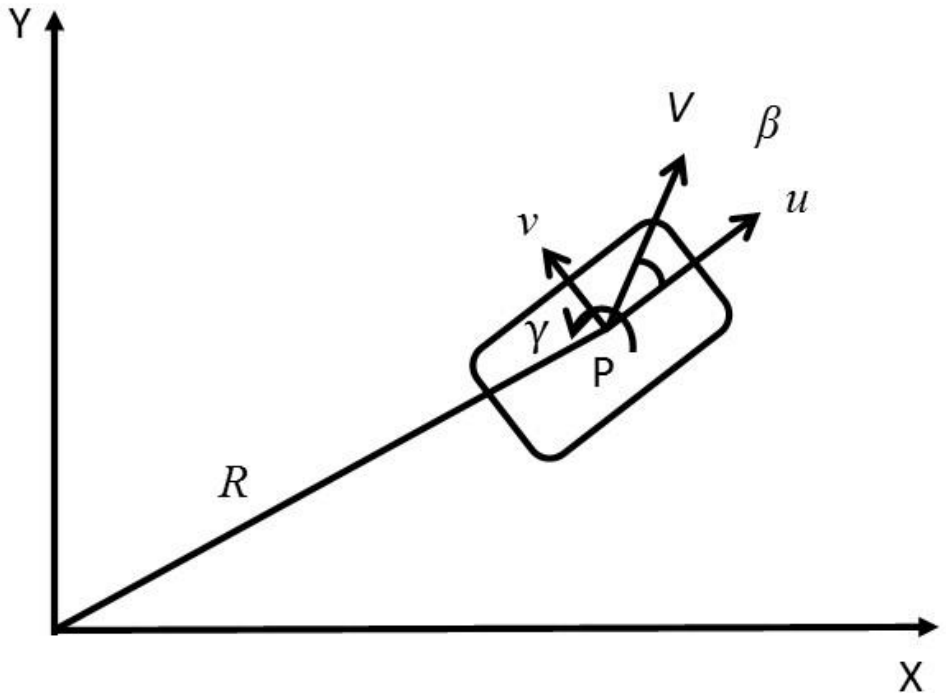

Figure 3-3 Coordinate axes for vehicle plane motion

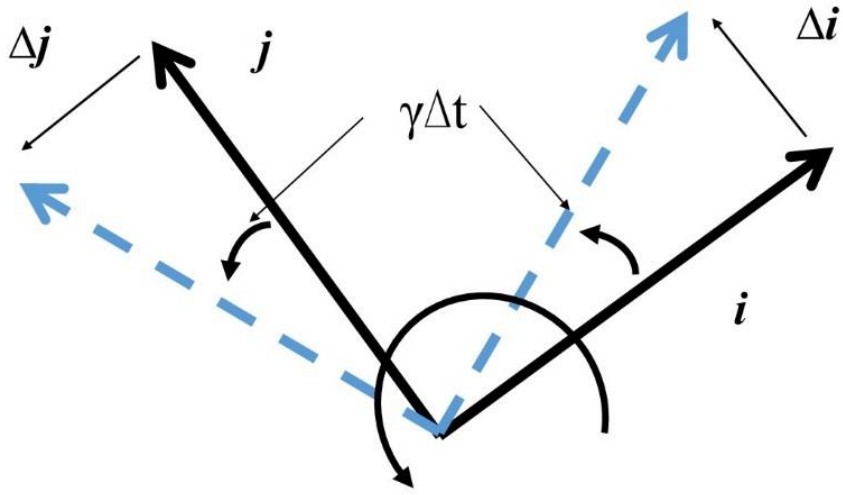

Figure 3-4 Time derivative of unit vectors

The final acceleration vector of point P, $\ddot{R}$ is

$$\ddot{R} = (\dot{u} - v\gamma)i + (\dot{v} + u\gamma)j \quad (3\text{-}2)`$$

The angle between the vehicle traveling direction and longitudinal direction or side slip angle of the vehicle at the center of gravity, β is expressed by,

$$\beta = \tan^{-1}\left(\frac{u}{v}\right) \quad (3\text{-}3)$$

If we consider $u>>v$, then β can be regarded to be very small. Thus,

$$u = V\ cos\ \beta\ \approx V$$
$$\dot{u} = -V\ sin\beta \times \dot{\beta}\ \approx V\beta\dot{\beta}$$
$$v = V\ sin\ \beta\ \approx V\beta$$
$$\dot{v} = V\ cos\ \beta \times \dot{\beta}\ \approx V\dot{\beta}$$

Which, equation (3-2)` of $\ddot{R}$ can be written as;

$$\ddot{R} = -V\left(\dot{\beta} - \gamma\right)\beta i + V\left(\dot{\beta} - \gamma\right)j \quad (3\text{-}4)$$

Based on this, when the side slip angle β is small, a moving vehicle at a constant speed will only have an acceleration of $V\left(\dot{\beta} - \gamma\right)$ which is in the lateral and is perpendicular to the traveling direction. For this reason, no coupling exists between the yaw rotational speed and the vehicle's translational velocity. By obeying Based on the Newton's Second Law of Motion $F = ma$, the lateral dynamic equation and yaw dynamic equation can be written as;

$$\mathrm{m}V\left(\frac{d\beta}{dt} + \gamma\right) = 2Y_f + 2Y_r \quad (3\text{-}5)$$

$$\mathrm{I}\frac{d\gamma}{dt} = (2l_fY_f - 2l_rY_r)\cos\beta \quad (3\text{-}6)$$

It is to be noted that there is no difference in the characteristics of the left and right tires due to linearity. Thus, the total force generated by sum of two front and two rear wheels. The velocity component in x- and y direction for each tire is shown in Figure 3-5.

3.3.2 Linear tire characteristic for driving condition

The heading direction of the front wheels has an angular displacement of θ_F and the rear wheels has an angular displacement of θ_R with respect to the vehicle longitudinal direction, x. The heading direction of the rear wheels is the same as the vehicle longitudinal direction. Therefore, the side-slip angle for each tire could be written as below:

$$\beta_f = \beta + \frac{l_f}{V}\gamma - \theta_F \tag{3-7}$$

$$\beta_r = \beta - \frac{l_r}{V}\gamma - \theta_R \tag{3-8}$$

In linear form, the lateral force of the tire is proportional to the side slip angle of the tire. In this research, all angles in anti-clockwise direction are define as positive value. However, when the lateral force act in positive y-direction, the side slip angle rotates in clockwise and has negative value. Therefore, the lateral force can be calculated as follow;

$$Y_f = -K_f\beta_f = -K_f\left(\beta + \frac{l_f}{V}\gamma - \theta_F\right) \tag{3-9}$$

$$Y_r = -K_r\beta_r = -K_r\left(\beta - \frac{l_r}{V}\gamma - \theta_R\right) \tag{3-10}$$

K_f and K_r are the cornering stiffness of the front and rear wheels. Based on these equations, the lateral forces are influenced by the vehicle motion specifically the side slip angle of centre gravity β, yaw rotational speed at the centre gravity γ and the steering angle of front and rear wheels θ_F, θ_R. The above equations can be substituted into the linear lateral dynamic equation in equation (3-5) and the yaw dynamic equation in equation (3-6).

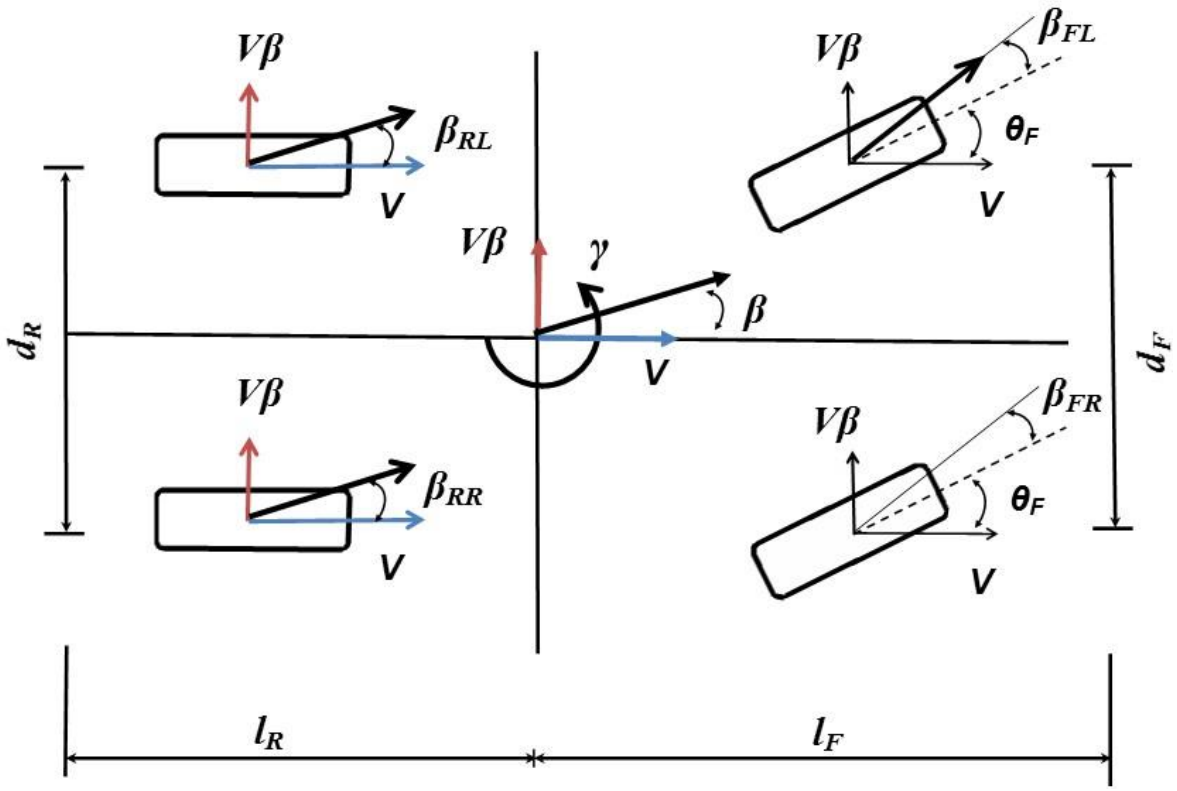

Figure 3-5 The force vector of the linear vehicle model with front two-wheel steering

3.4 Feedforward Control for Vehicle with Nonlinear Model

Every physical system in our life has nonlinearities and very little can be done to overcome them. In case of automobile, the dynamics motion of an actual vehicle also inherently a nonlinear system [3-9]. A feedback control cannot be executed directly to nonlinear system because of the yaw rotational speed coupled with the velocity components as expressed in the nonlinear dynamic equation of motion in previous section. However, modelling a control method based on a linear dynamic equation is considered not suitable and inaccurate. Other parameters that could influenced the dynamic motion of the vehicle are neglected and the modelled control system deem low precision

Figure 3-6 shows a simulation block diagram to justify our claims. In this simulation block, the vehicle model, which is a small electric vehicle with oversteer characteristic equipped with 4WDIS, is calculated by a nonlinear dynamic equation of motion. Then, a state observer unit, which is modelled by a linear feedback control system, is fed forward to the vehicle model. The state observer unit of the simulation block will be explained in detail in the following sections.

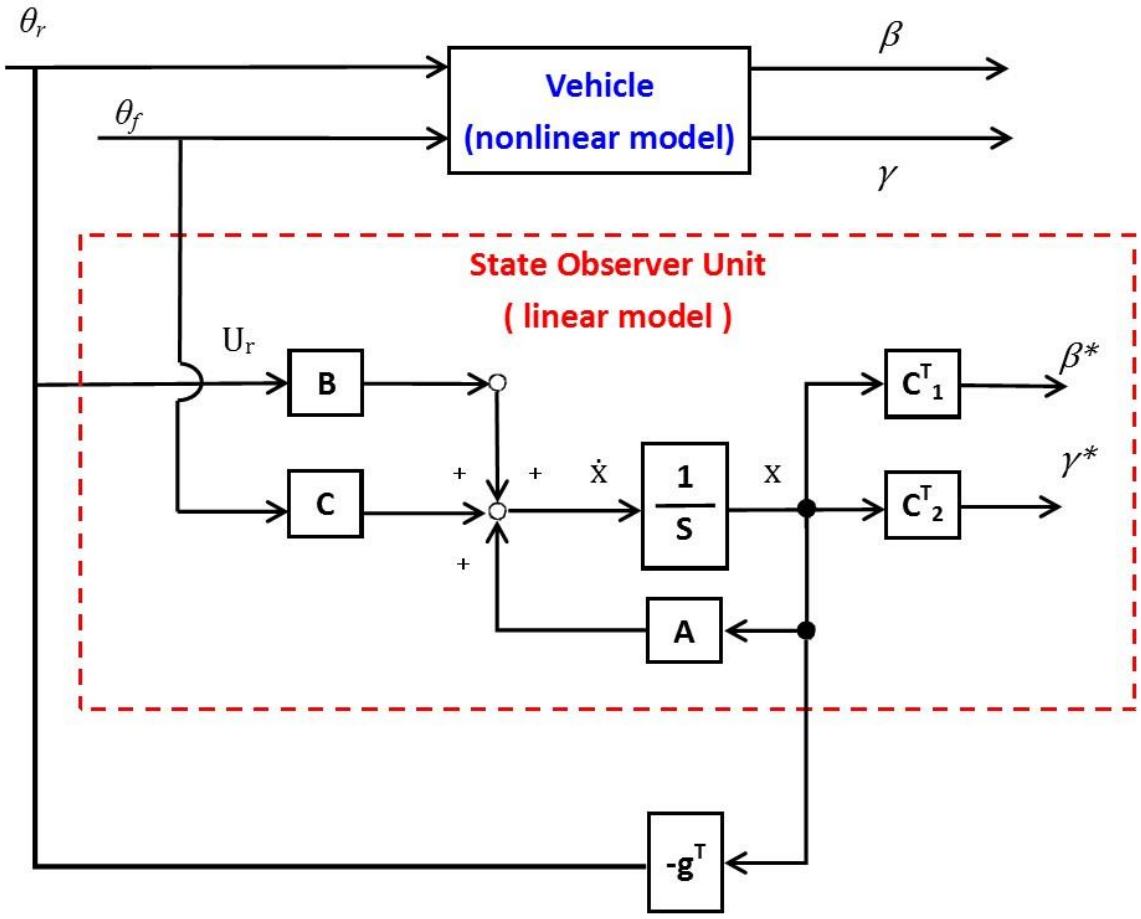

Figure 3-6 Simulation block of a feedforward control for vehicle with nonlinear model

3.4.1 Vehicle model

In a linear equation of motion, we describe that the lateral velocity *v* is small in comparison to *u*. However, in real condition *u* isn't necessarily always constant. Therefore, the side slip angle is not assumed as small and the use of β in the description of the vehicle motion is avoided. The vehicle longitudinal and lateral accelerations are better expressed by $(\dot{u} - vr)$ and $(\dot{v} + ur)$, respectively. Based on the Newton's Second Law of Motion *F=ma*, the vehicle lateral and yaw dynamic equations of motion inclusive of the longitude dynamic equations of motion can be expressed by the following equations:

$$\mathrm{m}\left(\frac{du}{dt} - v\gamma\right) = \sum X_F + \sum X_R$$

$$\mathrm{m}\left(\frac{dv}{dt} + u\gamma\right) = \sum Y_F + \sum Y_R$$

$$\mathrm{I}\frac{d\gamma}{dt} = l_F \sum Y_F - l_R \sum Y_R$$

A nonlinear vehicle dynamic equation of motion was introduced in chapter 2 for front wheel steering. However, a four-wheel vehicle nonlinear dynamic model has been used obtain the basic understanding of a four-wheel drive and independent steering small electric vehicle dynamic motion in this chapter. The vehicle model has six degrees of freedom: three translational along the *x, y,* and *z*-axes, and three rotational about the *x, y* and *z*-axes. However, a planar motion is assumed so that a translation along the z-axis and rotations about the x and y-axes are disregarded. Figure 3-6 depicts the force vector of a vehicle with four-wheel drive and four-wheel steering. The front and rear steering angle that are define as θ_F and θ_R cannot be assumed as small. Thus, the sum of forces and yaw moment acted on each wheel can be written as follow:

$$\sum X_F = (X_{FR} + X_{FL})\cos\theta_F - (Y_{FR} + Y_{FL})\sin\theta_F$$

$$\sum X_R = (X_{RR} + X_{RL})\cos\theta_R - (Y_{RR} + Y_{RL})\sin\theta_R$$

$$\sum Y_F = (X_{FR} + X_{FL})\sin\theta_F + (Y_{FR} + Y_{FL})\cos\theta_F$$

$$\sum Y_R = (X_{RR} + X_{RL})\sin\theta_R + (Y_{RR} + Y_{RL})\cos\theta_R$$

$$N_z = l_F[(X_{FR} + X_{FL})\sin\theta_F + (Y_{FR} + Y_{FL})\cos\theta_F] + l_R[(X_{RR} + X_{RL})\sin\theta_R] + (Y_{RR} + Y_{RL})\cos\theta_R$$

$$N_t = \frac{d_F}{2}[(X_{FR} + X_{FL})\cos\theta_F + (Y_{FR} + Y_{FL})\sin\theta_F] + \frac{d_R}{2}[(X_{RR} + X_{RL})\cos\theta_R + (Y_{RR} + Y_{RL})\sin\theta_R]$$

Where $\sum X_F$ is the total longitude force of front right and left, $\sum X_R$ is the total longitude force of rear right and left, $\sum Y_F$ is the total lateral force of front right and left, $\sum Y_R$ is the total lateral force of rear right and left, N_z is the yaw moment generated by the longitude force of each wheels, N_t is the yaw moment generated by the lateral force of each wheels. The subscript FR and FL represent front right and front left and the RR and RL represent rear right and rear left. These total forces and yaw moments can be substituted in the equation below. The longitude, lateral and yaw dynamic equation of motion can be rewritten as follow;

$$m\left(\frac{du}{dt} - v\gamma\right) = (X_{FR} + X_{FL})\cos\theta_F + (X_{RR} + X_{RL})\cos\theta_R - (Y_{FR} + Y_{FL})\sin\theta_F - (Y_{RR} + Y_{RL})\sin\theta_R \quad (3\text{-}11)$$

$$m\left(\frac{dv}{dt} + u\gamma\right) = (X_{FR} + X_{FL})\sin\theta_F + (X_{RR} + X_{RL})\sin\theta_R + (Y_{FR} + Y_{FL})\cos\theta_F + (Y_{RR} + Y_{RL})\cos\theta_R \quad (3\text{-}12)$$

$$I\frac{d\gamma}{dt} = l_F[(X_{FR} + X_{FL})\sin\theta_F + (Y_{FR} + Y_{FL})\cos\theta_F] + l_R[(X_{RR} + X_{RL})\sin\theta_R + (Y_{RR} + Y_{RL})\cos\theta_R] + \frac{d_F}{2}[(X_{FR} + X_{FL})\cos\theta_F + (Y_{FR} + Y_{FL})\sin\theta_F] + \frac{d_R}{2}[(X_{RR} + X_{RL})\cos\theta_R + (Y_{RR} + Y_{RL})\sin\theta_R] \quad (3\text{-}13)$$

Each wheels of the vehicle are modelled as a brush tire. Due to this, the equations for friction and lateral forces are dependent on the value of slip ratio, tire side-slip angle, and weight distribution. The model's deformation of the tire tread rubber is also used to derive the following equations,

$$\xi_p = 1 - \frac{K_\rho}{3\mu W_z}\lambda$$

Where,

$$\lambda = \sqrt{\rho^2 + \left(\frac{K_\beta}{K_\rho}\right)^2 (1+\rho)^2 \tan^2\beta}$$

$$K_\rho = \frac{b{l_T}^2}{2} K_x \quad , \quad K_\beta = \frac{b{l_T}^2}{2} K_y$$

When $\xi_\rho > 0$, the contact surface comprises of adhesive and slip region. Thus, longitude force and lateral force can be written as;

$$X = -K_\rho \rho {\xi_p}^2 - 6\mu W_z \frac{\rho}{\lambda}\left(\frac{1}{6} - \frac{1}{2}{\xi_p}^2 + \frac{1}{3}{\xi_p}^3\right) \tag{3-14}$$

$$Y = -K_\beta (1+\rho)\tan\beta\, {\xi_p}^2 - 6\mu W_z \left(\frac{K_\beta \tan\beta (1+\rho)}{K_\rho \lambda}\right)\left(\frac{1}{6} - \frac{1}{2}{\xi_p}^2 + \frac{1}{3}{\xi_p}^3\right) \tag{3-15}$$

However, when $\xi_\rho \leq 0$, the contact surface only holds the slip region. Therefore, the longitude force and lateral force can be written as;

$$X = -\mu W_z \frac{\rho}{\lambda} \tag{3-16}$$

$$Y = -\mu W_z \left(\frac{K_\beta \tan\beta (1+\rho)}{K_\rho \lambda}\right) \tag{3-17}$$

Generally, when a vehicle is traveling in a straight line, the heading direction of the wheel coincides with the traveling direction. In other words, the wheel traveling direction is in line with the wheel rotational plane. However, when the vehicle has lateral motion and yaw motion, the traveling direction can be out of line with the rotational plane. Tire side slip angle is defined as the angle between the tire traveling direction and the tire heading direction or the tire rotation plane.

As we explained in chapter 2, the vehicle has a velocity component of *u* in the longitudinal direction, and *v* in the lateral direction. The vehicle also has an angular velocity of γ around the center of gravity. Consequently, each tire will have the velocity component of the center of gravity, and velocity component due to rotation around the center of gravity. The equation for side-slip angle for front and rear wheels with steer angle are given as follows;

$$\beta_{FR} = \tan^{-1}\left(\frac{v + l_F\gamma}{u + d_F\gamma/2}\right) - \theta_F$$

$$\beta_{FL} = \tan^{-1}\left(\frac{v + l_F\gamma}{u - d_F\gamma/2}\right) - \theta_F$$

$$\beta_{RR} = \tan^{-1}\left(\frac{v - l_R\gamma}{u + d_R\gamma/2}\right) - \theta_R$$

$$\beta_{RL} = \tan^{-1}\left(\frac{v - l_R\gamma}{u - d_R\gamma/2}\right) - \theta_R \quad (3\text{-}18)$$

The slip ratio ρ can be represented in terms of the traction between the road and the tire surface, which is defined as

$$\rho = \frac{r\omega - u}{r\omega} \quad (3\text{-}19)$$

Then the coefficient of friction μ can be approximated by the following equation

$$\mu = -1.10\mathrm{k} \times (e^{35\rho} - e^{0.35\rho}) \quad (3\text{-}20)$$

where

$$\begin{cases} k = 1.0 \ \ (dry\ asphalt) \\ k = 0.2 \ \ (icy\ road) \end{cases}$$

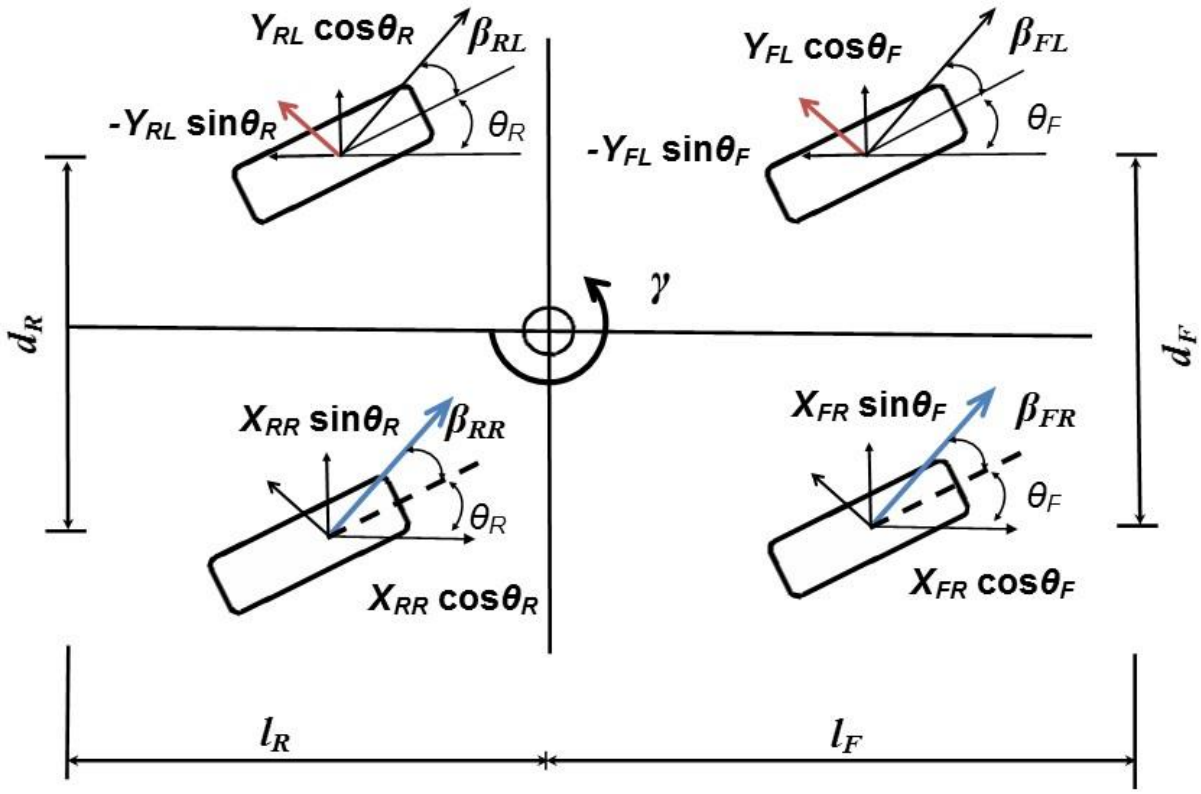

Figure 3-7 The force vector of the nonlinear vehicle model with 4WDIS

3.4.2 State observer unit

In control theory, a state observer is a system that provides an estimate of the internal state of a given real system, from measurements of the input and output of the real system. In this study, this state observer unit estimates the yaw rotational speed and side-slip angle of the vehicle. The linearized differential equation represents the linear vehicle dynamic equation of motion for the state observer. It is arranged as a set of first-order ordinary differential equations in the vector state form:

$$\begin{aligned} \dot{\mathrm{x}} &= \mathrm{A}\mathrm{x} + \mathrm{B}\mathrm{U}_r + \mathrm{C}\mathrm{U}_f \\ y_\beta &= \beta^* = \mathbb{C}_1{}^T\mathrm{x} \\ y_\gamma &= \gamma^* = \mathbb{C}_2{}^T\mathrm{x} \end{aligned} \tag{3-21}$$

where,

$$\mathrm{x} = [\beta^* \quad \gamma^*]^T,$$

$$\mathbb{C}_1{}^T = [1 \quad 0]^T, \qquad \mathrm{U}_f = \theta_F,$$

$$\mathbb{C}_2{}^T = [0 \quad 1]^T, \qquad \mathrm{U}_r = \theta_R,$$

$$\mathrm{A} = \begin{bmatrix} a & b \\ c & d \end{bmatrix} = \begin{bmatrix} -\dfrac{2(K_f + K_r)}{mv} & -1 - \dfrac{2(K_f l_f - K_r l_r)}{mv^2} \\ -\dfrac{2(l_f K_f - l_r K_r)}{I} & \dfrac{2(l_f{}^2 K_f + l_r{}^2 K_r)}{Iv} \end{bmatrix},$$

$$\mathrm{B} = \begin{bmatrix} e \\ f \end{bmatrix} = \begin{bmatrix} \dfrac{2K_r}{mv} \\ -\dfrac{2l_r K_r}{I} \end{bmatrix}, \qquad \mathrm{C} = \begin{bmatrix} k \\ l \end{bmatrix} = \begin{bmatrix} \dfrac{2K_f}{mv} \\ \dfrac{2l_f K_f}{I} \end{bmatrix},$$

The state vector x represents the side-slip angle and yaw rotational speed of the vehicle. The steering angles of the front and rear wheels are the inputs of this system. The value for the front-wheel angle θ_F is a driver-selected input whereas the rear-wheel angle θ_R is initially 0 degrees. During high-speed cornering, the rear-wheel steering is used as the control input by introducing a feedback gain $-g^T$.

$$\mathrm{U}_r = -g^T\mathrm{x} + \theta_r \tag{3-22}$$

3.4.3 Optimal control

In order to find the optimal control for the linearized differential equation, the following evaluation function *J* is employed.

$$J = \int_0^\infty (q_{11}\mathrm{x}^2 + q_{22}\dot{\mathrm{x}}^2 + w\theta_r^2)dt = \int_0^\infty (\mathrm{x}^T Q\mathrm{x} + w\theta_r^2)dt \tag{3-23}$$

where,

$$\mathrm{Q} = \begin{bmatrix} q_{11} & 0 \\ 0 & q_{22} \end{bmatrix}$$

in which q_{11}, q_{22}, and w are appropriately chosen constant weighting matrices for the side-slip angle, yaw rotational speed, and rear-wheel steering angle, respectively. The optimal solution for *J* can be designed if Q is a positive definite matrix and the state observer control input $\mathrm{U_r}$ is given by

$$\mathrm{U}_r = -\frac{1}{w}B^T P\mathrm{x} + \theta_R \tag{3-24}$$

where,

$$-\mathrm{g}^T = -\frac{1}{w}B^T P$$

With $\mathrm{P} = \mathrm{P}^\mathrm{T} \geq 0$ being the unique positive-semidefinite solution of the algebraic Riccati equation,

$$A^T\mathrm{P} + \mathrm{PA} - w^{-1}PBB^TP = -Q$$

$$\begin{bmatrix} a & b \\ c & d \end{bmatrix}^T P + P\begin{bmatrix} a & b \\ c & d \end{bmatrix} - w^{-1}P\begin{bmatrix} e \\ f \end{bmatrix}[e \quad f]^T P = -\begin{bmatrix} q_1 & 0 \\ 0 & q_2 \end{bmatrix} \tag{3-25}$$

The unique positive-semidefinite *P* can also be expressed as,

$$P = \begin{bmatrix} \varepsilon & \phi \\ \psi & \epsilon \end{bmatrix}$$

Thus, eq. (18) can be expanded as;

$$\begin{bmatrix} a & c \\ b & d \end{bmatrix}\begin{bmatrix} \varepsilon & \phi \\ \psi & \epsilon \end{bmatrix} + \begin{bmatrix} \varepsilon & \phi \\ \psi & \epsilon \end{bmatrix}\begin{bmatrix} a & b \\ c & d \end{bmatrix} - w^{-1}\begin{bmatrix} \varepsilon & \phi \\ \psi & \epsilon \end{bmatrix}\begin{bmatrix} e \\ f \end{bmatrix}[e \quad f]\begin{bmatrix} \varepsilon & \phi \\ \psi & \epsilon \end{bmatrix} = -\begin{bmatrix} q_1 & 0 \\ 0 & q_2 \end{bmatrix}$$

$$\begin{bmatrix} a\varepsilon + c\psi & a\phi + c\epsilon \\ b\varepsilon + d\psi & b\phi + d\epsilon \end{bmatrix} + \begin{bmatrix} a\varepsilon + c\phi & b\varepsilon + d\phi \\ a\psi + c\epsilon & b\psi + d\epsilon \end{bmatrix} - w^{-1}\begin{bmatrix} \varepsilon & \phi \\ \psi & \epsilon \end{bmatrix}\begin{bmatrix} e^2 & ef \\ ef & f^2 \end{bmatrix}\begin{bmatrix} \varepsilon & \phi \\ \psi & \epsilon \end{bmatrix}$$

$$= -\begin{bmatrix} q_1 & 0 \\ 0 & q_2 \end{bmatrix}$$

$$\begin{bmatrix} a\varepsilon + c\psi & a\phi + c\epsilon \\ b\varepsilon + d\psi & b\phi + d\epsilon \end{bmatrix} + \begin{bmatrix} a\varepsilon + c\phi & b\varepsilon + d\phi \\ a\psi + c\epsilon & b\psi + d\epsilon \end{bmatrix}$$

$$-w^{-1}\begin{bmatrix} e^2\varepsilon + ef\phi & ef\varepsilon + f^2\phi \\ e^2\psi + ef\epsilon & ef\psi + f^2\epsilon \end{bmatrix}\begin{bmatrix} \varepsilon & \phi \\ \psi & \epsilon \end{bmatrix} = -\begin{bmatrix} q_1 & 0 \\ 0 & q_2 \end{bmatrix}$$

$$\begin{bmatrix} a\varepsilon + c\psi & a\phi + c\epsilon \\ b\varepsilon + d\psi & b\phi + d\epsilon \end{bmatrix} + \begin{bmatrix} a\varepsilon + c\phi & b\varepsilon + d\phi \\ a\psi + c\epsilon & b\psi + d\epsilon \end{bmatrix}$$

$$-w^{-1}\begin{bmatrix} [e^2\varepsilon + ef\phi]\varepsilon + [ef\varepsilon + f^2\phi]\psi & [e^2\varepsilon + ef\phi]\phi + [ef\varepsilon + f^2\phi]\epsilon \\ [e^2\psi + ef\epsilon]\varepsilon + [ef\psi + f^2\epsilon]\psi & [e^2\psi + ef\epsilon]\phi + [ef\psi + f^2\epsilon]\epsilon \end{bmatrix}$$

$$= \begin{bmatrix} -q_1 & 0 \\ 0 & -q_2 \end{bmatrix}$$

$$\begin{cases} a\varepsilon + c\psi + a\varepsilon + c\phi - \dfrac{1}{w}([e^2\varepsilon + ef\phi]\varepsilon + [ef\varepsilon + f^2\phi]\psi) = -q_1 \\ a\phi + c\epsilon + b\varepsilon + d\phi - \dfrac{1}{w}([e^2\varepsilon + ef\phi]\phi + [ef\varepsilon + f^2\phi]\epsilon) = 0 \\ b\varepsilon + d\psi + a\psi + c\epsilon - \dfrac{1}{w}([e^2\psi + ef\epsilon]\varepsilon + [ef\psi + f^2\epsilon]\psi) = 0 \\ b\phi + d\epsilon + b\psi + d\epsilon - \dfrac{1}{w}([e^2\psi + ef\epsilon]\phi + [ef\psi + f^2\epsilon]\epsilon) = -q_2 \end{cases} \quad (3\text{-}26)$$

3.4.4 Simulation procedures

Based on the equation provided in previous section, numerical simulations of steady state cornering test were performed to justify that a control method based on a linear dynamic equation is unsuitable for a nonlinear vehicle model. The modelled small electric vehicle with oversteer characteristic was used as vehicle model. The simulation parameters are as follow:

Road Condition: Dry asphalt

Steering System: Four-wheel steering

Vehicle velocity V = 50 km/h and 10 km/h

Front steer angle $\theta_F = 10^0$(constant)

Steering initiate time t =10s.

Maximum time t_{max} = 40s

In the simulation, the vehicle will accelerate until it reaches the velocity of 50 km/h. Then, the vehicle will maintain a constant speed. The front wheels will initiate rotation $\theta_F = 10^0$ at t =10s as shown in figure 3-8. The simulation time length is 40s. The steady state yaw rotational speed, steady state side slip angle, wheel steer angle and trajectory during the steady state cornering test are recorded. The process was repeated for the velocity of 10 km/h. The difference in the velocity is to observe the effect under maximum high speed low speed cornering. The linear feedback control input is fed forward to the vehicle with nonlinear model

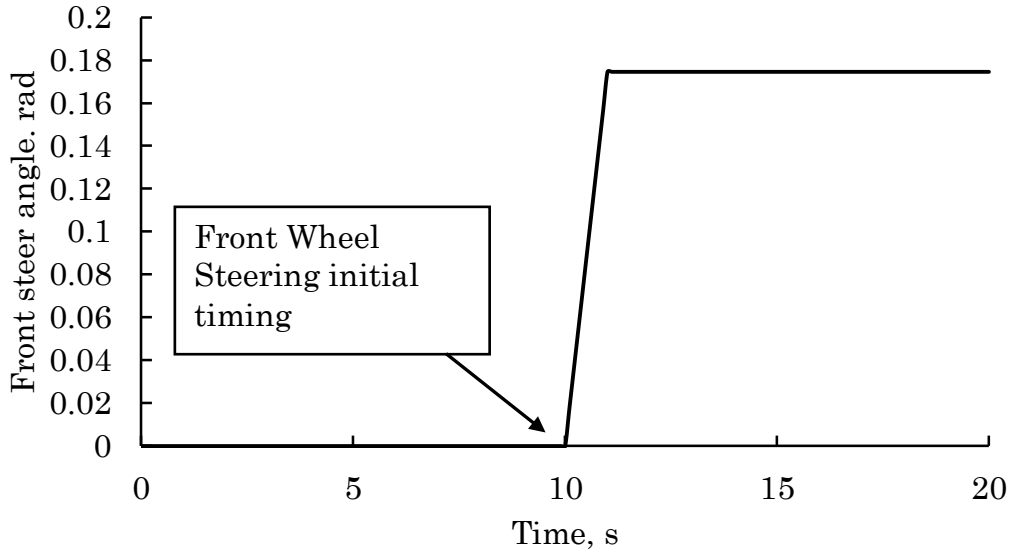

Figure 3-8 Front steer angle initiate timing

3.5 Feedback Control for Vehicle with Nonlinear Model

3.5.1 Error elimination

In order to use the state observer's linear feedback control, the error between outputs of both model has to be resolves. In conventional vehicles, there is no other method to measure the value of its side slip angle. However, yaw rotational speed of a vehicle can be calculated using gyro sensors.

The Figure 3-9 shows the renewed control method. the output of the vehicle model and the state observer was compared to form a close loop system. In general, there is no other method to direct measure the output of side slip angle. However, yaw rotational speed of a vehicle can be calculated with gyro sensors. In this system, the estimated yaw rotational speed output of state observer unit and the measured yaw rotational speed output of the vehicle model are compared and multiplied by high gain *H*. Then, this gain is fed back into the linear model. The linearized differential equation of equation (3-21) becomes,

$$\dot{\hat{\mathrm{x}}} = \mathrm{Ax} + \mathrm{BU}_r + \mathrm{CU}_f + H\tilde{r}$$

$$\tilde{r} = \gamma - \gamma^* = \mathbb{C}_2{}^T\hat{\mathrm{x}} - \mathbb{C}_2{}^T\mathrm{x}$$

$$= \mathbb{C}_2{}^T(\hat{\mathrm{x}} - \mathrm{x}) \qquad (3\text{-}27)$$

The renewed state observer control input can also be redefined as follow;

$$\mathrm{U}_r = -\frac{1}{r}B^T P(\hat{\mathrm{x}} - \mathrm{x}) + \theta_R \qquad (3\text{-}28)$$

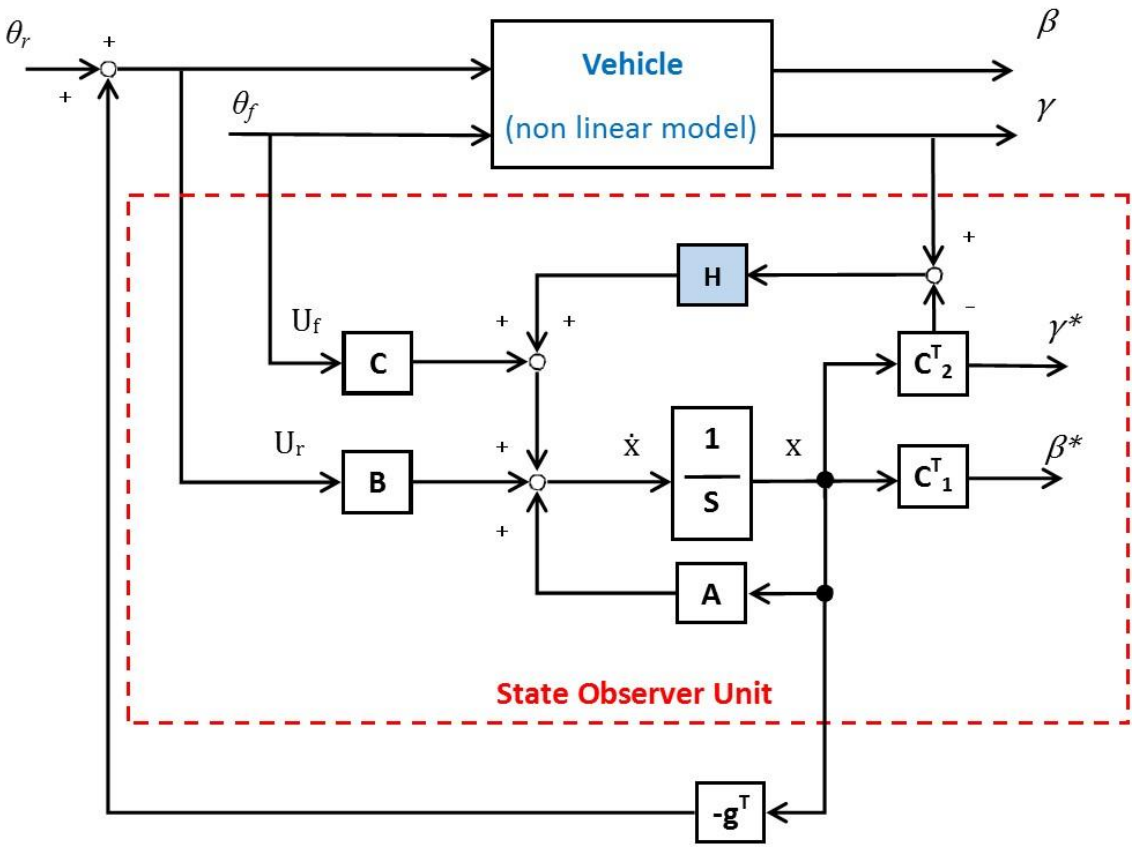

Figure 3-9 Simulation block of a feedback control for vehicle with nonlinear model

3.5.2 Simulation procedure

Numerical simulations of steady state cornering test were performed to examine the improvement of the feed forward control system on nonlinear vehicle model with yaw rotational speed error elimination. The modelled small electric vehicle with oversteer characteristic was used as vehicle model. The simulation parameters are as follow:

Road Condition: Dry asphalt

Steering System: Four-wheel steering

Vehicle velocity V = 50 km/h and 10 km/h

Front steer angle $\theta_F = 10^0$(constant)

Steering initiate time t =10s.

Maximum time t_{max} = 40s

In the simulation, the vehicle will accelerate until it reaches the velocity of 50 km/h. Then, the vehicle will maintain a constant speed. The front wheels will initiate rotation $\theta_F = 10^0$ at t =10s. The simulation time length is 40s. The steady state yaw rotational speed, steady state side slip angle, wheel steer angle and trajectory during the steady state cornering test are recorded. The process was repeated for the velocity of 10 km/h. The results of feedforward control (FFC) are compared with the renewed feedback control (FBC) for vehicle with nonlinear model.

3.6 Overall Steering Characteristic of 4WDIS Small Electric Vehicle

Linear feedback control can be feed forward to the vehicle nonlinear model with an error elimination of the output of both systems. Lastly, we have to examine the steer characteristic of the system.

3.6.1 Simulation procedure

Numerical simulations of steady state cornering test were performed to examine the overall steering characteristic of the modelled over steer small electric vehicle with yaw moment control by four-wheel drive and independent steering.

Road Condition: Dry asphalt

Steering System: Four-wheel steering

Vehicle velocity V = 50 km/h and 10 km/h

Front steer angle $\theta_F = 10^0$(constant)

Steering initiate time t =10s.

Maximum time t_{max} = 40s

In the simulation, the vehicle will accelerate until it reaches the desired velocity. Then, the vehicle will maintain a constant speed. The front wheels will initiate rotation $\theta_F = 10^0$ at t =10s. The simulation time length is 40s. The steady state yaw rotational speed, steady state side slip angle and wheel steer angle during the steady state cornering test are recorded. The process was repeated for each velocity. The results are compared with the previous results of steady state cornering by two-wheel steering.

3.7 Simulation Result and Discussion

3.7.1 Feedforward control for vehicle with nonlinear model

In this first part, we will discuss the result of steady state cornering at 50km/h. Figure 3-10 shows the front steer angle from the driver input 10 (deg), which is equivalent to 0.175 (rad), and the rear steer angle fed forward from state observer unit during the steady state cornering at 50 (km/h). Figure 3-11 shows the result of the trajectory during the steady state cornering at 50 (km/h) in regard to constant front steer angle. Figure 3-12 and Figure 3-13 show the output results of the steady state yaw rotational speed and steady state side slip angle during this steady state cornering simulation.

In figure 3-10, the black line represents front steer angle and the red dash line represent rear steer angle. During steady state cornering at 50 km/h in regards to 10 (deg) front steer input. In order to maintain stability, the state observer generated a positive steer angle at the rear wheels as a control input. The positive value indicates that the rear wheels steered in anti-clockwise direction that is similar direction to the front wheels. This value is fed forward to the vehicle with nonlinear model.

In regards to same velocity and steer angle input, we could clearly see the difference in the results of trajectory, yaw rotational speed and side slip angle. The red line represent State observer and blue line represent vehicle with nonlinear model. In the trajectory result, the vehicle with nonlinear model shows a wider cornering radius in compassion to state observer that produce a sharper turning. The trajectory of the state observer is an approximation calculation based on the output. The variation of the trajectory is caused by the output of both vehicle and state observer. In Figure 3-11, the vehicle has a lower steady state yaw rotational speed than the output of state observer. On the other hand, the steady state side slip angle of the vehicle in Figure 3-12 also shows a higher value than the output of state observer.

We can conclude that the state observer generated the rear steer angle based on the yaw rotational speed and side slip angle calculated by linear dynamic equation. The low output values gave a low control input which was insufficient for the vehicle with nonlinear model.

Next, we will discuss the result of steady state cornering at 10km/h.

Figure 3-14 shows the front steer angle from the driver input 10 (deg) and the rear steer angle fed forward from state observer unit during the steady state cornering at

10 (km/h). Figure 3-15 shows the result of the trajectory during the steady state cornering at 10 (km/h) in regard to constant front steer angle. Figure 3-16 and Figure 3-17 show the output results of the steady state yaw rotational speed and steady state side slip angle during this steady state cornering simulation.

In figure 3-14, the black line represents front steer angle and the red dash line represent rear steer angle. In contrast to the cornering at 50 (km/h), during steady state cornering at 10 km/h in regards to 10 (deg) front steer input, the state observer generated a negative steer angle at the rear wheels. The negative value indicates that the rear wheels steered in clockwise direction that is opposite to the front wheel. This value is fed forward to the vehicle with nonlinear model.

The red line represent State observer and blue line represent vehicle with nonlinear model. In this low speed cornering, the end result is reverse than the results of the previous high speed steady state cornering. The vehicle with nonlinear model shows a tighter cornering radius in compassion to state observer. This is due to the fed forward control input that was excessive giving higher yaw rotational speed and side slip angle in an absolute magnitude.

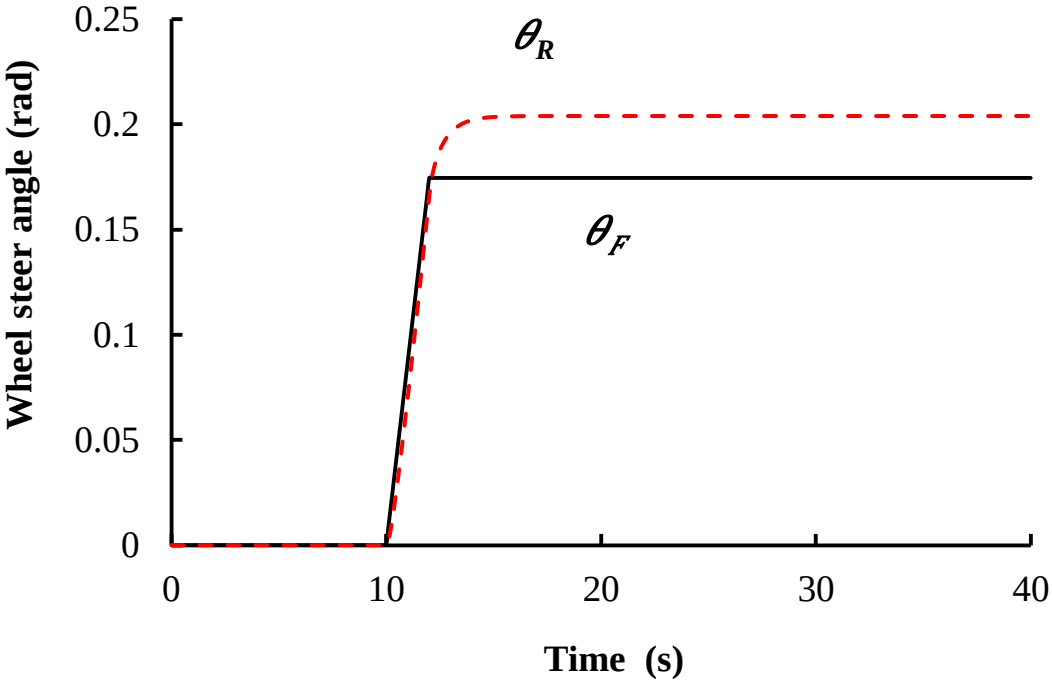

Figure 3-10 the front steer angle from the driver input and the rear steer angle

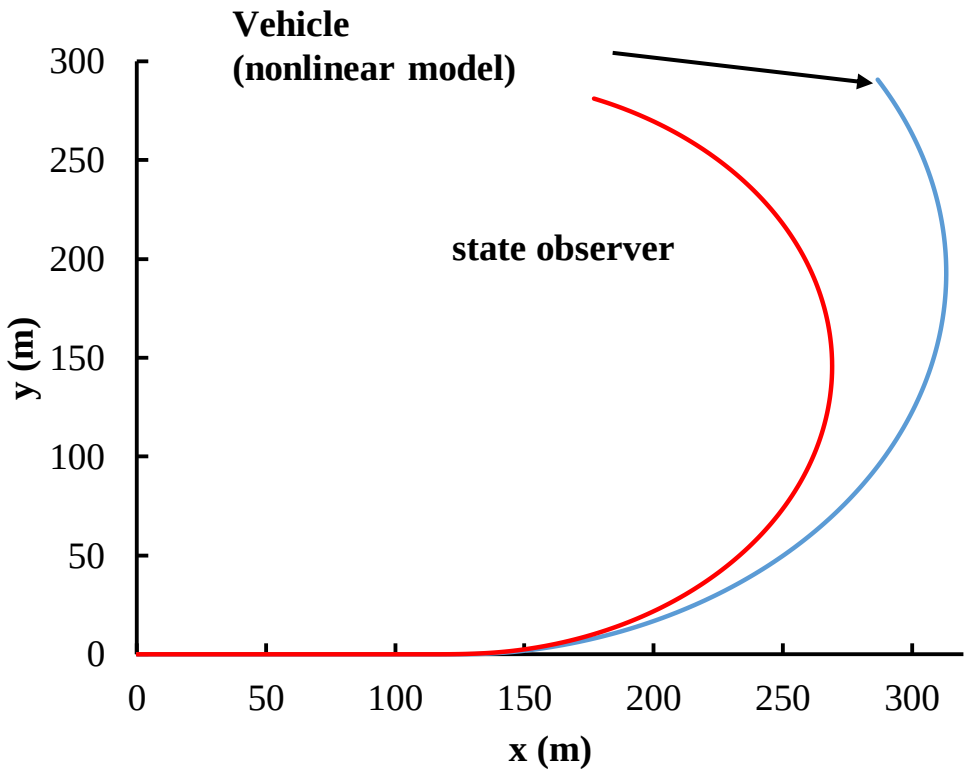

Figure 3-11 the trajectory during the steady state cornering

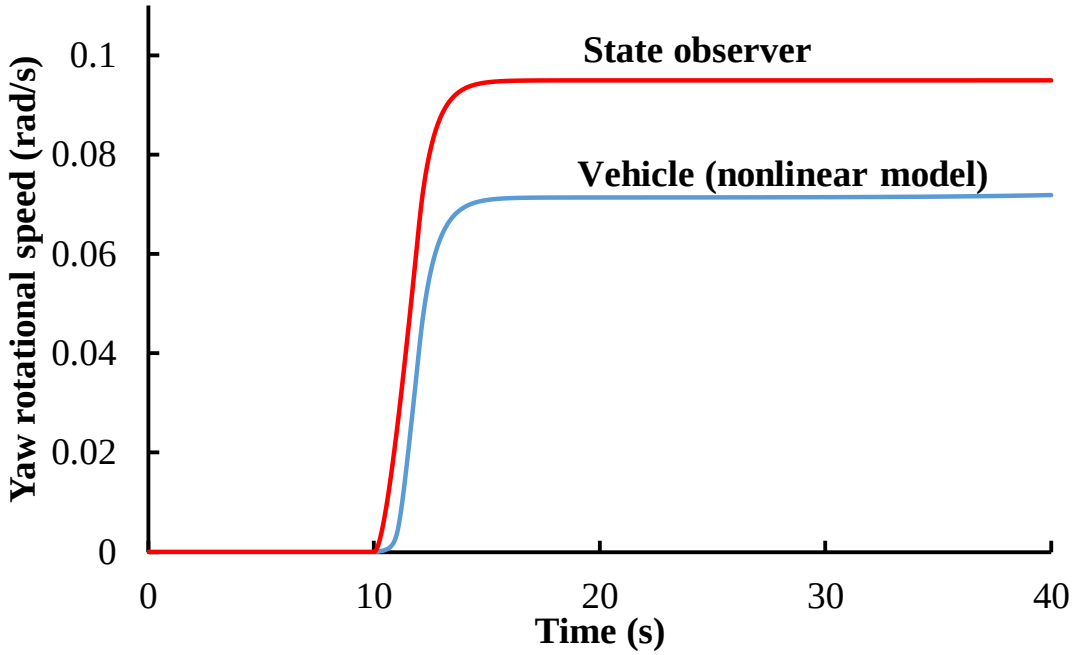

Figure 3-12 the output results of the steady state yaw rotational speed during this steady state cornering

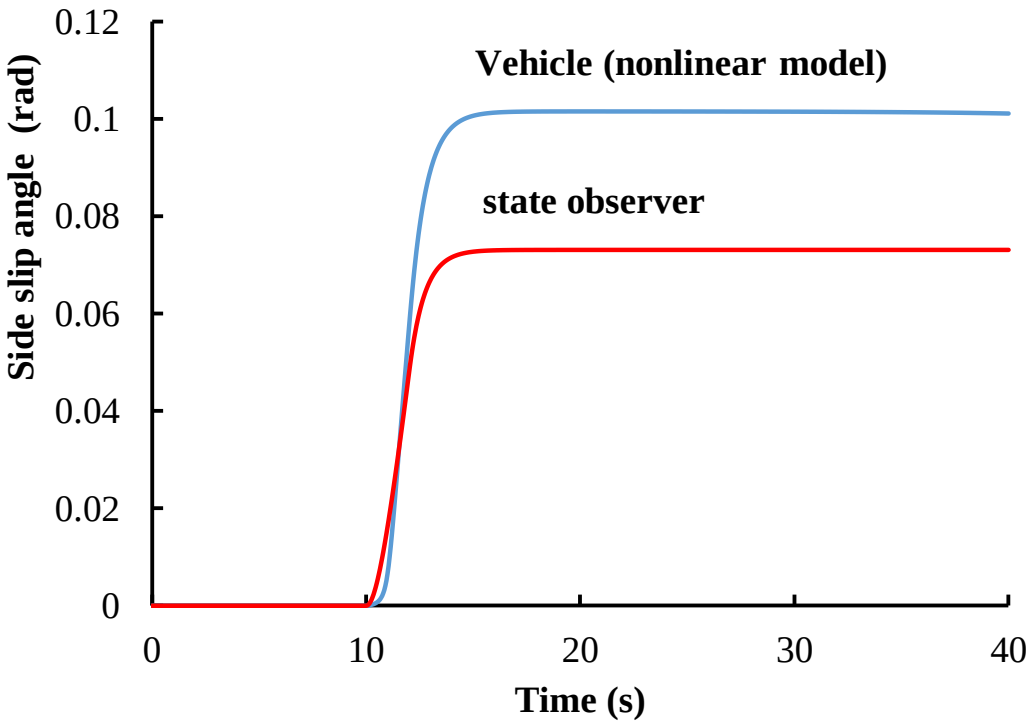

Figure 3-13 the output results of the steady state side slip angle during this steady state cornering

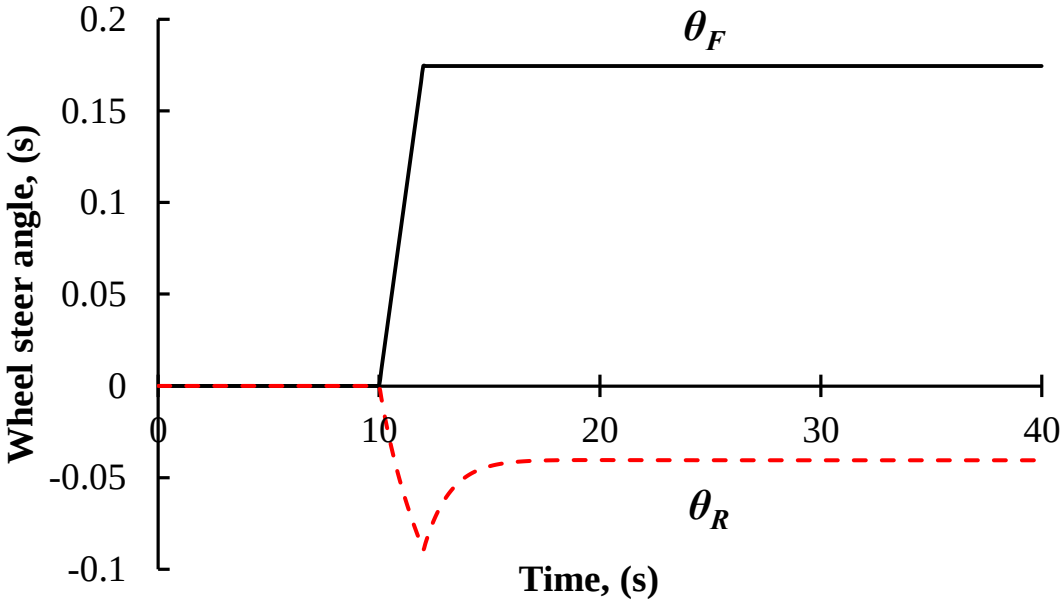

Figure 3-14 the front steer angle from the driver input 10 (deg) and the rear steer angle fed forward from state observer unit

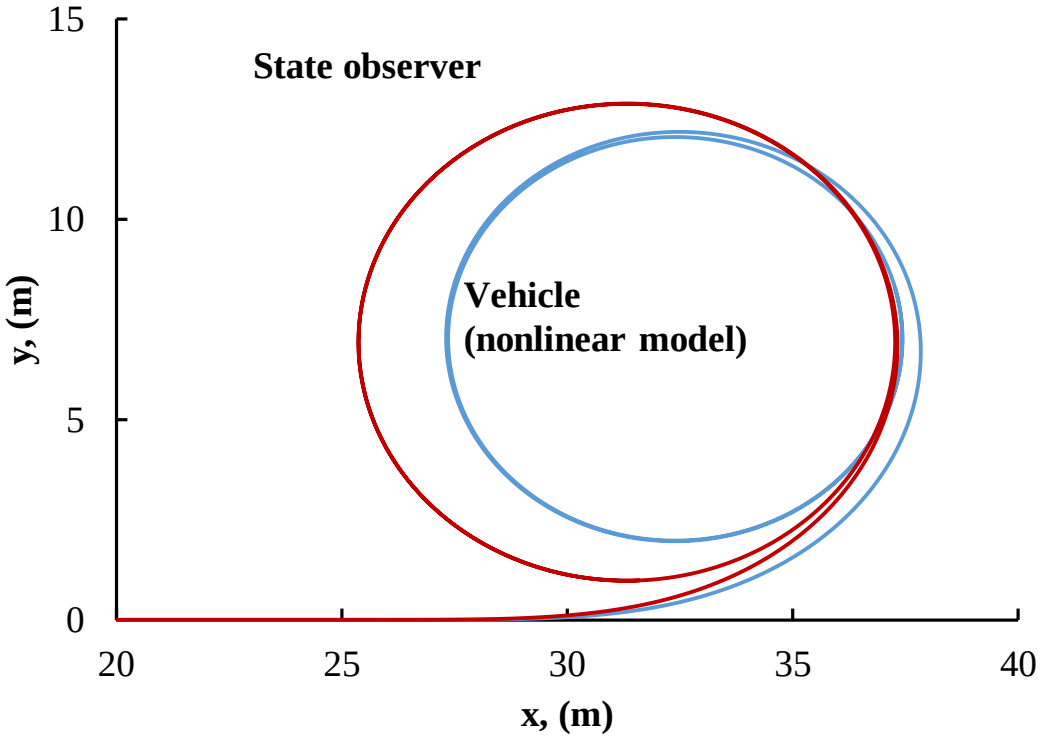

Figure 3-15 the trajectory during the steady state cornering at 10 (km/h)

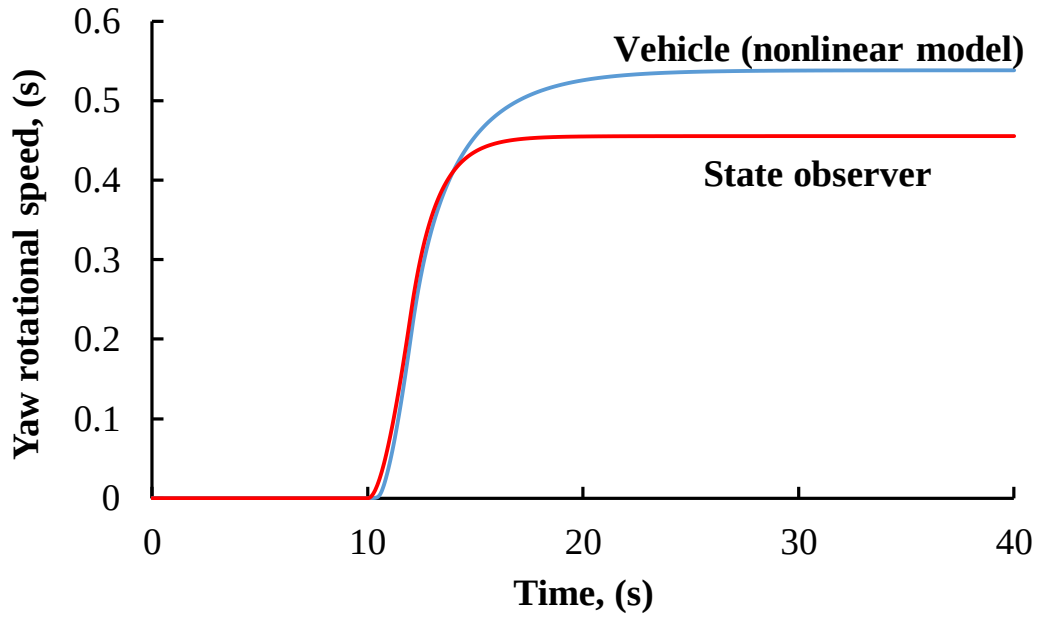

Figure 3-16 the output results of the steady state yaw rotational speed during this steady state cornering

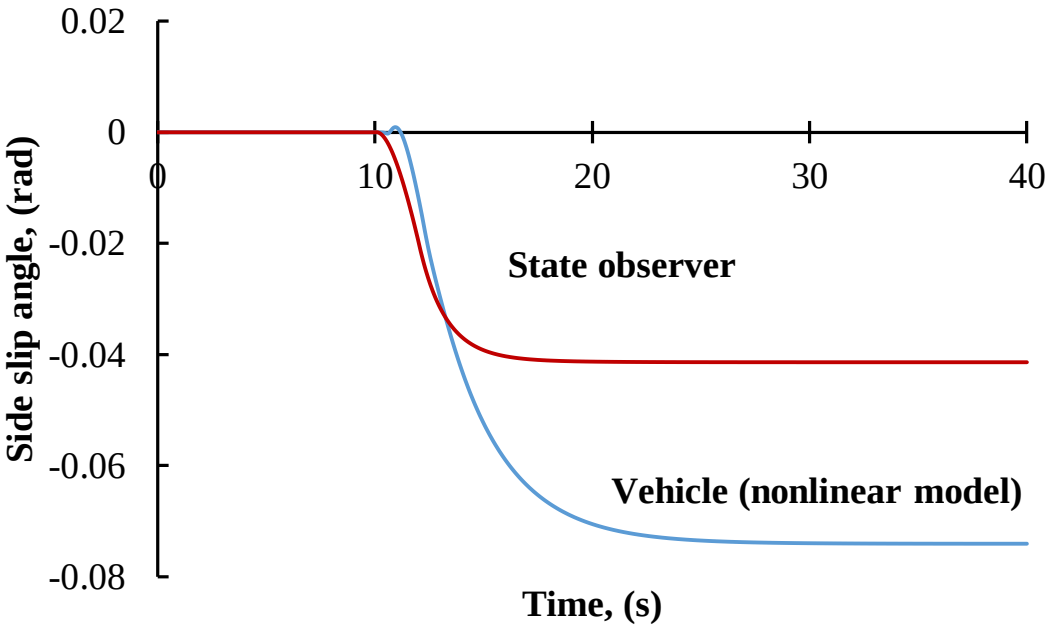

Figure 3-17 the output results of the steady state side slip angle during this steady state cornering

3.7.2 Feedback control for nonlinear vehicle model

In order to use the state observer's linear feedback control, the error between outputs of vehicle model and state observer has to be reduced. The side slip angle of a vehicle can't be measured. However, yaw rotational speed of a vehicle can be calculated using gyro sensors. The estimated yaw rotational speed of the state observer unit and the measured yaw rotational speed of the vehicle nonlinear model are compared and multiplied by high gain, fed back to the linear model to produce a rectified control input and lastly fed back to the vehicle model. The previous results of feedforward control (FFC) for vehicle with nonlinear model are compared with the renewed feedback control (FBC).

In this first part, we will discuss the result of steady state cornering at 50km/h by FFC and FBC system. Figure 3-18 shows the front steer angle from the driver input 10 (deg), and the rear steer angle from FFC and FBC during the steady state cornering at 50 (km/h). Figure 3-19 shows the result of the FFC and FBC trajectory during the steady state cornering at 50 (km/h) in regard to constant front steer angle. Figure 3-20 and Figure 3-21 show the output results of the steady state yaw rotational speed and steady state side slip angle by FFC and FBC during this steady state cornering simulation.

In figure 3-18, the black line represents front steer angle. While, the red solid and dash lines represent rear steer angle with FFC and FBC, respectively. During steady state cornering, the state observer with FBC generated a slightly higher steer angle at the rear wheels than the FFC. A few second delay from the front wheel steer initial time can be observed at the rear steer angle with FBC. However, the rear steer angle increased instantly when it initiated.

Due to this, we could see progress from the previous result at the trajectory, yaw rotational speed and side slip angle. The solid blue and red lines represent vehicle and state observer with FBC while dash blue and red line represents vehicle and state observer with FFC. In the trajectory result, the trajectory of the vehicle is similar to the state observer after FBC is applied. The slight increase of the rear steer angle caused the steady state yaw rotational speed to increase considerably and lower the steady state side slip angle of the vehicle with FBC. However, the changes of the state observer output when FBC was applied are small and can be considered insignificant.

Next, we will discuss the result of steady state cornering at 10km/h by FFC and

FBC system. Figure 3-22 shows the front steer angle from the driver input 10 (deg), and the rear steer angle from FFC and FBC during the steady state cornering at 10 (km/h). Figure 3-23 shows the result of the FFC and FBC trajectory during the steady state cornering at 50 (km/h) in regard to constant front steer angle. Figure 3-24 and Figure 3-25 show the output results of the steady state yaw rotational speed and steady state side slip angle by FFC and FBC during this steady state cornering simulation.

In figure 3-22, the black line represents front steer angle. While, the red solid and dash lines represent rear steer angle with FFC and FBC, respectively. A few second after the rear steer angle initiate, the angle increase in negative value for both FFC and FBC. However, when the rear steer angle started to decreased, the state observer with FBC generated a lower steer angle in the negative value at the rear wheels in comparison to the FFC.

Unlike the steady state cornering at high speed, the FBC has an impact on output of both vehicle model and state observer. In Figure 3-23, the trajectory of vehicle and state observer with FBC is identical and are present in between the trajectory of previous vehicle and state observer with FFC. The same occurrence can be observed for the steady state yaw rotational speed and steady state side slip angle which the output exists in between the previous output of vehicle and state observer with FFC. Furthermore, in this FBC system, only the error of yaw rotational speed was eliminated. Thus, the steady state side slip angle had a small variation. This small error merely effected the face of direction of the vehicle. Nonetheless, the outcome trajectory of the vehicle and state observer are the same.

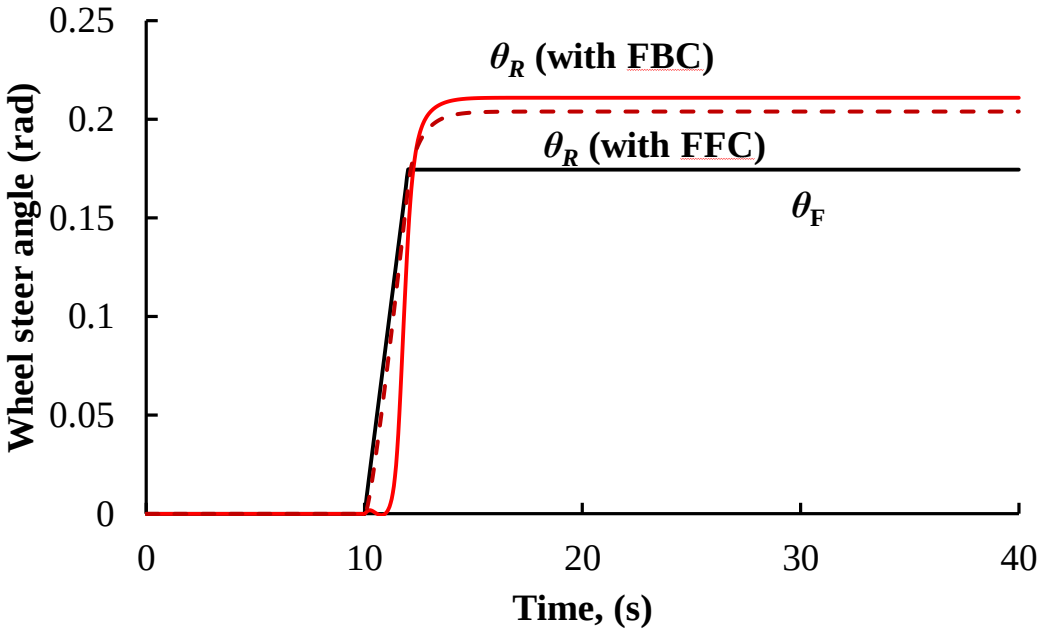

Figure 3-18 the front steer angle from the driver input 10 (deg), and the rear steer angle from FFC and FBC during the steady state cornering at 50 (km/h)

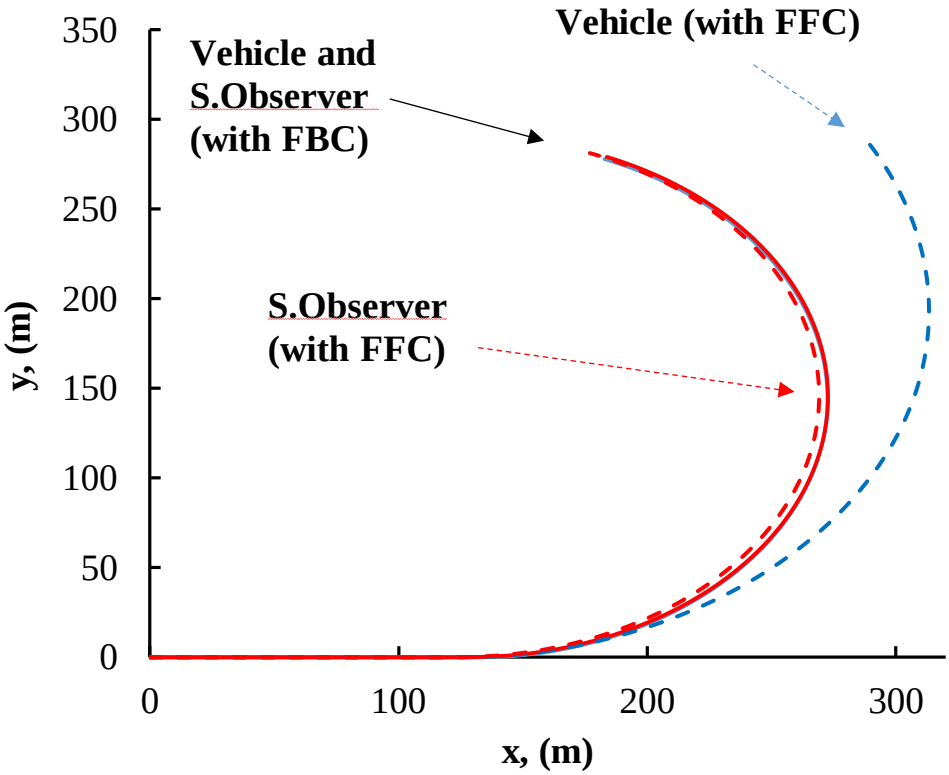

Figure 3-19 the FFC and FBC trajectory during the steady state cornering at 50 (km/h)

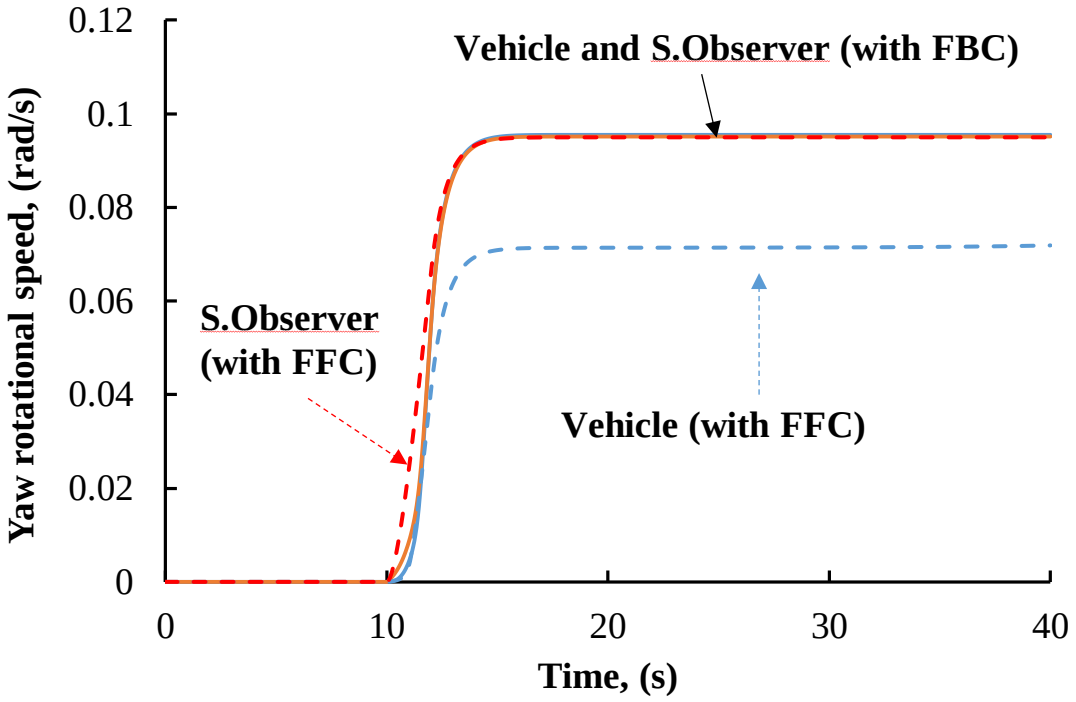

Figure 3-20 the steady state yaw rotational speed by FFC and FBC during steady state cornering at 50km/h

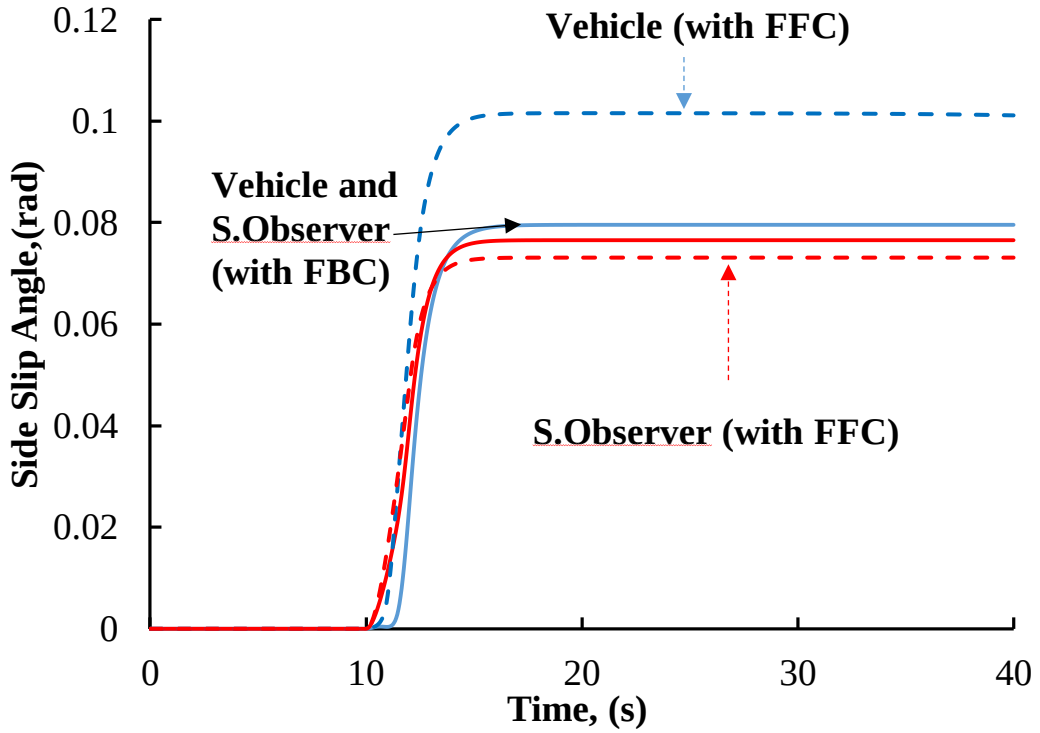

Figure 3-21 the steady state side slip angle by FFC and FBC during steady state cornering simulation at 50km/h

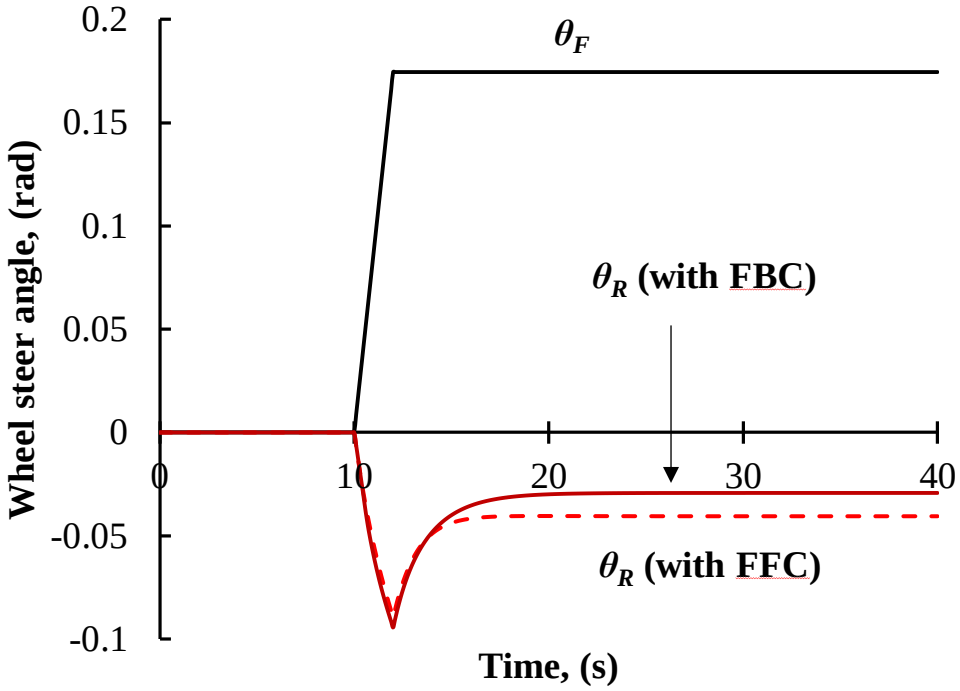

Figure 3-22 the front steer angle from the driver input 10 (deg), and the rear steer angle from FFC and FBC during the steady state cornering at 10 (km/h)

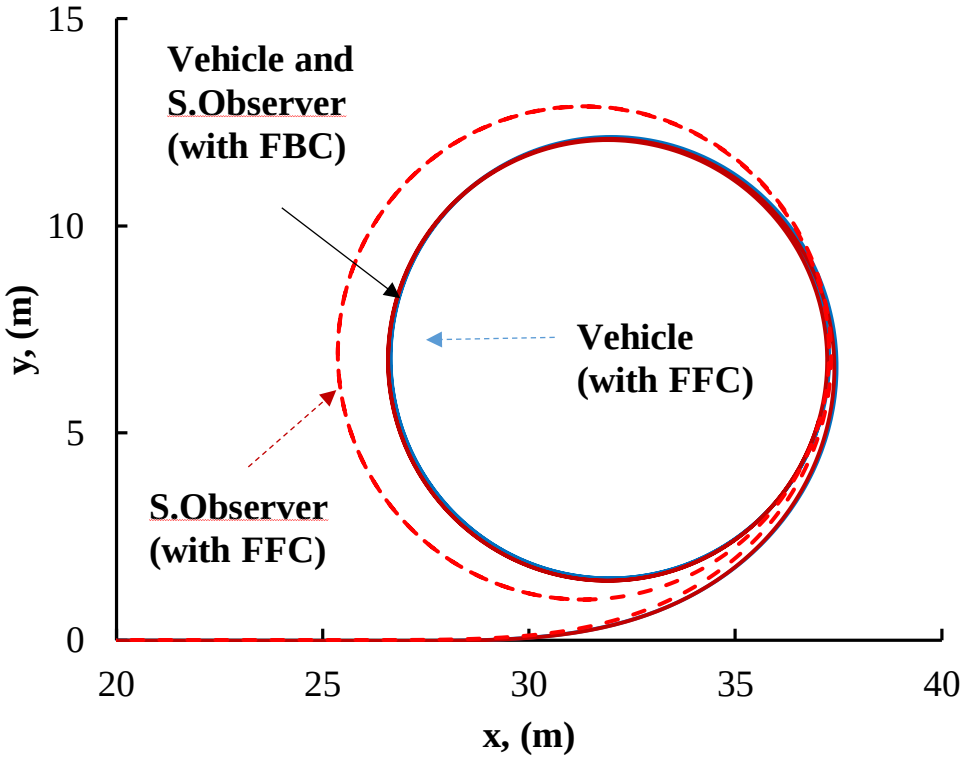

Figure 3-23 the FFC and FBC trajectory during the steady state cornering at 10 (km/h)

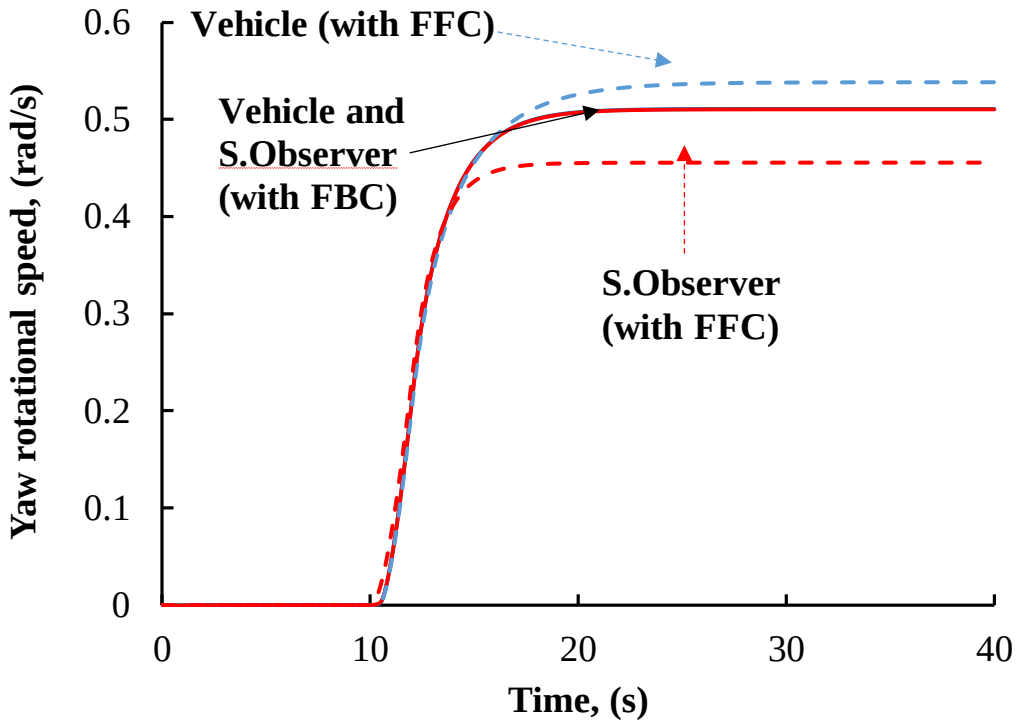

Figure 3-24 the steady state yaw rotational speed by FFC and FBC during steady state cornering at 10km/h

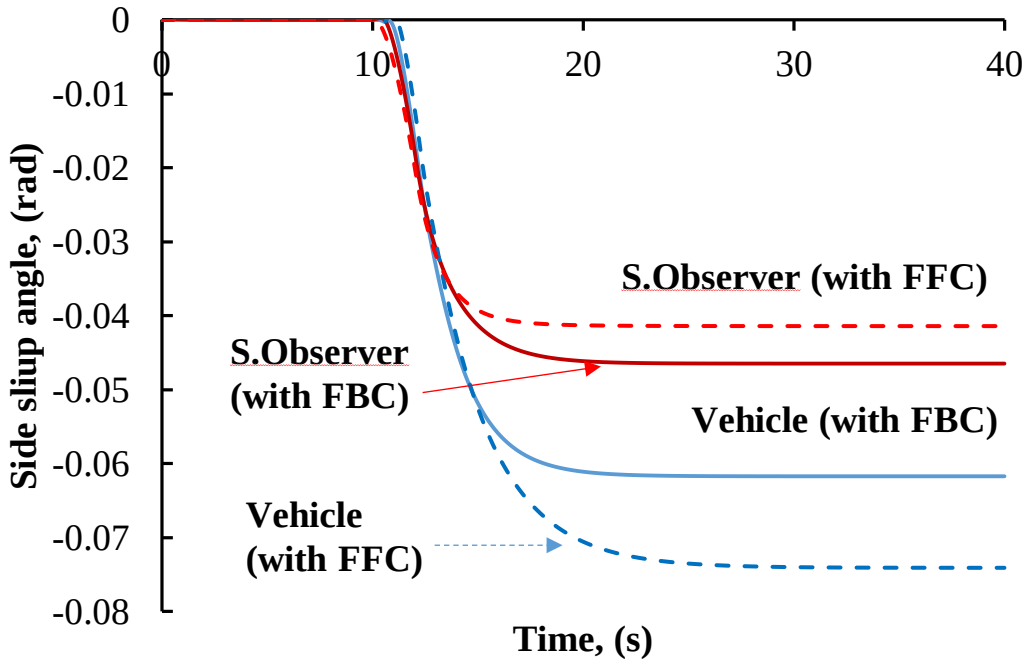

Figure 3-25 the steady state side slip angle by FFC and FBC during steady state cornering simulation at 10km/h

3.7.3 Overall Steering Characteristic of OS Small Electric Vehicle with 4WDIS

The stability limit velocity of the modelled OS in-wheel small EV has been determined in the chapter 2. In this chapter, we implemented 4WDIS onto the vehicle as a yaw moment control. The previous steady state cornering simulation condition in chapter 2 is repeated again. In order to have a deep understanding, the discussion is separated between the stability regions.

In this first section, the control effect of the 4WDIS on an OS in-wheel small EV during steady state cornering over the stability limit velocity in regards to constant front steer angle 10^{o} is investigated. Figure 3-26 shows the result of the steady state yaw rotational speed for the vehicle model with 4WDIS. From this figure, the yaw rotational speed decreased as the velocity of the vehicle model increased. However, if we observe closely, the time to produce a constant steady state yaw rotational speed is instantaneous, especially at velocity range of 30 km/h to 50 km/h. The results of steady state side-slip angle for this simulation in Figure 3-27 shows a reverse pattern from the yaw rotational speed. The side-slip angle increased as the velocity of the vehicle model increased. Based on these results, we can assume that the 4WDIS control input suppressed the output of yaw rotational speed and side slip angle considerably as the velocity of the vehicle model increased.

In order to understand the control method of the 4WDIS, we have to examine the input of the system. Figure 3-28 shows the rear wheel steering angle during the steady state cornering simulation of the 4WDIS vehicle model. In the first few second after the front wheel steering angle initiated, a rear wheel steering angle in minus value was generated that gave the instantaneous yaw rotational speed mention before. The minus angle of the rear wheel was smaller as the steady state velocity increased because the excess yaw rotational speed produce by OS vehicle model also increased. As time progressed, the rear wheel steer angle was increased to counter the excess yaw rotational speed and maintain a constant value. The angle of the rear wheel is larger at the velocity range over 15 km/h which proofs our early assumption was correct. Based on these results, an OS in-wheel small EV can achieve a stable steady state cornering even when the velocity is over the stability limit velocity with the implementation of 4WDIS.

Theoretically, OS vehicles can already produce high yaw rotational speed and stability when cornering below the stability limit velocity. Logically, any control system is unnecessary in the stable region. Based on the previous result of 2WS in chapter 2, we can assume that the cornering performance in the stable region of the OS in-wheel small EV will be suppressed in the presents of the 4WDIS.

In this section, the control effect of 4WDIS implementation onto an OS in-wheel small EV during steady state cornering below the stability limit velocity in regards to constant front steer angle 10^{o} is presented. Figure 3-29 and figure 3-30 show the results of the steady state yaw rotational speed and steady state side-slip angle for the vehicle model with 4WDIS, respectively. The average time for the yaw rotational speed to reach constant value was also reduced to 25s in comparison to the 2WS vehicle model. The 4WDIS had increased the steering response time in regards to the front wheel steer input initiated at t=10s. Even with high yaw rotational speed, the steady state side slip angle also remains constant.

For better comparison, the relation between steady state yaw rotational speed and steady state side-slip angle to the velocity of the vehicle model with 4WDIS and 2WS were plotted in Figure 3-31 and Figure 3-32. The steady state yaw rotational speed of the vehicle model with 4WDIS was approximately two folds the value of vehicle model with normal 2WS at velocity of 0 to 10 km/h. When the velocity of the vehicle increased from 10 km/h to 15 km/h, the steady state yaw rotational speed gradually decreased. A similar pattern occurred for the side-slip angle when we observe in absolute magnitude value.

In order to comprehend these matters, we have to examine the input of the control system. Figure 3-33 shows the rear wheel steering angle during the steady state cornering of the 4WDIS vehicle model. As soon as the front wheel steer initiated at t=10s, the rear wheel steer at the opposite direction as the front wheel. Unlike the situation in the unstable region, the rear wheel steering angle maintained an opposite angle as the front wheel which boost the yaw rotational speed. As the velocity approach near the stability limit, the outputs need to be suppressed.

In order to conclude the overall steer characteristic of the OS small electric vehicle with 4WDIS during steady state cornering in regards to front steer angle 10 (deg), Figure 3-34 shows the relationship of steady state yaw rotational speed and velocity while Figure 3-35 shows the relationship of steady state side slip angle and velocity in comparison to

the conventional 2WS vehicle. On the other hand, Figure 3-36 shows the relationship of the output rear wheel steer angle and velocity in regards to front steer angle 10 (deg).

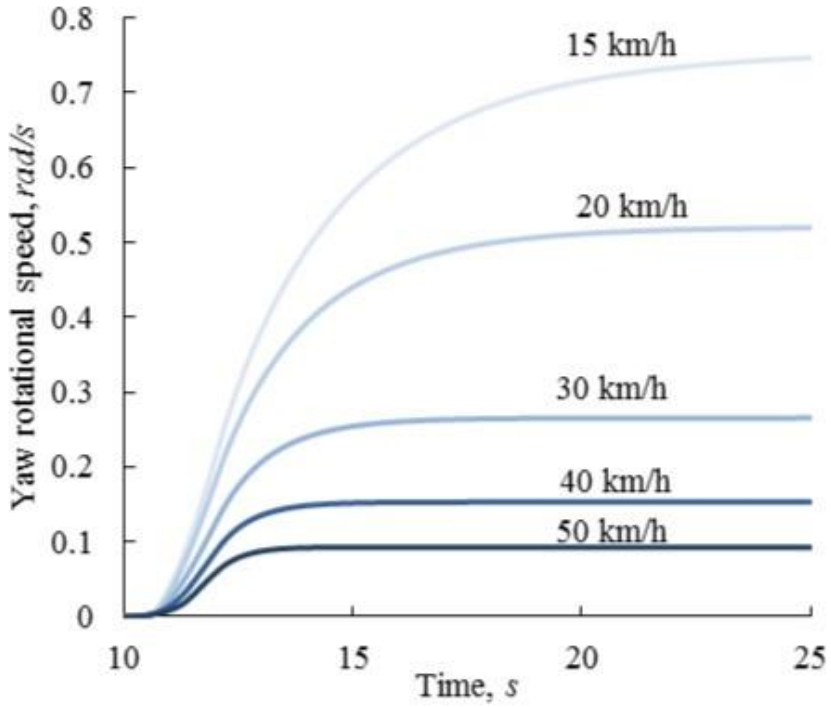

Figure 3-26 Change of time for steady state yaw rotational speed during cornering above stability limit velocity with 4WDIS

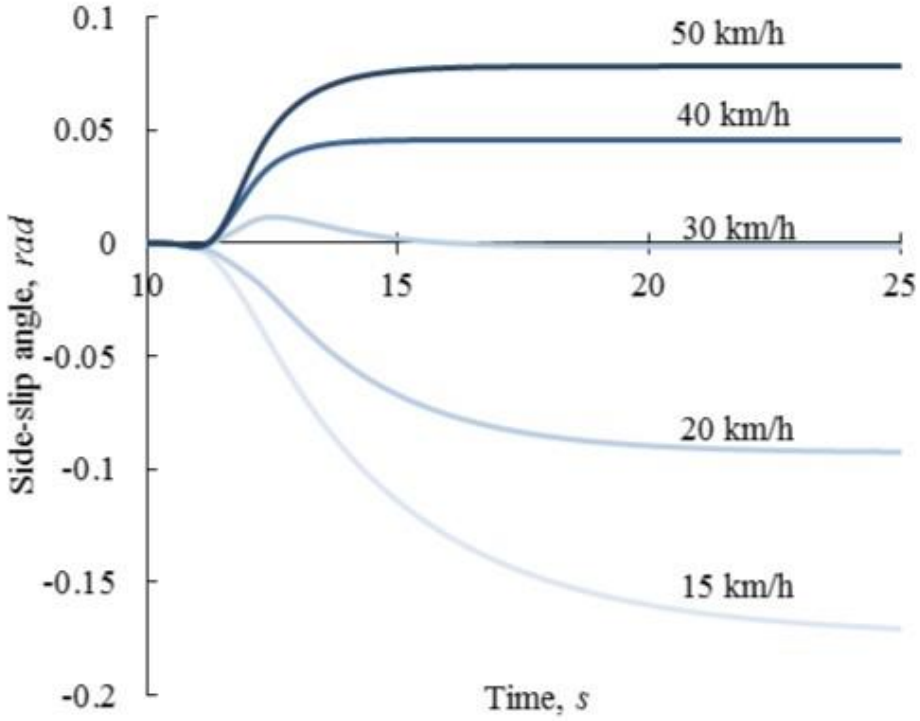

Figure 3-27 Change of time for steady state side slip angle during cornering above stability limit velocity with 4WDIS

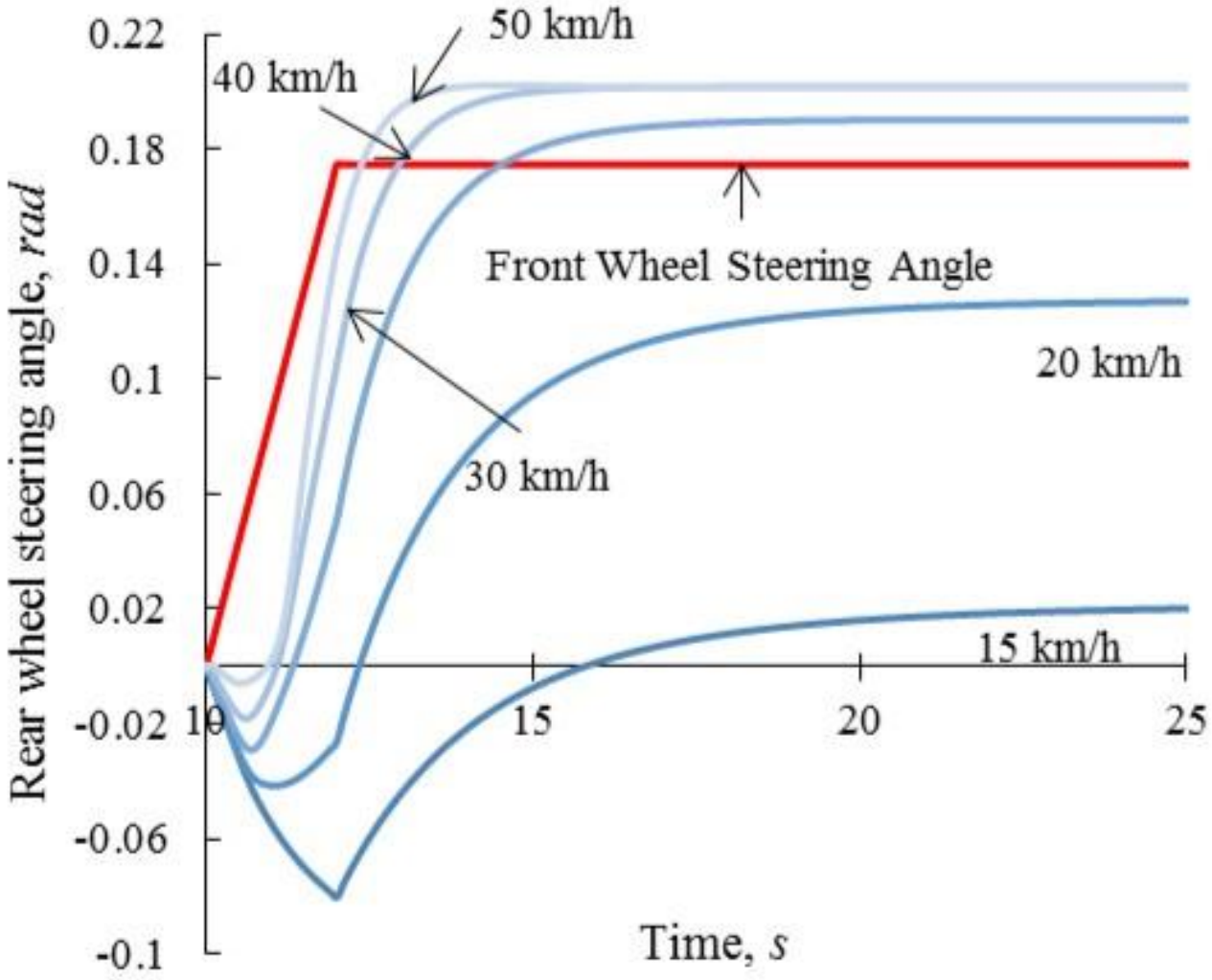

Figure 3- 28 Front and rear wheel steer angle during cornering above stability limit velocity with 4WDIS

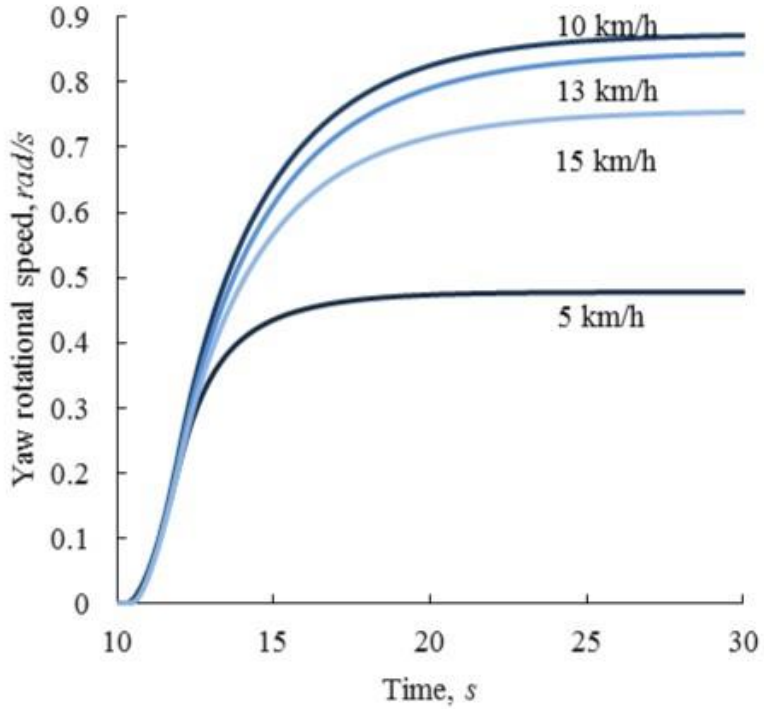

Figure 3-29 Change of time for steady state yaw rotational speed during cornering above stability limit velocity with 4WDIS

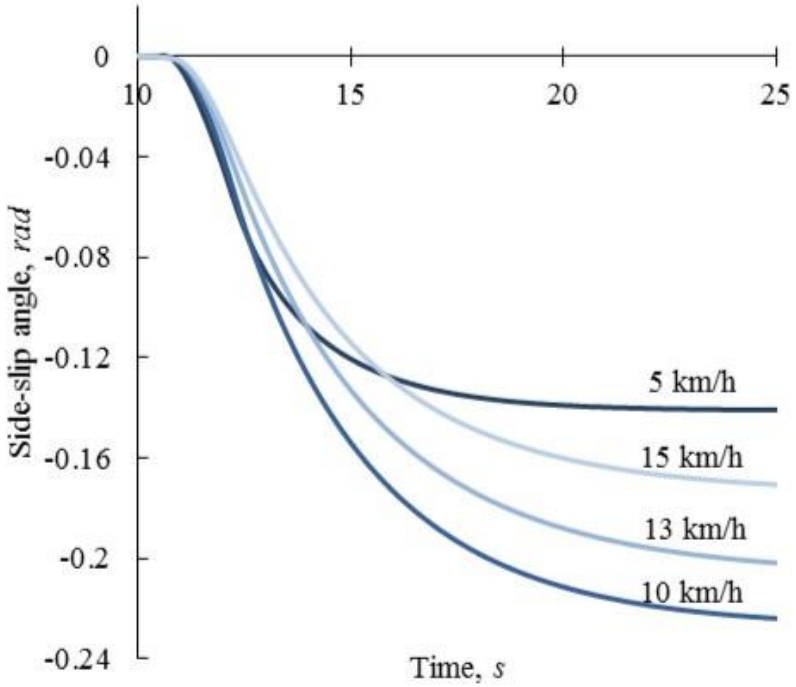

Figure 3-30 Change of time for steady state side slip angle during cornering above stability limit velocity with 4WDIS

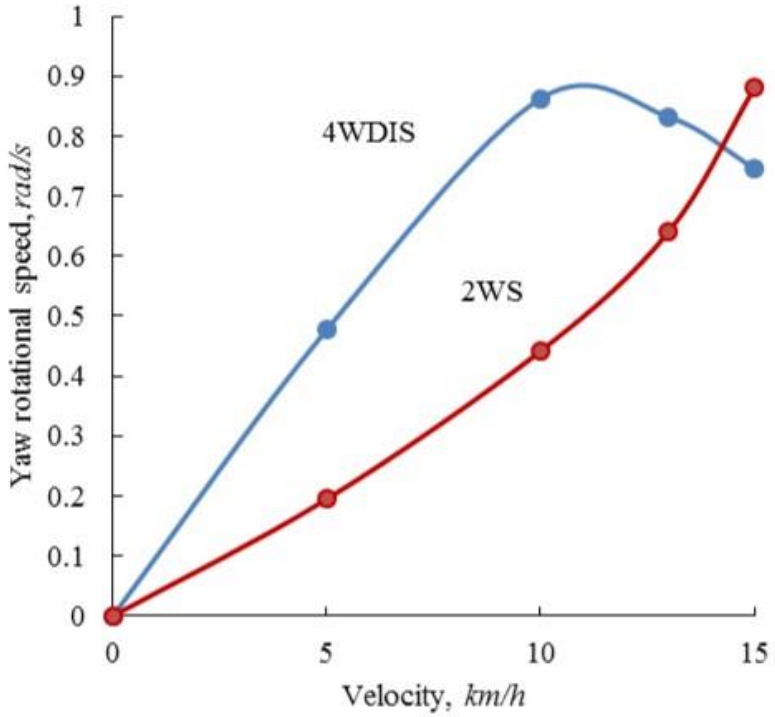

Figure 3-31 Comparison of the steady state yaw rotational speed to velocity during cornering below stability velocity limit for 4WDIS and 2WS

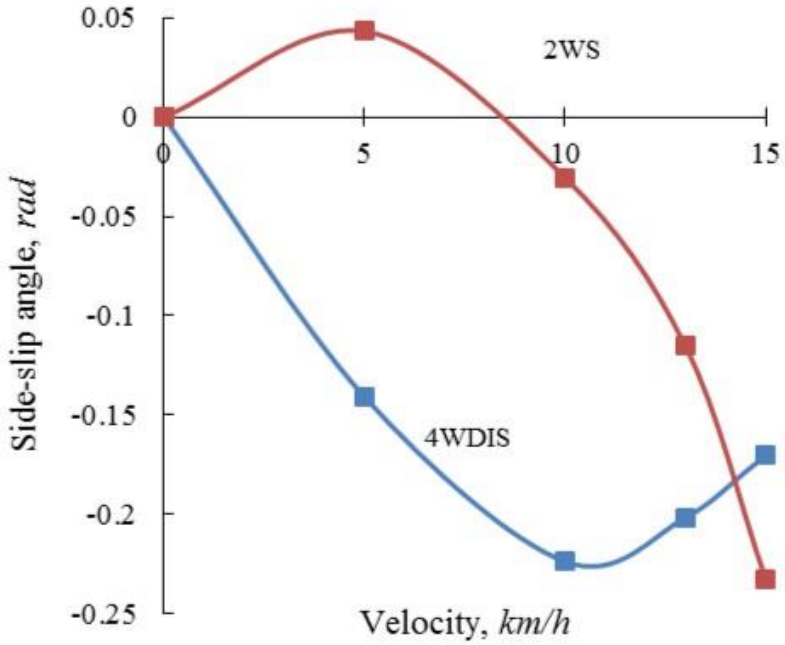

Figure 3-32 Comparison of the steady state side slip angle to velocity during cornering below stability velocity limit for 4WDIS and 2WS

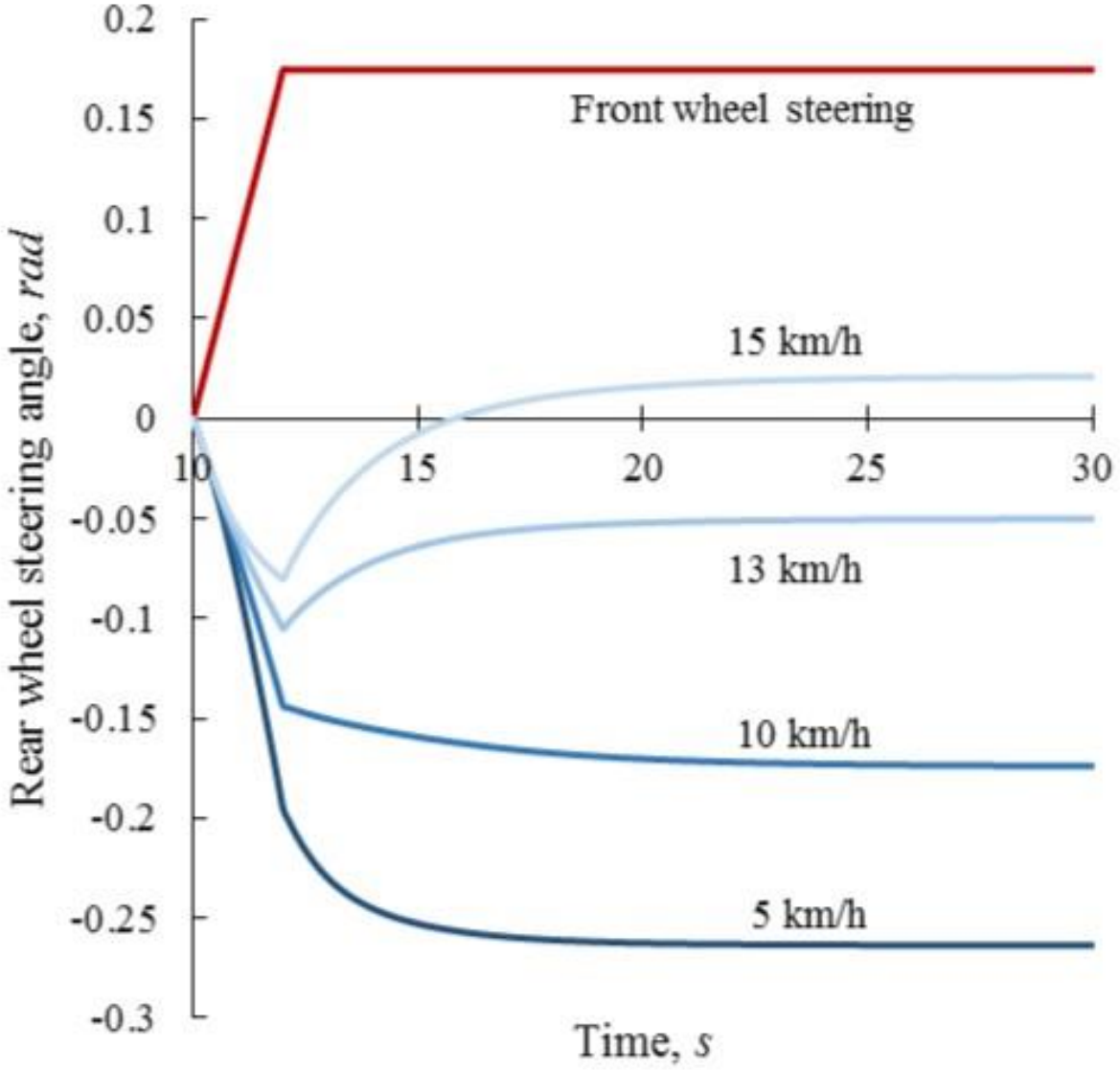

Figure 3- 33 Front and rear wheel steer angle during cornering below stability limit velocity with 4WDIS

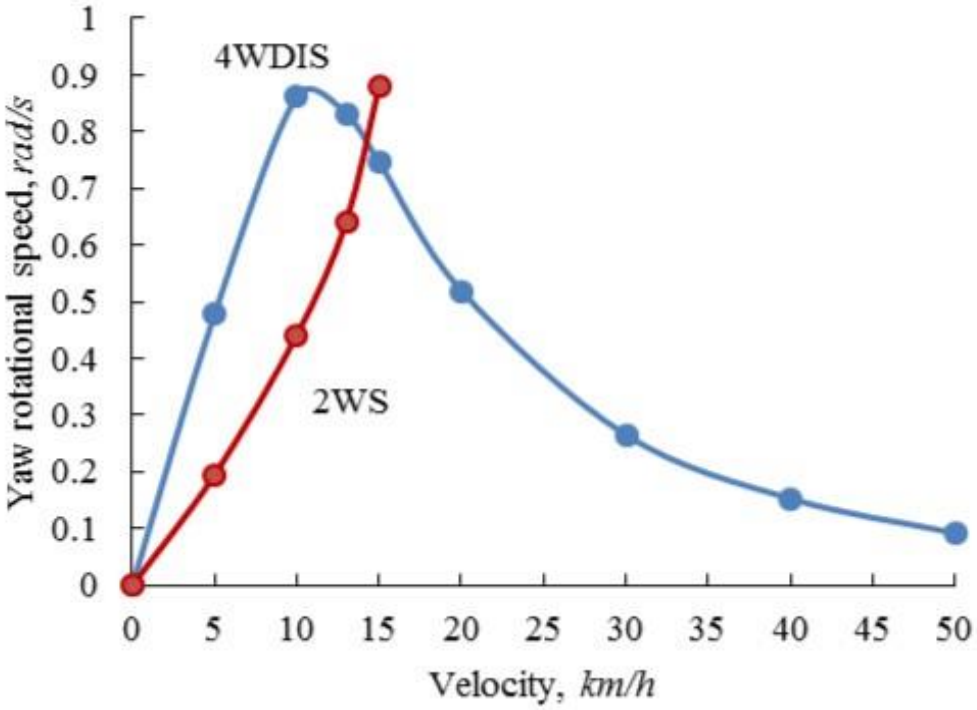

Figure 3-34 The overall steady state yaw rotational speed to velocity for 4WDIS in comparison to 2WS

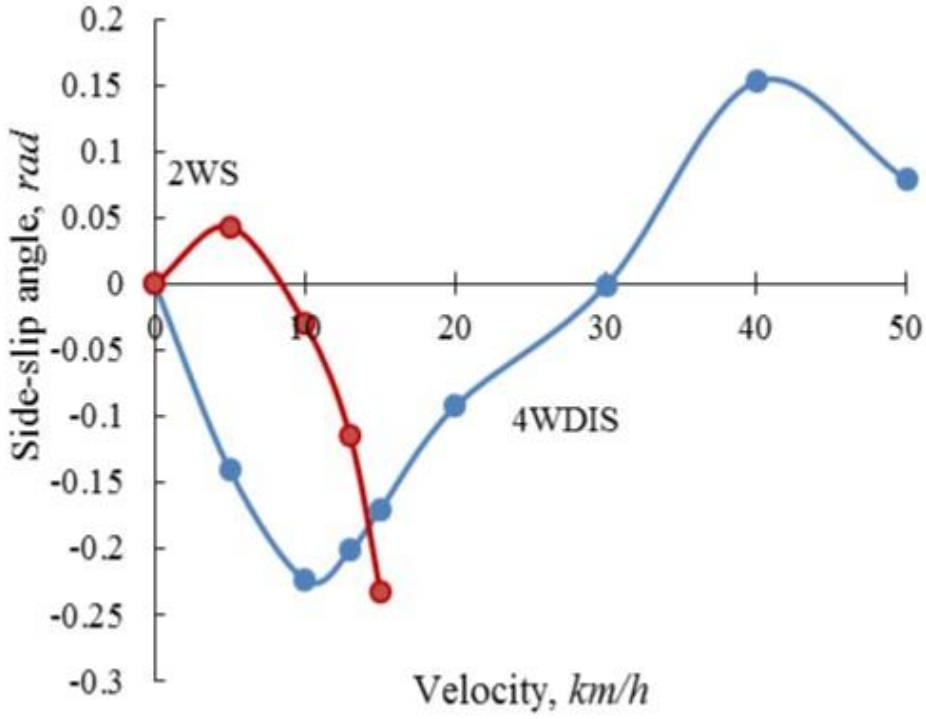

Figure 3-35 The overall steady state side slip angle to velocity for 4WDIS in comparison to 2WS

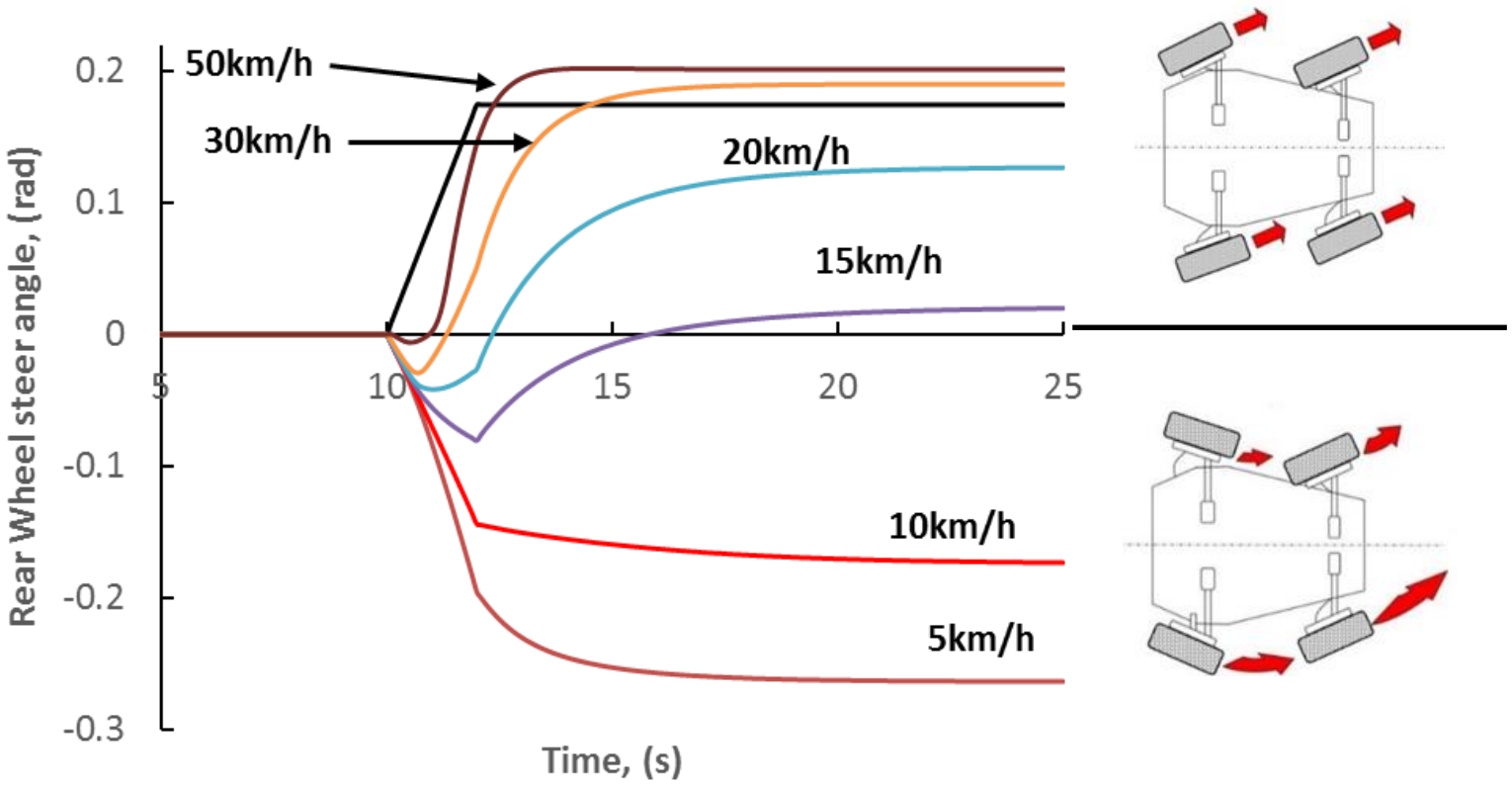

Figure 3- 36 The overall steering characteristic of the 4WDIS

3.8 Summary

In order to use the state observer's linear feedback control on the vehicle with nonlinear model, the error between outputs of both model has to be resolves. The estimated output of the state observer unit and the measured output of the vehicle nonlinear model are compared and multiplied by high gain *H* which is then fed back to the linear model to produce a rectified control input. Then, the rectified control input is send to the vehicle.

The steering characteristic of the OS small electric vehicle integrated with 4WDIS was determined by performing steady state cornering test in regards to a constant front steer angle and at constant velocity. The results were compared with the 2WD OS small electric vehicle from chapter 2. We found that the 4WDIS eliminates the stability velocity limit of the modelled OS small electric vehicle. The yaw moment control system does not only maintain stability at high speed, but also increase mobility at low speed. Furthermore, the system utilized opposite steering at low speed and parallel steering at high speed.

Chapter 4

Regenerative Brake Control as Skid Control System

4.1 Introduction

Chapter 4 is the skid control system by regenerative brake control. Even though we have achieved in increasing the mobility and steering performance of the small electric vehicle in the previous chapter 2 and 3, the system is feeble if traction can't be managed. A normal anti-lock brake system can't be installed on an in-wheel motor due to space limitation. In this chapter, based on the characteristics of in-wheel motor, which are fast torque response and easiness in obtaining an accurate torque feedback, the regenerative brake control was developed as a substitute to an anti-lock brake system. The ABS controls the slip ratio of the tire so that friction coefficient can be maximized. In case of regenerative brake control, if the slip ratio is greater than the optimum value, the regenerative brake turns off and the current produced is transferred to charge the battery. However, when the slip ratio is smaller than the optimum value, the regenerative brake is restored to regain the brake force. From the simulation results, during braking on an icy road, the regenerative brake control has the same control effect as an ABS. Thus, for an in-wheel small electric vehicle, the regenerative brake control can be a substituted to ABS and be utilized as a skid control system

4.2 Anti-lock Brake System

4.2.1 ABS structure unit

Anti-lock brake system (ABS) is one of the skid control system in automobile that allows the wheels of a vehicle to maintain traction with the surface of the road disregarding the drivers braking force preventing the wheels from locking up or stop rotating while the vehicle is still in motion [4-1] - [4-4]. ABS offers a huge improvement in vehicle stability and decrease stopping distances on dry and slippery road conditions. Figure 4-1 shows the simple structure of an ABS unit.

Speed Sensor

In order for the anti-lock brake system to supervise the wheel during lock up, a speed sensor located on each wheel is need.

Electronic Control Unit (ECU)

The ECU is the controller in the vehicle which receive feedback from each individual wheel speed sensor, in case if there a variation in the wheel speed causing traction lose the signal is sent to the controller. The controller will then limit the brake force by activate the braking valve on and off.

Hydraulic Unit

The hydraulic consist of three-channel piping model, each piping for the front wheels and one that connects to the power cylinder that controls the mechanical brakes for the rear wheels. The hydraulic unit receives the braking pressure directly from the master cylinder. The separation on the front wheels provides particular control for maximum braking efficiency while the rear wheels are control simultaneously. In the hydraulic unit contains 3 IN-valves, 3 OUT-valves and a piston pump.

- Valve

  The ECU send a signal to the IN and the OUT valve to control the pressure generate from the master cylinder. In normal braking condition, the IN-valves open allowing the pressure from the master cylinder to pass through to the wheel cylinder. However, when the driver pushes the pedal too hard, the IN-valves close isolating the pressure from the master cylinder. Lastly, when in skidding condition the OUT-valves open to release pressure from the wheel cylinder, decreasing the braking force.

- Pump

  When the valves release the pressure from the brakes, the pump is used to regain the pressure back to the wheel cylinder.

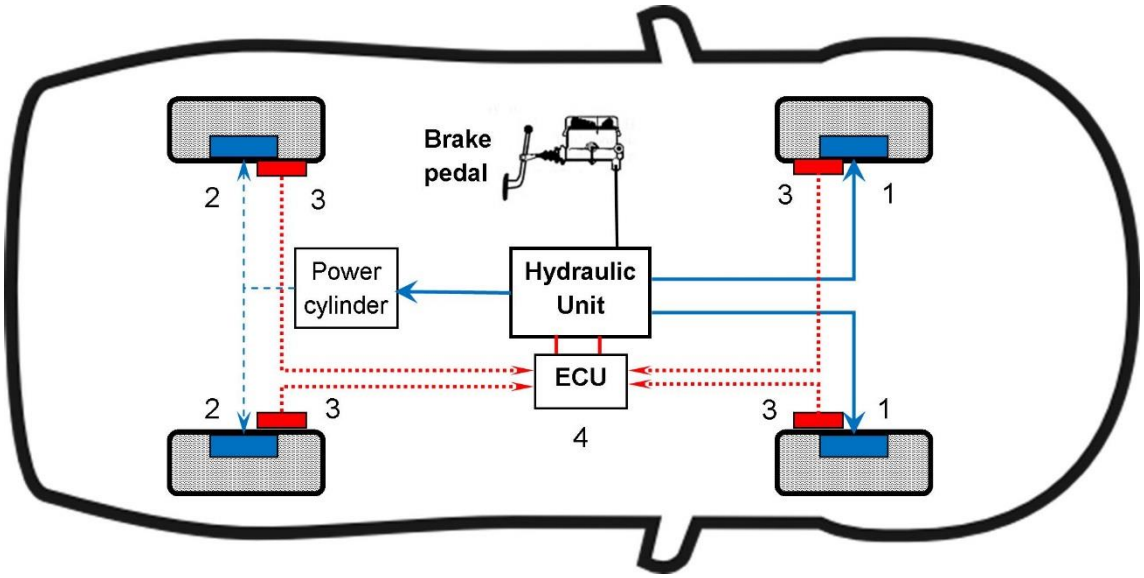

1: hydraulic brake line, 2: mechanical linkage, 3: signal cable connection to speed sensor, 4: electric control unit

Figure 4-1: ABS structure Unit

4.2.2 ABS Operation

The slip ratio formula is crucial for the ABS to operate by expressing the traction characteristics between the vehicle's tire and road surface. Equation 4-1 proposed the definition of slip ratio ρ. Where u indicates the body speed, ω denotes the rotational speed of the tire, and r denotes the radius of the tire.

$$\begin{cases} \rho = \dfrac{u - r\omega}{u} & \text{(braking)} \\ \rho = \dfrac{r\omega - u}{r\omega} & \text{(driving)} \end{cases} \tag{4-1}$$

By using the value of slip ratio, an approximation of the friction coefficient μ of the tire and the road surface can be calculated in the following equation 4-2;

$$\begin{cases} \mu = 1.10k \times (e^{35\rho} - e^{0.35\rho}) & \text{(braking)} \\ \mu = -1.05k \times (e^{-45\rho} - e^{-0.45\rho}) & \text{(driving)} \end{cases} \tag{4-2}$$

Where k is the parameter of the road condition, for which the values are as follow;

$$\begin{cases} k = 1.0 & \text{(dry asphalt)} \\ k = 0.2 & \text{(icy road)} \end{cases}$$

Utilizing slip ratio and friction coefficient equations, a typical tire characteristic curve is produced as such in Figure 4-2. When the tire is locked, the slip ratio becomes 1.0, and the friction coefficient decreases and becomes approximately zero. As a result, the braking force is reduced, and the motion of the vehicle becomes uncontrollable.

The ABS controls the slip ratio so that the friction coefficient is maximized. When tire lock occurs, i.e., when the slip ratio becomes 1.0, the IN valve is closed, the OUT valve is opened, and the pump begins to operate. The pressure in the wheel cylinder and the braking force are decreased. As a result, the slip ratio becomes small, and the friction co-efficiency and the side force become larger. When the slip ratio becomes too small, the IN valve opens and the OUT valve closes again. The pressures in the wheel cylinder and the braking force are increased, and the slip ratio then becomes large.

It is suggested that in ABS controller unit, when the slip ratio reaches the value between ρ_{up} =0.2 and ρ_{dn} = 0.3, the vehicle can obtain the maximum value of friction coefficient and a high degree of cornering force shown in Figure 4-2.

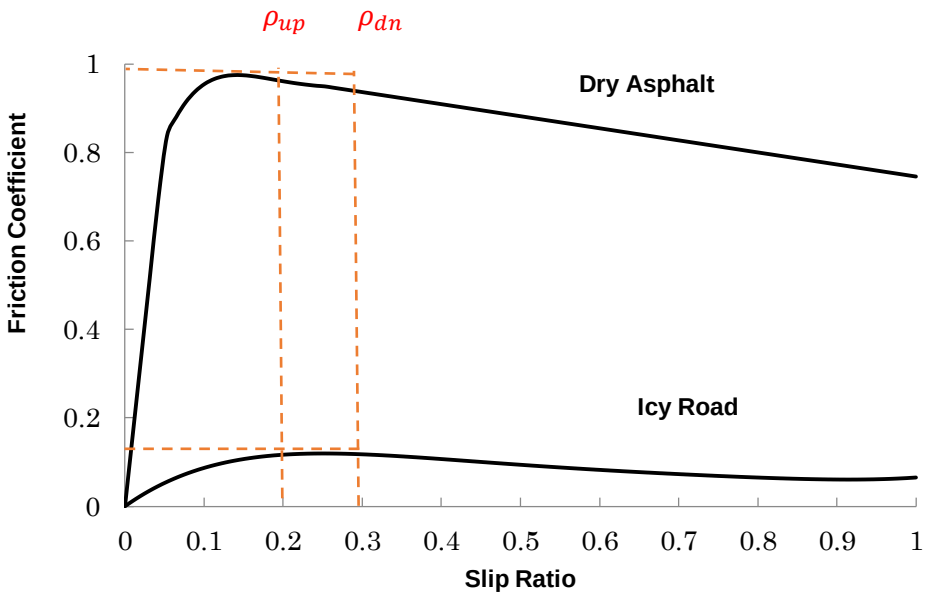

Figure 4-2: ABS Control Unit by Typical Tire Characteristic

4-3 Regenerative Brake System

4.3.1 Mechanism of regenerative brake system

Regenerative braking is often related to vehicle that applies electric motor. Nearly all electric motors are based on magnetism. When an electric is directed to the stator and rotor, different magnetic poles are formed between them and give rise to a force, which produces torque (kinetic energy). In reverse process or electric generator, the rotor is force to turn in opposite direction, the motor become an electric generator converting kinetic energy into output of electric energy. The electrical load produced generates the braking effect.

From the mechanism of electric motor as generator, it clearly understood that regenerative brake force of a vehicle is proportional to the rotational speed of the rotor, which in this case is the motor shaft. When the vehicle is braking, the motor shaft forces the rotor to turn by the wheels' momentum causing electrical load. As the vehicle gradually slows down, the rotational speed of the wheel decreases and so thus the electrical current produced. The declination of braking effect shows that the regenerative brake force diminished.

Generally, a mechanical brake system is installed at the wheels where in-wheel motor is located. Therefore, the total amount of brake force on the wheels with in-wheel motors can be written as;

$$F_{rear} = (\mathrm{C} \times \omega) + F_{mechanical} \qquad (4\text{-}3)$$

Where, F_{actual}*:* actual rear tire brake force, *C:* regenerative brake coefficient*,* ω*:* rotational speed of tire, and $F_{mechanical}$*:* mechanical brake force

Figure 4-3 shows the regenerative brake and mechanical brake system in the ideal braking force distribution.

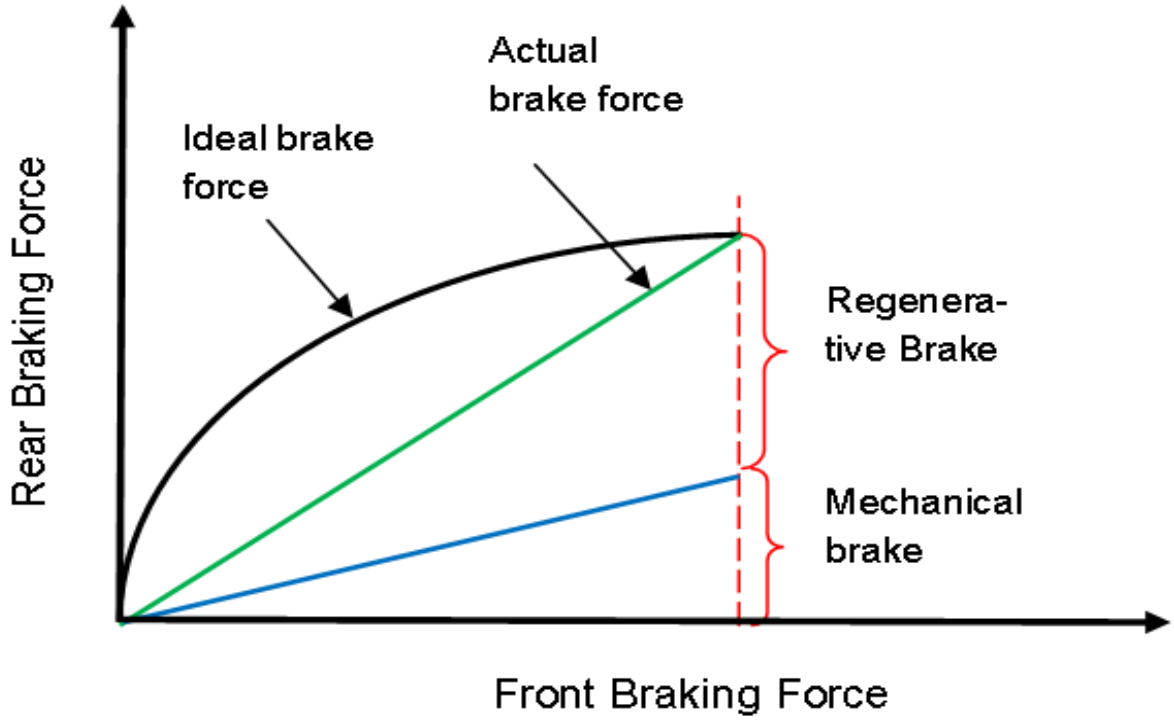

Figure 4-3 Ideal Braking Force Distribution

4.3.2 Regenerative brake control

In general, an in-wheel motor on each wheel provides the possibility of enhanced vehicle motion control [4-5]. However, the excessive regenerative braking torque can result in the locked-up of the EV's wheel especially during braking on an icy road and emergency braking. On the other hand, the introduction of the ABS has contributed to improve the safety of the vehicles decisively by automatically controlling the brake force during braking in potentially dangerous conditions [4-6]. Due to the characteristics of the in-wheel motor, which is the torque response is fast and accurate, the in-wheel motor can be an actuator of ABS to control the regenerative braking torque on the driving tire.

Figure 4-4 illustrates the typical friction coefficient and slip ratio curves for the dry asphalt an icy road [4-7]. This figure is used as a reference in the regenerative brake control. Wheel skid will occur when the large regenerative braking torque rapidly generated at the wheel. This will cause the wheel to lock-up and the vehicle to skid. The slip ratio is used to know either the wheel is locked or not and the equation of slip ratio during braking is:

$$\rho = \frac{u - r\omega}{r\omega} \tag{4-4}$$

Where u is the wheel absolute velocity or vehicle chassis velocity in the longitudinal direction. r and ω are the wheel radius and tire angular velocity respectively. When the slip ratio rapidly increases towards 1.0, the braking force and the side force generation on the wheel will be disappeared. This causes unstable vehicle motion and can be a dangerous spin motion.

In this study, based on the Figure 4-3, the regenerative brake control timing is proposed. The regenerative brake control timing operates similar as ABS, which is based on the slip ratio. If $\rho > \rho_{dn}$, the regenerative brake turns off and the current produced is transferred to charge the battery. However, if $\rho < \rho_{up}$, the regenerative brake is turned back on to regain the ideal brake force. From this mechanism, the braking force on the rear tire can be maximized and prevent wheel locked during braking on an icy road or emergency braking.

4.4 Analysis Vehicle Model

4.4.1 Vehicle braking system

In order to observe the effectiveness of regenerative brake control, we compared the braking effect of regenerative brake control with anti-lock brake system on an in-wheel small electric vehicle. The figure 4-4 shows the braking system of the analysis vehicle model. The front brake system consists of a hydraulic brake system and the rear wheels, which the in-wheel motor located, consists of mechanical brake system and regenerative brake system.

Figure 4-5 shows the construction of a hydraulic and mechanical brake system represented as a bicycle model where both left and right side of the brake system have the same mechanism. The front brake system is a hydraulic braking system while the rear brake system is a mechanical braking system. In hydraulic brake system, the braking force of the front drum brake is monotonous to the force acted from master cylinder (M/C) pressure. The total force is defined as equation 3;

$$F_{hydraulic} = (pressure) \times (master\ cylinder\ cross\ section\ \ area)$$
$$= \rho g H \times \frac{\pi d^2}{4} \quad (4\text{-}5)$$

In mechanical brake system, the braking pressure generated in the master cylinder is directed into a power cylinder. The piston from power cylinder pulls a wire connected to the rear drum brake that moves the brake shoe. Every power cylinder is represented by a spring-mass-damper system and the wire connecting from the power cylinder to the drum brake is represented as a spring. The dynamic force equation from the power cylinder to the wire of a mechanical brake system can be shown in below;

$$m_p \frac{d^2 x_p}{dt^2} = \rho g H A - k_w (x_p - x_d) - k_p x_p - d_p \frac{dx_p}{dt} \quad (4\text{-}6)$$

In the simulation, the displacement of power cylinder spring x_p is calculated by using finite-differential method on the dynamic force equation above. When assuming a uniform partition in time Δt, so the difference between two consecutive spaces is donated as (A) for the first order and (B) second order.

$$m_p \frac{d\dot{x}_p}{dt} = \rho g H A - k_w (x_{p(A)} - x_{d(A)}) - k_p x_{p(A)} - d_p \dot{x}_{p(A)}$$

$$m_p \frac{\dot{x}_{p(B)} - \dot{x}_{p(A)}}{\Delta t} = \rho g H A - k_w\left(x_{p(A)} - x_{d(A)}\right) - k_p x_{p(A)} - d_p \dot{x}_{p(A)} \quad (4\text{-}6)`$$

Let consider,

$$F_{tot} = \rho g H A - k_w\left(x_{p(A)} - x_{d(A)}\right) - k_p x_{p(A)} - d_p \dot{x}_{p(A)}$$

The velocity of the power cylinder spring,

$$\dot{x}_{p(B)} = \dot{x}_{p(A)} + \frac{\Delta t}{m_p}(F_{tot}) \quad (4\text{-}7)$$

Thus, the displacement of the spring can be written as,

$$\dot{x}_{p(B)} = \frac{dx_p}{dt} = \dot{x}_{p(A)} + \frac{\Delta t}{m_p}(F_{tot})$$

$$\frac{x_{p(B)} - x_{p(A)}}{\Delta t} = \dot{x}_{p(A)} + \frac{\Delta t}{m_p}(F_{tot})$$

$$x_{p(B)} = x_{p(A)} + \Delta t\left(\dot{x}_{p(A)} + \frac{\Delta t}{m_p}(F_{tot})\right) \quad (4\text{-}8)$$

However, the dynamic force equation from the wire to the rear drum brake of a mechanical drum brake system is as follow;

$$m_d \frac{d^2 x_d}{dt^2} = k_w\left(x_p - x_d\right) - k_d x_d - d_d \frac{dx_d}{dt} \quad (4\text{-}9)$$

In order to calculate the displacement of drum brake spring x_d, the same method of finite-differential was used.

$$m_d \frac{d\dot{x}_d}{dt} = k_w\left(x_p - x_d\right) - k_d x_d - d_d \dot{x}_d$$

$$m_d \frac{\dot{x}_{d(B)} - \dot{x}_{d(A)}}{\Delta t} = k_w\left(x_{p(A)} - x_{d(A)}\right) - k_d x_{d(A)} - d_d \dot{x}_{d(A)} \quad (4\text{-}9)`$$

The velocity of the drum brake spring,

$$\dot{x}_{d(B)} = \dot{x}_{d(A)} + \frac{\Delta t}{m_d}\left(k_w\left(x_{p(A)} - x_{d(A)}\right) - k_d x_{d(A)} - d_d \dot{x}_{d(A)}\right)$$

Thus the displacement of the spring is

$$x_{d(B)} = x_{d(A)} + \Delta t\left(\dot{x}_{d(A)} + \frac{\Delta t}{m_d}\left(k_w\left(x_{p(A)} - x_{d(A)}\right) - k_d x_{d(A)} - d_d \dot{x}_{d(A)}\right)\right) \quad (4\text{-}10)$$

Finally, by obtaining the displacement of drum brake spring x_d, the total braking force for the mechanical brake equation is;

$$F_{mechanical} = k_d x_{d(P)} - d_d \dot{x}_{d(P)} \quad (4\text{-}11)$$

Figure 4-6 shows the simulation model of the whole hydraulic-mechanical brake system. The master cylinder was modeled by a constant pressure of 1.8 MPa. The power cylinder and the drum brakes of front and rear wheels were modeled by spring-mass-damper model. The spring coefficient used was $k = 6.36 \times 10^7 N/m$ and the viscous damping coefficient was $d = 9.81 \times 10^2 Ns/m$. The wire connecting the link and rear drum brake was modeled also as a spring with coefficient of $k = 2.82 \times 10^8 N/m$.

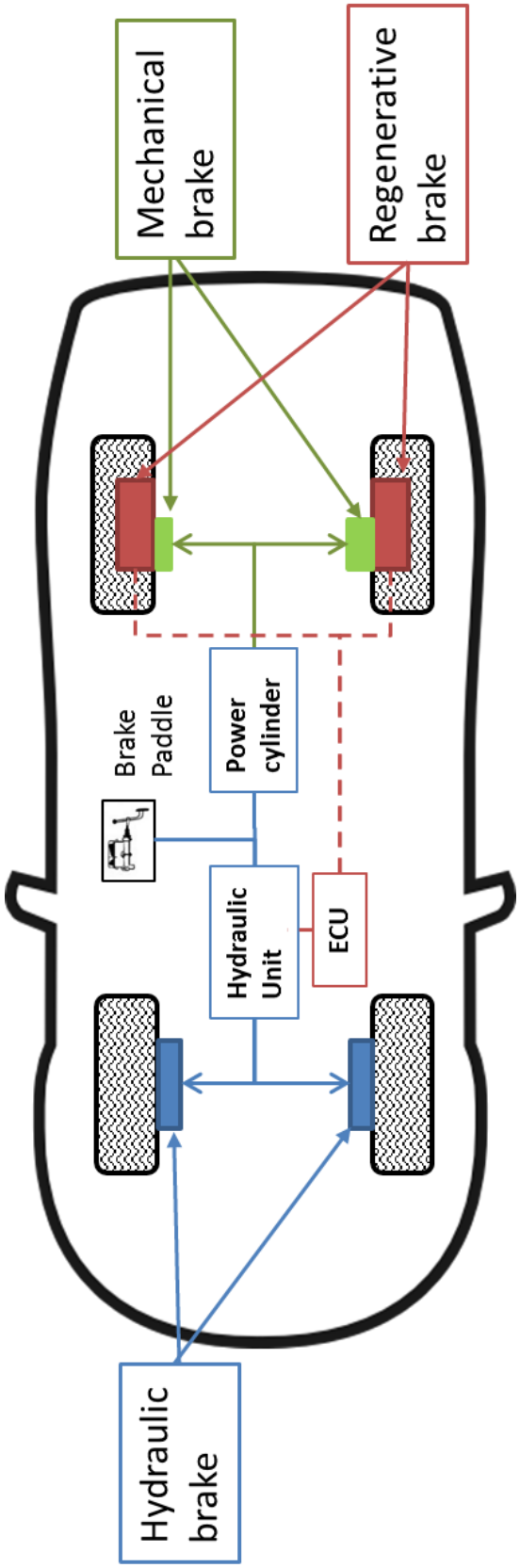

Figure 4-4 braking system of the analysis vehicle model.

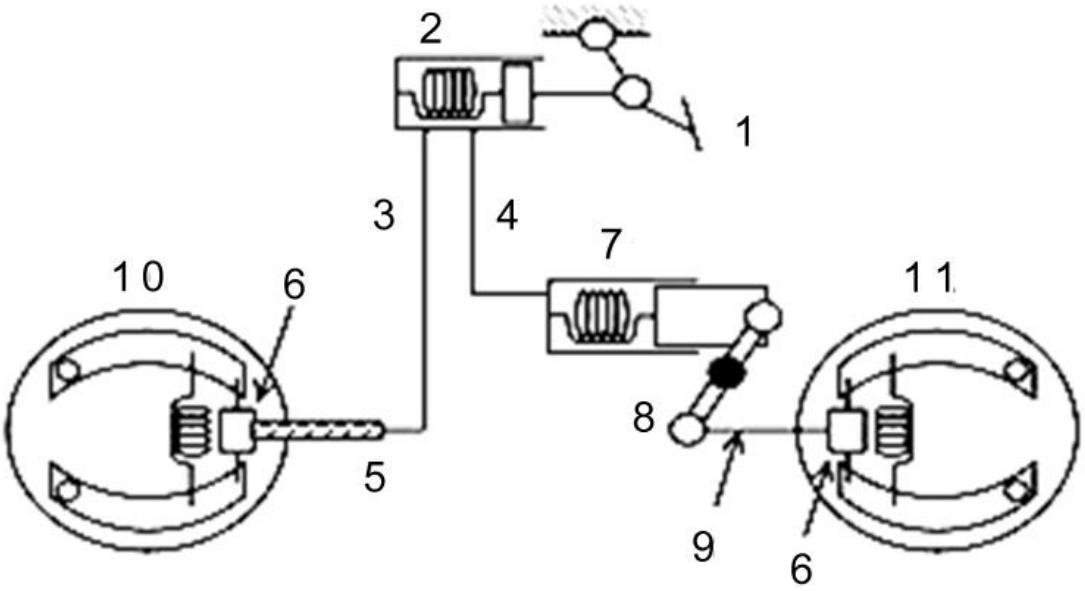

1: Brake Pedal 2: Master Cylinder 3: Front Brake Tube 4: Rear Brake Tube 5: Brake Hose 6: Wheel Cylinder 7: Power Cylinder 8: Link 9: Wire 10: Front Drum Brake 11: Rear Drum Brake

Figure 4-5 Bicycle model of hydraulic and mechanical brake system

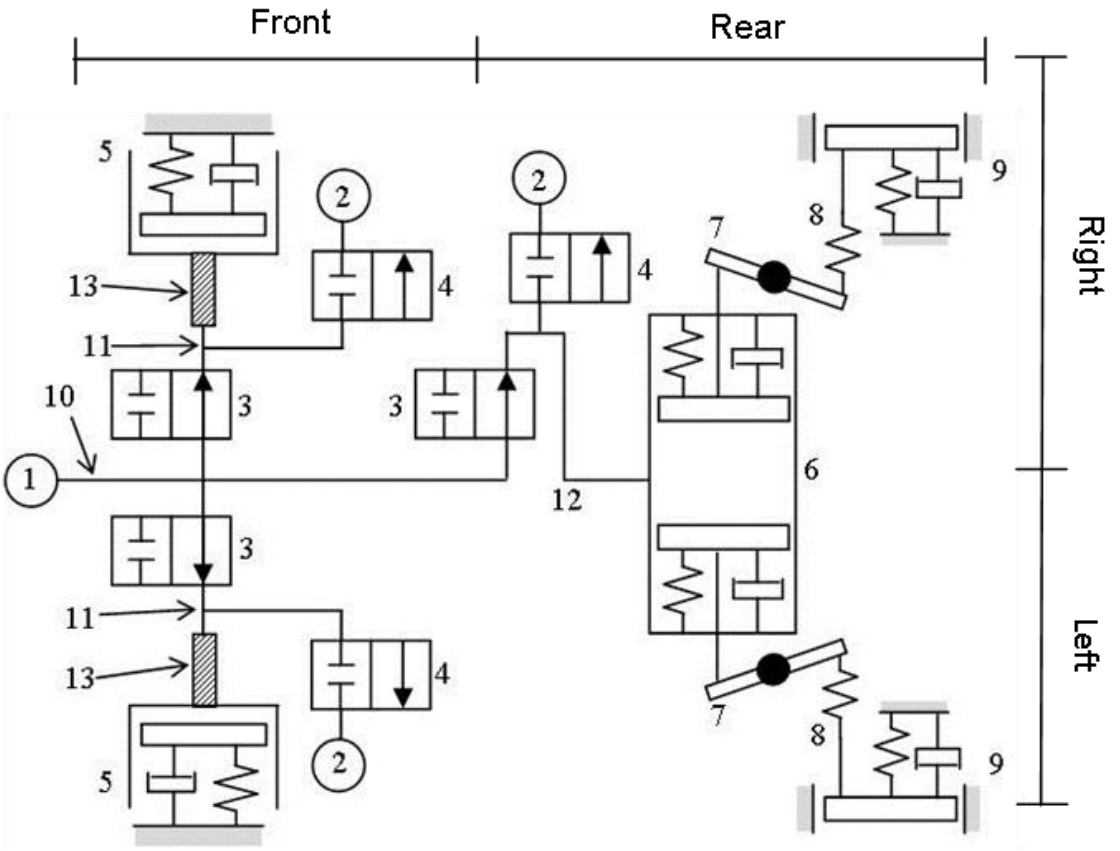

1: Master Cylinder 2: Low Pressure Source 3: In Valve 4: Out Valve 5: Front Drum Brake 6: Power Cylinder 7: Link 8: Wire 9: Rear Drum Brake 10: Master Cylinder Line 11: Front Hydraulic Line 12: Rear Hydraulic Line 13: Front Brake Hose

Figure 4-6 Simulation model of hydraulic and mechanical brake system

4.4.2 Nonlinear dynamic equation of motion for braking condition

Figure 4-7 shows the modification of force vector for the construction of basic motion equation. In this chapter, in order to study the skid control system, a cornering during braking is simulated. Thus, below are the equations of motion for longitude, lateral and yaw direction of the vehicle:

$$m\left(\frac{du}{dt} - v\Upsilon\right) = \left(-X_{fr} - X_{fl}\right)\cos\theta + \left(-Y_{fr} - Y_{fl}\right)\sin\theta - X_{rr} - X_{rl} \tag{4-12}$$

$$m\left(\frac{dv}{dt} + u\Upsilon\right) = \left(Y_{fr} + Y_{fl}\right)\cos\theta + \left(-X_{fr} - X_{fl}\right)\sin\theta + Y_{rr} + Y_{rl} \tag{4-13}$$

$$\begin{aligned} I\frac{d\omega}{dt} = {} & l_f\left(Y_{fr}\cos\theta + Y_{fl}\cos\theta - X_{fr}\sin\theta - X_{fl}\sin\theta\right) - l_r(Y_{rr} + Y_{rl}) \\ & + \frac{d_f}{2}\left(-X_{fr}\cos\theta + X_{fl}\cos\theta - Y_{fr}\sin\theta + Y_{fl}\sin\theta\right) \\ & + \frac{d_r}{2}(-X_{rr} + X_{rl}) \end{aligned} \tag{4-14}$$

Where u, v donate the velocity of longitude, traverse axis, Υ is the vehicle yaw rotational speed, X_{fr}, X_{fl}, X_{rr}, X_{rl} are the friction force while Y_{fr}, Y_{fl}, Y_{rr}, Y_{rl} are the lateral force for each front and rear tire and θ is the front steer angle.

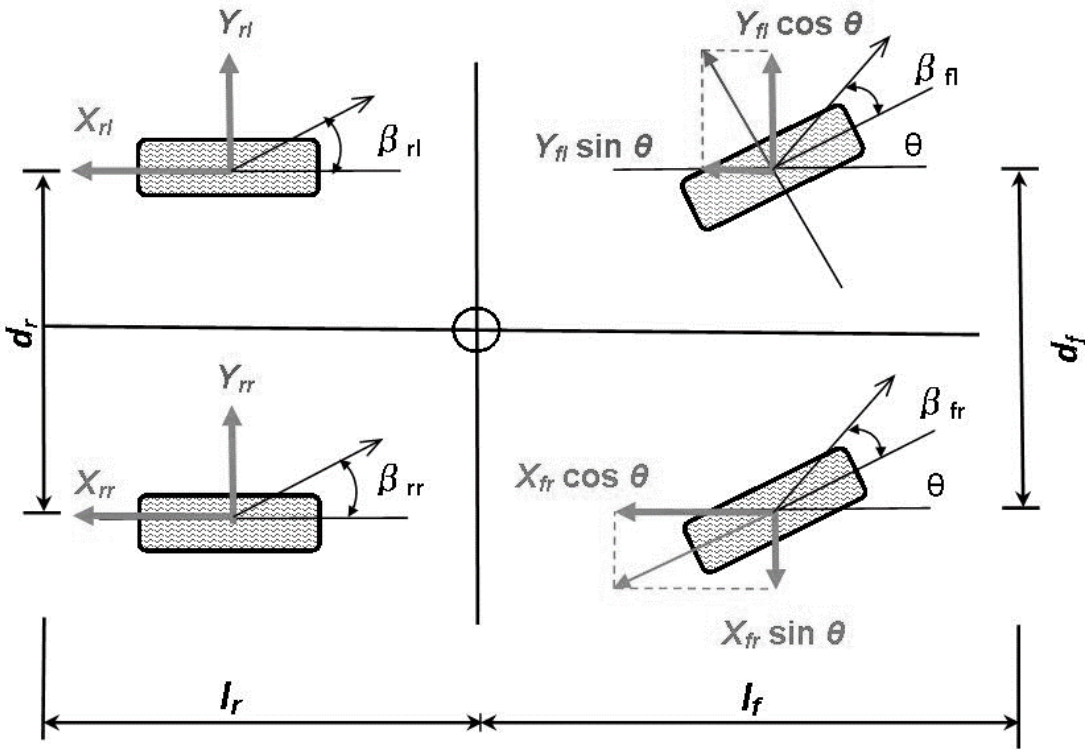

Figure 4-7 Modification of Force Vector for braking

4.4.3 Nonlinear tire characteristic for braking condition

The lateral force and the friction force between interacting surface of tire and road surface for braking are correlate with slip ratio, tire side slip angle and weight distribution is shown in the equations below. The model of deformation of tire tread rubber in the previous chapter was also used to calculate these equations. Moreover, during braking, due to inertia at the center gravity point, a weight distribution at the longitude and to the side of the vehicle is put into consideration. So the tire weight W_z is already represented as weight distribution of each tire. The equations below were used to calculate the longitudinal lateral forces for braking condition;

$$\xi_p = 1 - \frac{K_s}{3\mu W_z}\frac{\lambda}{1-\rho}$$

Where,

$$\lambda = \sqrt{\rho^2 + \left(\frac{K_\beta}{K_s}\right)^2 \tan^2 \beta_T}$$

$$K_s = \frac{b{l_T}^2}{2}K_x \quad , \quad K_\beta = \frac{b{l_T}^2}{2}K_y$$

When $\xi_\rho > 0$, the contact surface comprises of adhesive and slip region. Thus, longitude force and lateral force can be written as;

$$X = -\frac{K_s\rho}{1-\rho}{\xi_p}^2 - 6\mu W_z\frac{\rho}{\lambda}\left(\frac{1}{6} - \frac{1}{2}{\xi_p}^2 + \frac{1}{3}{\xi_p}^3\right) \tag{4-15}$$

$$Y = -\frac{K_\beta \tan\beta_T}{1-\rho}{\xi_p}^2 - 6\mu W_z\frac{K_\beta \tan\beta_T}{K_s\lambda}\left(\frac{1}{6} - \frac{1}{2}{\xi_p}^2 + \frac{1}{3}{\xi_p}^3\right) \tag{4-16}$$

However, when $\xi_\rho \leq 0$, the contact surface only holds the slip region. Therefore, the longitude force and lateral force can be written as;

$$X = -\mu W_z\frac{\rho}{\lambda} \tag{4-17}$$

$$Y = -\mu W_z\ \frac{K_\beta \tan\beta_T}{K_s\lambda} \tag{4-18}$$

Where, *b, l:* width and length of interacted tire surface, K_x, K_y*:* stiffness of vertical and horizontal axis of tire. In this research, *b*=10 *cm*, *l*=15 *cm*, $K_x = 3.33 \times 10^7 N/m^3$,$K_y = 3.33 \times 10^7 N/m^3$ was set as constant.

4.4.4 Load transfer effect

The tire friction force and the tire literal force changes with weight distribution. When there is a load transfer from rear tire to the front tire during braking, the sum of friction force for the front tire is much higher than the rear tire. This effect also implies during cornering where when there is a load transfer between the left and the right wheels, the sum of their lateral force will be lower than when load transfer is not considered.

Figure 4-8 is used to explain the load transfer for braking of a vehicle. There is an inertial force *F* acting to the front of the vehicle from the center gravity during braking. At that moment, consider that the moment around the rear wheel is balance by the moment due to the load transfer acting on the front wheel, and balance that moment to the moment of inertia force acting on the center of gravity, so the load transfer for braking is equal to;

$$l \times \Delta W = h \times F$$

$$l\Delta W = h \times \frac{W}{g} a$$

$$\Delta W_{braking} = \mathrm{W} \cdot \frac{a_X}{g} \cdot \frac{h}{l} \tag{4-19}$$

The same principle is used to calculate the load transfer cause by cornering. From Figure 4-9, the inertia force is substitute with the centripetal force acting from the center gravity of the vehicle during cornering.

$$\Delta W_{cornering} = \mathrm{W} \cdot \frac{a_Y}{g} \cdot \frac{h}{d} \tag{4-20}$$

In the simulation, if considering that the vehicle is in the condition of braking and turning to the left, the most weight will concentrate on the front right wheel and the least weight will be at the rear left wheel. As a conclusion of the load transfer, the weight distribution of the vehicle during cornering and braking are shown below.

$$W_{fr} = W_{fr} + \Delta W_{braking} + \Delta W_{cornering}$$

$$W_{fl} = W_{fl} + \Delta W_{braking} - \Delta W_{cornering}$$

$$W_{rr} = W_{rr} - \Delta W_{braking} + \Delta W_{cornering}$$
$$W_{rl} = W_{rl} - \Delta W_{braking} - \Delta W_{cornering} \quad (4\text{-}21)$$

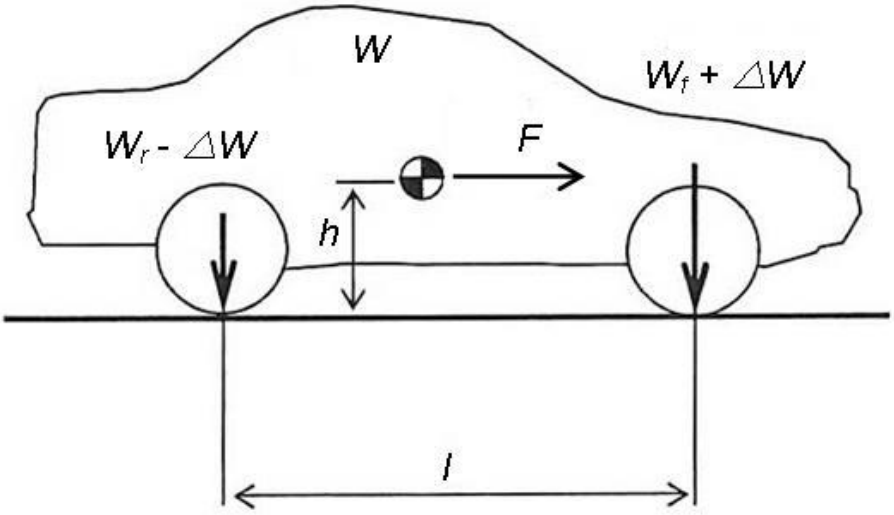

Figure 4-8 load transfer for braking

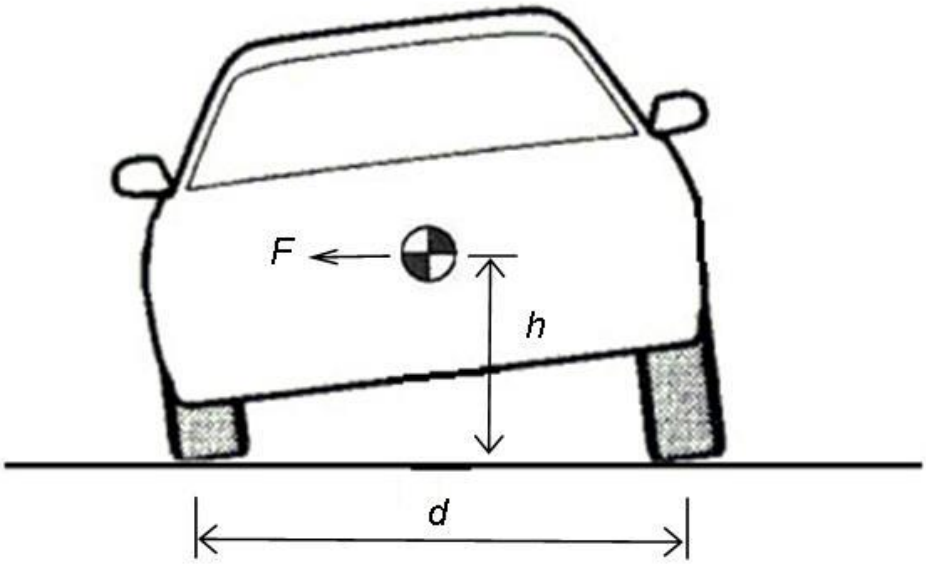

Figure 4-9 load transfer for cornering

4.5 Regenerative Brake Coefficient

As mention before, during braking the wheel's momentum force the rotor to turn in opposite direction that leads to electrical load that makes up the braking effect on the vehicle. In order to precisely obtain those electrical loads means to dissect the in-wheel motor and examine the magnet strength itself, which is cost-inefficient and time consuming.

A simple experiment is proposed to determine the regenerative brake coefficient by comparing the experimental result of vehicle stopping time during braking with simulation result.

4.5.1 Experimental methods for identifying the regenerative brake coefficient

Toyota COMS EV was used as the experimental vehicle. The vehicle was driven in a straight line on a dry asphalt surface until it reaches a constant velocity. A lever on the braking pedal, as shown in Figure 4-10, was pulled for braking. The velocity of the vehicle, rotational speed of front and rear wheel, and the hydraulic braking pressure was recorded. Figure 4-11 shows the motor shift switch. When the motor shift switch is in 'driving', the in-wheel motors are engaged and regenerative brake is available during braking.

4.5.2 Simulation methods for verifying the regenerative brake coefficient

The experimental conditions (velocity, brake pressure) of a straight line braking are duplicated in a numerical simulation. The stopping time result is then compared to the experimental result to obtain the approximate regenerative brake coefficient.

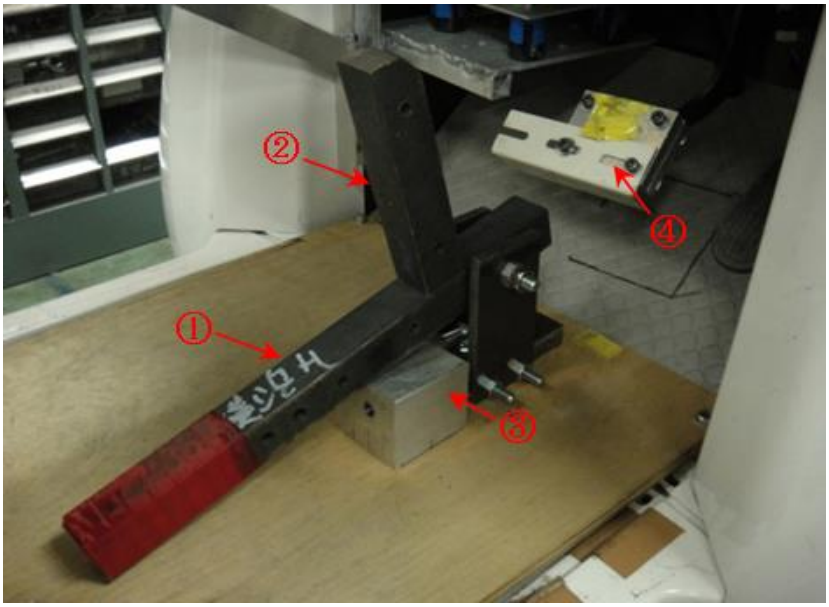

Figure 4-10 Brake lever and stopper

Figure 4-11 Motor shift switch set to ‘drive’

4.6 Effectiveness of Regenerative Brake Control as Skid Control System

4.6.1 Simulation procedure

In the objective to observe the effectiveness of regenerative brake control system for in-wheel small electric vehicle based on steer performance, three cases of braking condition on icy road were investigated using numerical simulation. The cases are as follows;

- Case 1: braking on icy road without any skid control system
- Case 2: braking on icy road with anti-lock brake system as a skid control system
- Case 3: braking on icy road with anti-lock brake system and regenerative brake control

In the simulation, the initial velocity was 14 [*km/h*] and the braking pressure was 1.8 [*MPa*]. Steer angle was set to 20 [*deg*].

4.7 Result and Discussion

4.7.1 Regenerative brake coefficient, *C*

After succeeding in the finding of the tire stiffness value, the same procedures were used to determine the value of regenerative brake coefficient. Several road tests were done by driving the in-wheel small electric vehicle in straight line until it reached a constant speed of 30 *km/h* and then make a sudden braking with 1.5 *MPa* pressure. The only variance was that the motor shift switch was left in driving mode indicating regenerative brake is at presence. Figure 4-12 shows best experimental result of the deceleration of vehicle body and tire speed with a linear approximation line for braking pressure.

The parameters from the experiment condition as shown below were used to reenact the straight line braking in a numerical simulation.

Vehicle velocity = 30 *km/h*,

Master cylinder pressure =1.54 *MPa*,

Road condition = dry asphalt

The value of the regenerative brake coefficient was determined by comparing the results of stopping time for the simulation and the experiment. From these procedures, when the regenerative brake coefficient value is set to 25 kg/s^2, the stopping time of the simulation is similar to the experiment result. Figure 4-13 shows the simulation result of deceleration of vehicle body and tire speed.

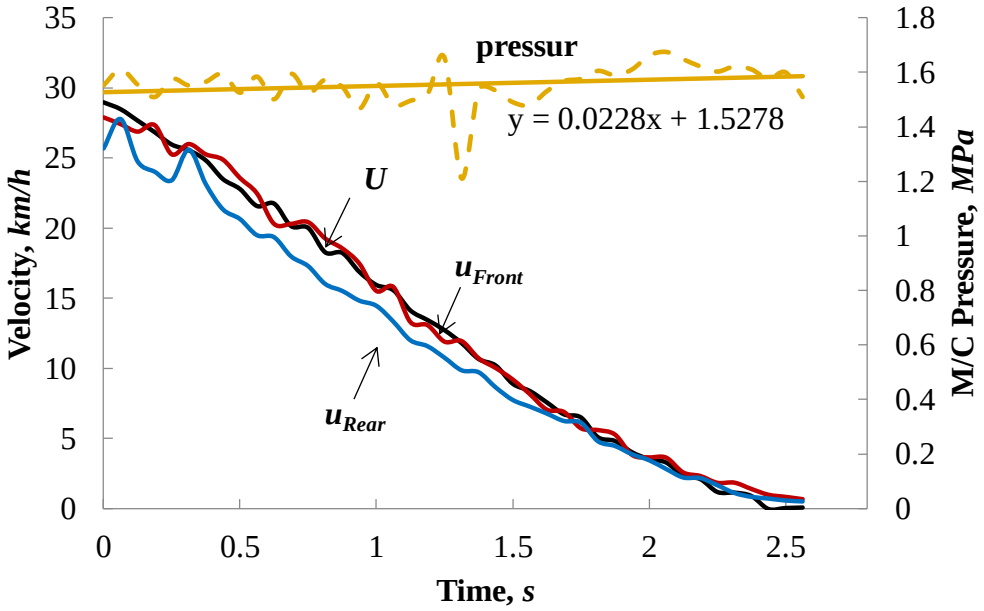

Figure 4-12 Vehicle and tire speed deceleration based on experiment

(U = 30 *km/h*, regenerative brake on)

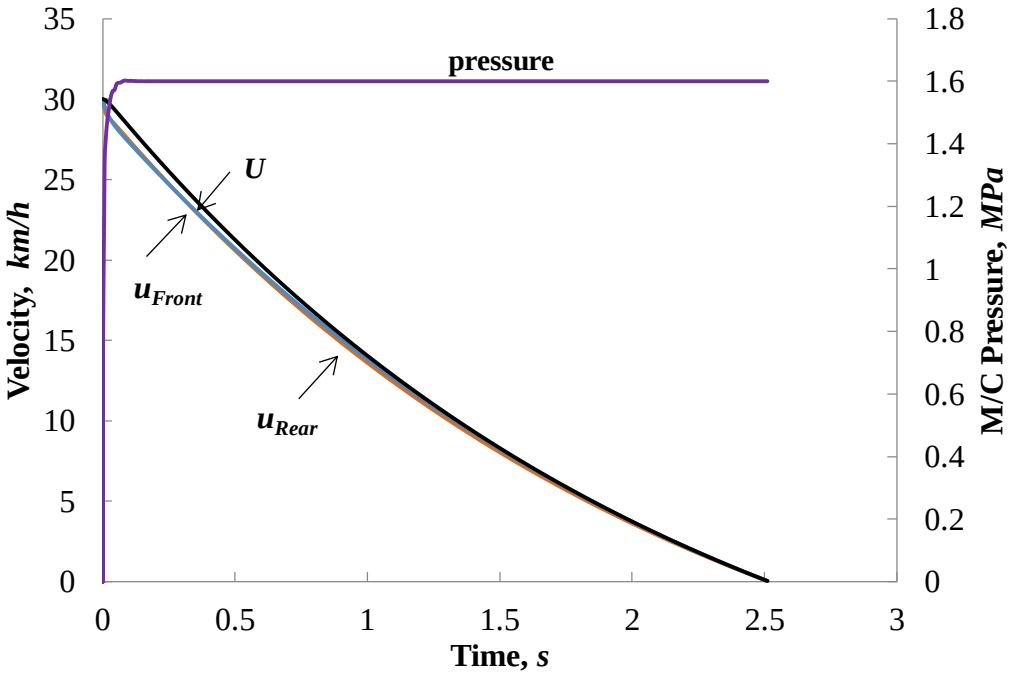

Figure 4-13 Vehicle and tire speed deceleration based on simulation

(U = 30 *km/h*, regenerative brake on)

4.7.2 Effectiveness of regenerative brake control as skid control system

Figure 4-14 shows the result of the longitude and lateral velocity while figure 4-15 shows the trajectory of in-wheel small electric vehicle during braking on icy road for all three cases based on similar initial velocity, braking pressure and steer angle. The black, red and blue lines represent case 1, case 2 and case 3, respectively for both figures. In figure 4-14, the dash and continuous lines represent longitude and lateral velocity, respectively. Each case descriptions are as follow;

- Case 1: braking on icy road without any skid control system
- Case 2: braking on icy road with anti-lock brake system at the front wheel
- Case 3: braking on icy road with anti-lock brake system and regenerative brake control

The results for case 1 prove that braking on icy road for in-wheel small electric vehicle is dangerous. It took 22 [*sec*] for the vehicle to complete stop from initial velocity 14 km/h. Based on the trajectory, the vehicle did not have any control even though steering input was applied.

In case 2, anti-lock brake system was exclusively installed as a skid control system at the front wheels of the in-wheel small electric vehicle. The stopping time had improved about 11 [*sec*] compared to the stopping time of case 1. The trajectory during braking shows that vehicle complied with the steer angle. However, observing from the result of the velocity, the longitude velocity reached a stop sooner than the lateral velocity. These suggest that the vehicle was moving side-ways cause by drifting of rear wheels where the in-wheel motors are located.

Figure 4-16 show the result of hydraulic brake force, while Figure 4-17 shows the results of slip ratio and friction coefficient for the front wheels during braking on ice in case 2. On the other hand, Figure 4-18 shows the result of regenerative brake and mechanical brake force, while Figure 4-19 shows the results of slip ratio and friction coefficient for the rear wheels during braking on ice in case 2. In the matter of front wheels, the ABS controls the brake force by releasing and regaining force based on the slip ratio value to produce a high friction coefficient. However, for the rear wheels, the regenerative brake force was initially high and decreased as the wheel stop rotating. The mechanical brake force is small but holds the wheel in lock condition. Due to this, the slip ratio was at high value that led to low friction coefficient. Thus, this gives out the early assumption

that the rear wheels were in slip condition. Even though the front wheels maintain traction during braking and steering, the cornering momentum and low traction of the rear wheels cause the vehicle to drift.

In case 3, ABS control method was implemented on the regenerative brake produced by the in-wheel motor as a skid control system. During braking on ice, the regenerative brake control operated synchronously with anti-lock brake system. Based on velocity results in figure 6, the stopping time for case 3 is higher than case 2. However, the longitude and lateral velocity stop at the same time. Moreover, the trajectory of the in-wheel small electric vehicle for case 3 shows a tighter radius than case 2.

Figure 4-20 show the result of hydraulic brake force of the front wheel and regenerative brake force from rear wheel during braking on ice in case 3. On the other hand, Figure 4-21 and Figure 4-22 shows the results of slip ratio and friction coefficient for the front and rear wheels during braking on ice in case 3, respectively. Even though regenerative brake adopted the same control method as anti-lock brake system, the braking force produced was not similar. In the event of ABS operational, the brake pressure from the master cylinder is constant. However, the regenerative brake force is proportional to the tire rotational speed. During alternating Off and On, the later value of regenerative brake force is lower than the previous brake force. Nonetheless, the braking force at a particular moment is sufficient to produce a high friction coefficient at the particular rotational speed. Consequently, the regenerative brake force will disappear when the wheel stop rotating and the mechanical brake will hold the wheel in place.

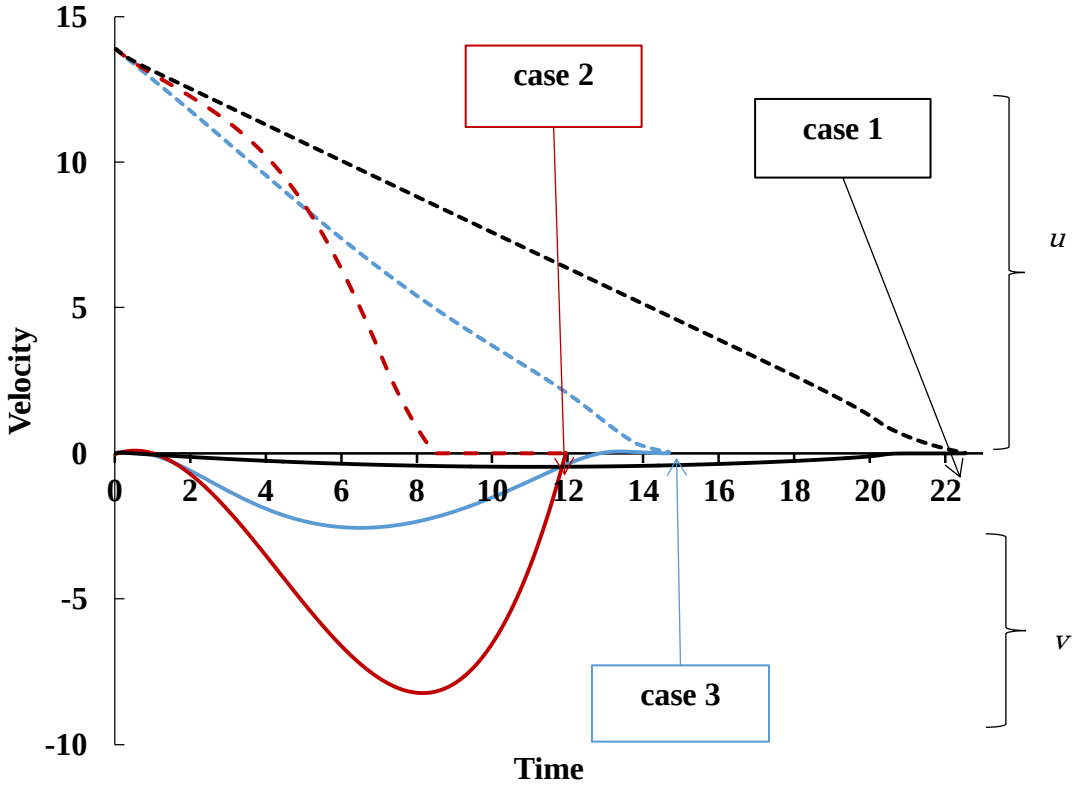

Figure 4-14 the longitude and lateral velocity

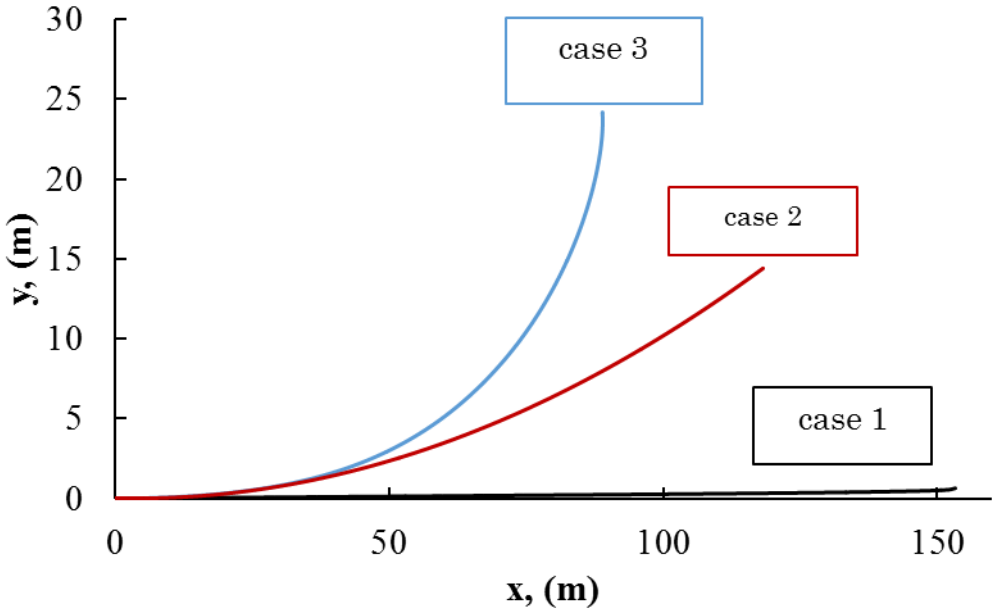

Figure 4-15 the trajectory of in-wheel small electric vehicle

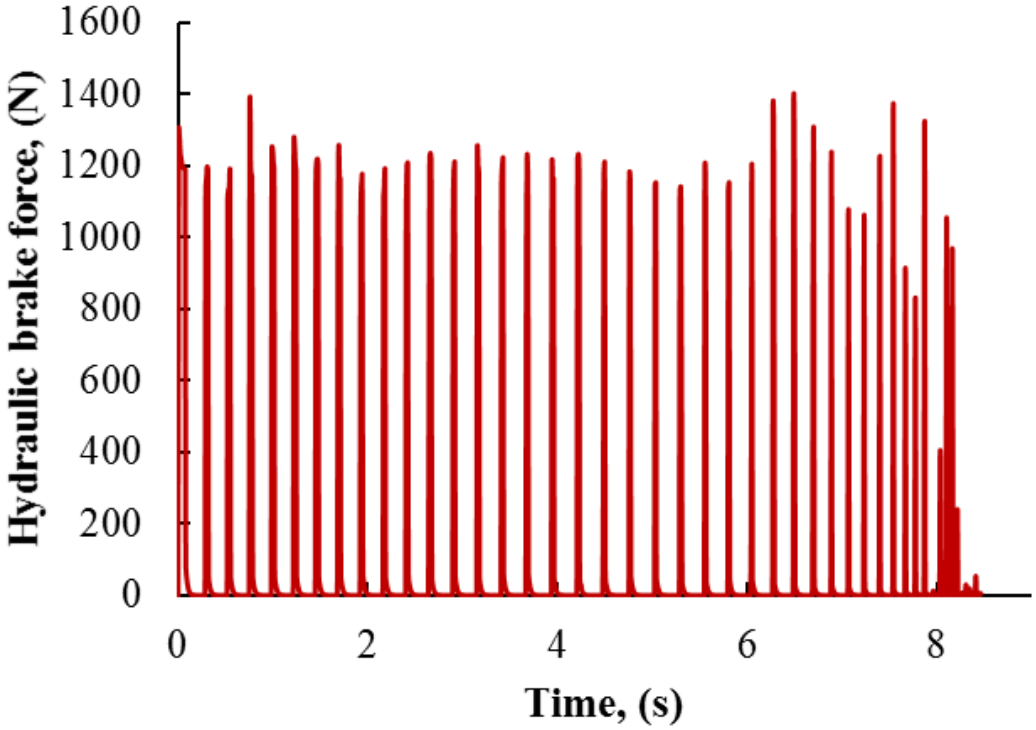

Figure 4-16 The hydraulic brake force during braking on ice road for case 2

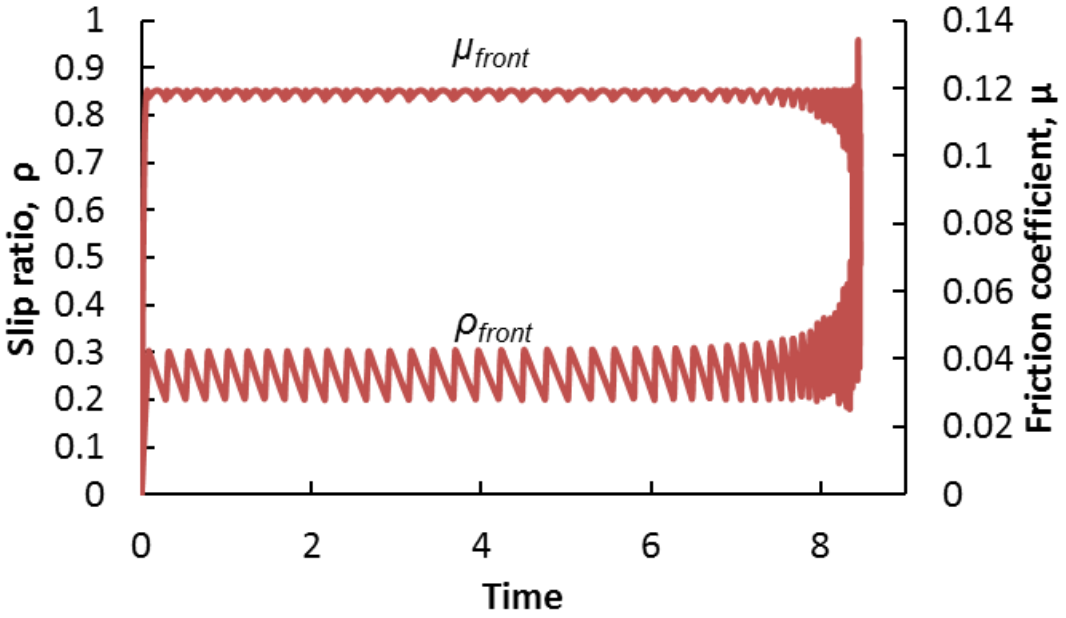

Figure 4-17 The slip ratio and friction coefficient for the front wheels during braking on ice road for case 2

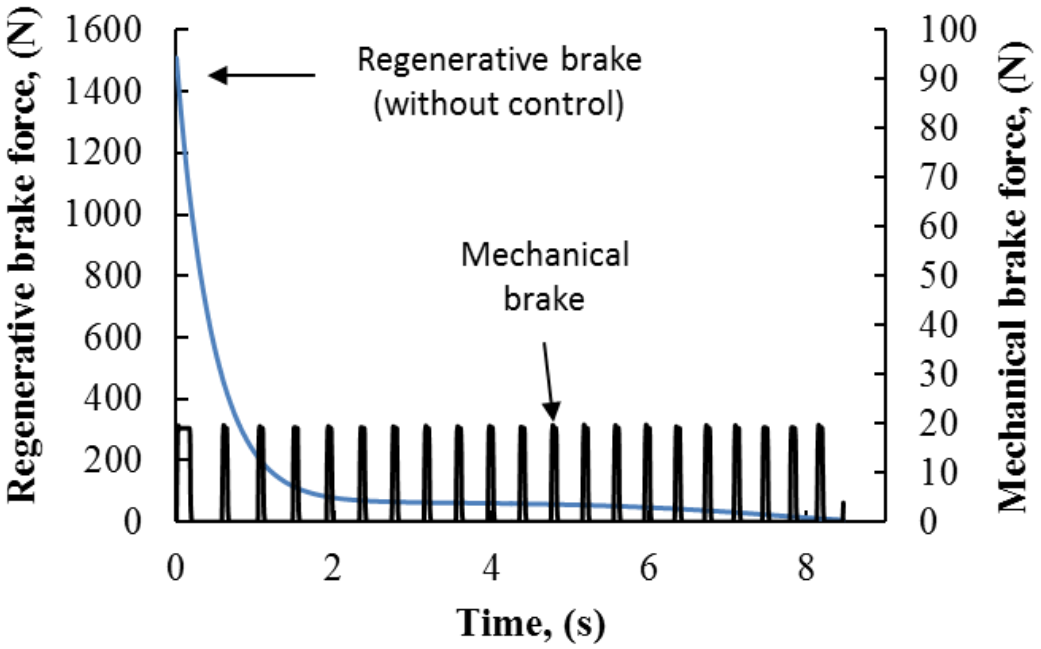

Figure 4-18 The regenerative brake and mechanical brake force during braking on ice road for case 2

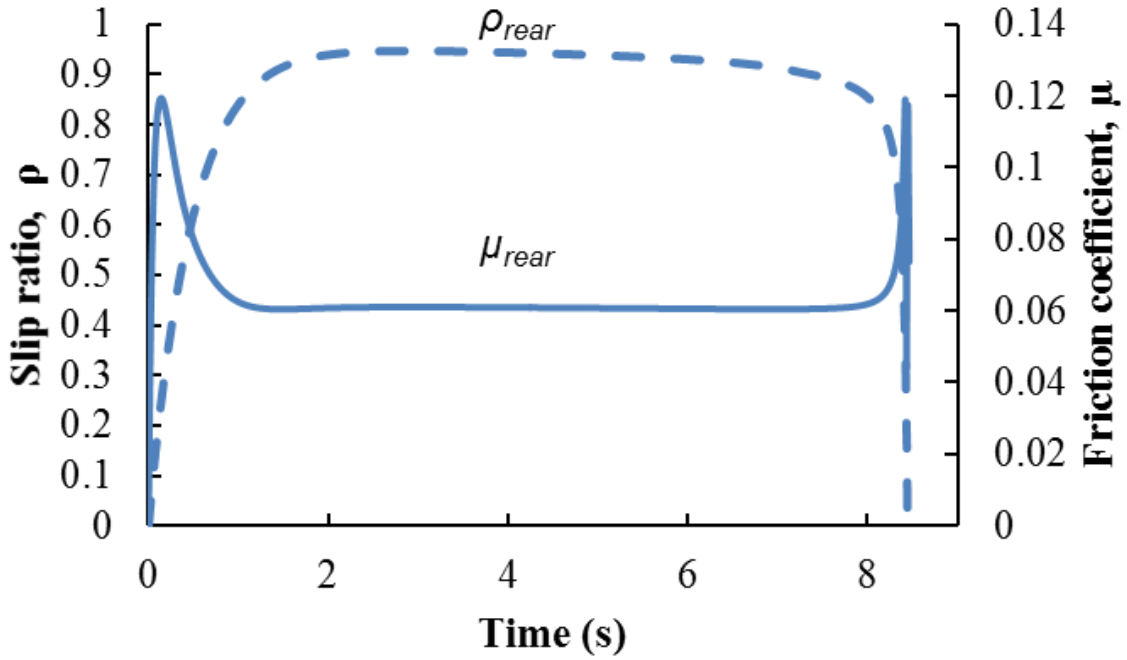

Figure 4-19 The slip ratio and friction coefficient for the rear wheels during braking on ice road for case 2

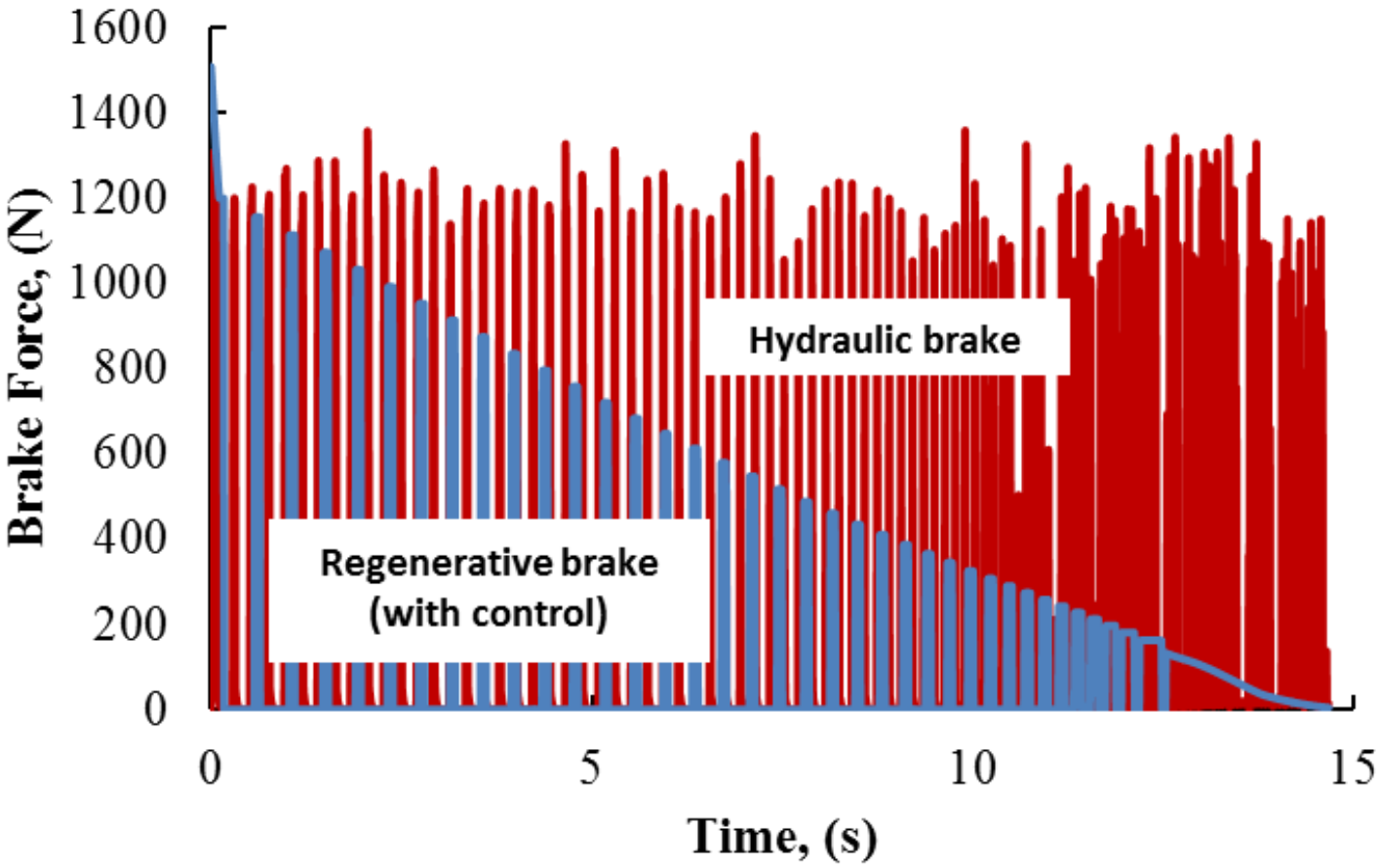

Figure 20 The brake force of hydraulic brake and regenerative brake during braking on ice road in case 3

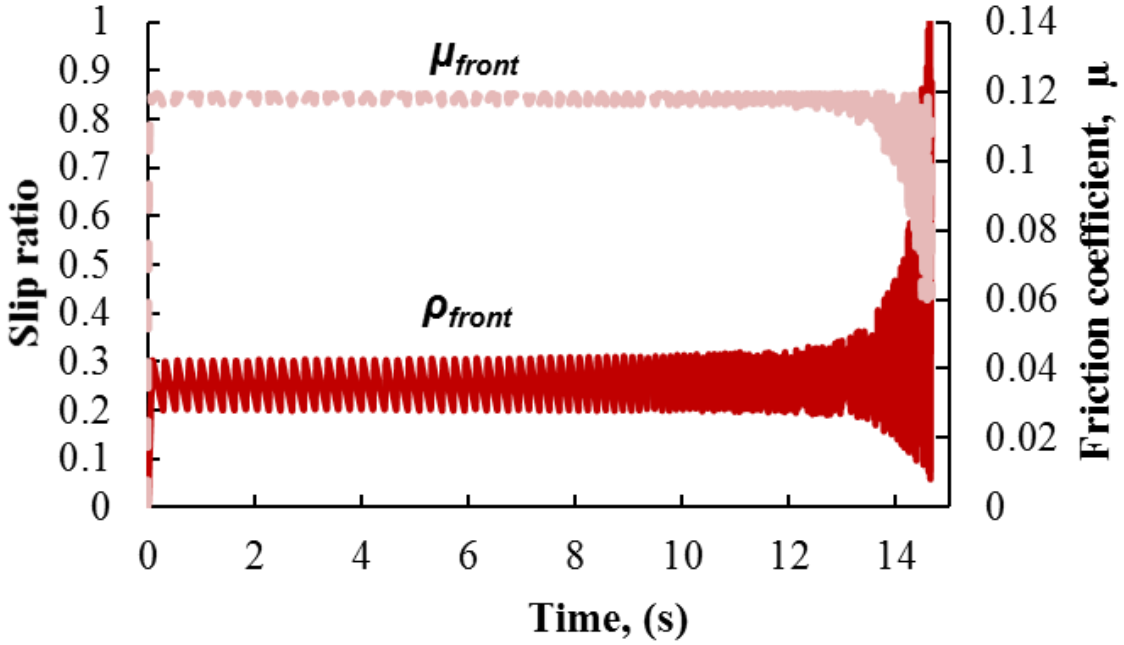

Figure 4-21 The slip ratio and friction coefficient for the front wheel and rear wheels during braking on ice in case 3

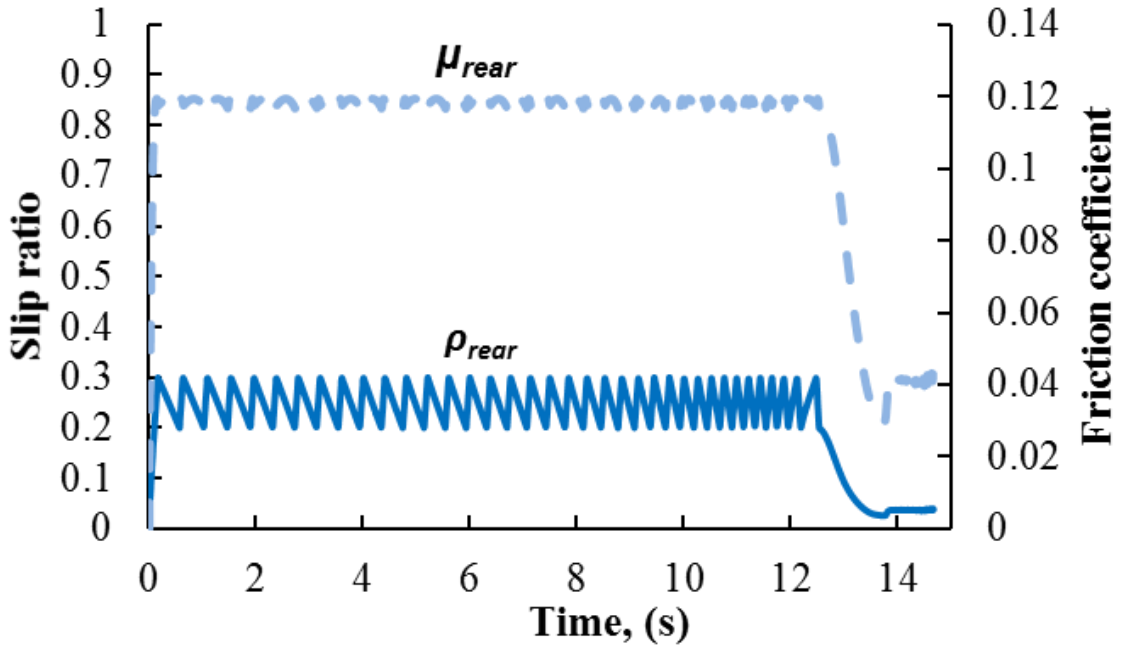

Figure 4-22 The slip ratio and friction coefficient for the rear wheel and rear wheels during braking on ice in case 3

4.8 Summary

In this chapter, the regenerative brake control was developed as a substitute to anti-lock brake system for in-wheel small electric vehicle. In order to observe the effectiveness of regenerative brake control, we compared the braking effect of regenerative brake control with anti-lock brake system. The findings of the experiment and simulation results are as follows:

1. Based on the comparison of experiment and simulation results, the regenerative brake coefficient value is 25 kg/s^2
2. During braking on an icy road, the regenerative brake can be controlled based on the slip ratio value to produce high friction coefficient.
3. The regenerative brake adopted the same control method as anti-lock brake system, but the braking force produced was not similar.
4. The regenerative brake force is proportional to the tire rotational speed.
5. Nonetheless, the braking force at a particular moment is sufficient to produce a high friction coefficient at the particular rotational speed.
6. Consequently, the regenerative brake force will disappear when the wheel stop rotating and the mechanical brake will hold the wheel in place.

Chapter 5

Conclusions

In this research, to increase the mobility and stability of the small electric vehicles (EVs), a small electric vehicle with oversteer characteristic that is integrated with a four-wheel drive and independent steering is developed. The outcome of this research has been written in 5 chapters and the summarization of each chapter is described as below.

Chapter 1 introduction

Over the 20th century, increasing carbon dioxide emission by petroleum-based transportations is one of the main contributor to global warming. Moreover, escalation of global human population has put a pressure on the amount of carbon dioxide emission especially in developing countries rather than developed countries. A research paper from the National Academy of Sciences of the USA concluded that climate change that takes place due to the global warming is largely irreversible for 1,000 years even after emissions of carbon dioxide stop. This environmental issues by petroleum-based transportations along with the issue of fossil fuel depletion around the world have led activist and lobbyist to pressure automotive manufacturers to redesign future vehicles.

Under the aspect of redesigning future vehicle, in the past few year car manufacturers have reintroduced hybrid electric vehicle (HEV) and full-electric vehicle (EV). Hybrid electric vehicle is a vehicle that incorporate a smaller and generate less emission fossil-fuel engine with an electric powertrain. On the other hand, a fully-electric vehicle is an automobile that is propelled exclusively by one or more electric motors. Since electric vehicles do not have internal combustion engine, they don't use any fuel and produce zero tail emission. This means that an electric vehicle benefits the environment more than a hybrid electric vehicle.

Similar to telephones and computers, new devices which was once a huge and shared-item has gotten smaller, faster and cheaper. The shrinking and personalization of technological device phenomena does not limit to computer and telephone. They have also spread to automotive. Small electric vehicle meets the consumer demand as they are practical, efficient and affordable. Moreover, Government and car manufacturer have join together to promote small electric. The reason government support small electric vehicles is because they can be used to improve the lives of people in cities. The small size electric vehicle can ease traffic congestion, and improving access to tourist areas and communities in a city

Mobility within a city such as Tokyo and Osaka along with its surrounding suburbs

can be difficult. The rapid development within a small concentrated area and high density population has led to construction of various narrow and complex roads. In order to drive in such roads mixed with vehicles and pedestrians, small electric vehicles nowadays have to face critical driving condition. For example, in the city when a small electric vehicle enters a narrow road and needs to reciprocate, due to space limitation the driver has to either advance until a turntable space is available or make an exit at a larger road. A small electric vehicle is also use to commute from a city to neighboring suburb. Without any lateral stability control system, maneuverability will become difficult in various cornering at various velocity. All of these situations are worsen when they occur on a slippery road surface during heavy rain or snow that would can be easily categories as a very dangerous state

Thus, the main objective of this research is to improve the mobility and stability of small electric vehicle. Firstly, we increase the mobility by modelling a small electric vehicle with oversteer characteristic. Then, as a lateral stability control system, we implement yaw moment control by four-wheel drive and independent steering. Lastly, a regenerative brake control is utilized as a skid control system.

Chapter 2 Modelling an In-Wheel Small Electric Vehicle with Oversteer Characteristic

In this chapter, an in-wheel small electric vehicle is modelled with an oversteer characteristic in a numerical simulation. High cornering performance vehicle such as sport or racing cars have OS characteristic. They have high steer ability and response with low steer input. The down side of OS is that they have stability velocity limit. Due to in-wheel motor, a small electric vehicle can have a ‘skateboard-shape’ chassis where the top of the chassis can be managed freely. Therefore, in order to model an oversteer characteristic of a small electric vehicle, we reposition the weight of the center of gravity to the more to the rear of the vehicle.

The steering characteristic of the OS small electric vehicle was determined by performing steady state cornering test in regards to a constant front steer angle and at constant velocity. The end results show that the modelled OS vehicle has a stability velocity limit at 15.5 km/h. Nonetheless, the vehicle can achieve high yaw rotational speed at below this velocity even with small steer angle. However, as the velocity increases, the longer time it will take for the vehicle to achieve steady state cornering.

Chapter 3 Yaw Moment Control by Four Wheel Drive and Independent Steering.

In chapter 2, theoretically the mobility of a small electric vehicle has increased by modelling the vehicle with an oversteer characteristic. However, when the vehicle velocity is beyond the stability velocity limit the yaw rotational speed and side slip angle of the modelled small electric vehicle with oversteer characteristic reach infinite value. In this chapter, we introduced a yaw moment control by integrating a four-wheel drive and independent steering (4WDIS) as a lateral stability system of the vehicle. Until now, there are extensive study of 4WS as a yaw moment control. However, many of these past researches adopt easier way of modelling a lateral control system based on vehicle model with linear characteristics. Thus, the control method can be considered unsuitable.

Firstly, to justify our claims, we connect a state observer unit that consist of a linear feedback control to a vehicle with nonlinear model. The control input of the state observer unit is fed forwarded to the vehicle. Two simulations of steady state cornering with regard to a constant front steer angle and at low and high velocity was performed. The results show that the output of the vehicle and state observer varies. In order to use the state observer's linear feedback control on the vehicle with nonlinear model, the error between outputs of both model has to be resolves. The estimated output of the state observer unit and the measured output of the vehicle nonlinear model are compared and multiplied by high gain H which is then fed back to the linear model to produce a rectified control input. Then, the rectified control input is send to the vehicle.

Lastly, the steering characteristic of the OS small electric vehicle integrated with 4WDIS was determined by performing steady state cornering test in regards to a constant front steer angle and at constant velocity. The results were compared with the 2WD OS small electric vehicle from chapter 2. We found that the 4WDIS eliminates the stability velocity limit of the modelled OS small electric vehicle. The yaw moment control system does not only maintain stability at high speed, but also increase mobility at low speed. Furthermore, the system utilized opposite steering at low speed and parallel steering at high speed.

Chapter 4 Regenerative Brake Control as Skid Control System

Even though we have achieved in increasing the mobility and steering performance of the small electric vehicle, the system is faulty if traction can't be managed. In this chapter, based on the characteristics of in-wheel motor, which are fast torque response and easiness in obtaining an accurate torque feedback, the regenerative brake timing

control was developed as a substitute to an anti-lock brake system. The ABS controls the slip ratio of the tire so that friction coefficient can be maximized. In case of regenerative brake control, if the slip ratio is greater than the optimum value, the regenerative brake turns off and the current produced is transferred to charge the battery. However, if the slip ratio is smaller than the minimum value, the regenerative brake is restored to regain the ideal brake force.

Two cases of braking condition on icy road were investigated to observe the effectiveness of regenerative brake control using numerical simulation. The cases are as follows;

Case 1: braking on icy road with ABS only

Case 2: Braking on icy road with ABS and regenerative brake control

From the simulation results, the regenerative brake adopted the same control method as anti-lock brake system, but the braking force produced was not similar. The regenerative brake force is proportional to the tire rotational speed. Nonetheless, the braking force at a particular moment is sufficient to produce a high friction coefficient at the particular rotational speed. Consequently, the regenerative brake force will disappear when the wheel stop rotating and the mechanical brake will hold the wheel in place.

Chapter 5 Conclusions

In this research, a small electric vehicle with oversteer characteristic that is integrated with a four-wheel drive and independent steering is developed to increase the mobility and stability of the small electric vehicles (EVs). Several findings on this study can be concluded as below:

1. The modelled OS vehicle has a stability velocity limit at 15.5 km/h. Nonetheless, the vehicle can achieve high yaw rotational speed at below this velocity even with small steer angle.
2. In order to use the state observer's linear feedback control on the vehicle with nonlinear model, the error between outputs of both model has to be resolves by eliminating the error between state observer unit and vehicle model
3. The 4WDIS eliminates the stability velocity limit of the modelled OS small electric vehicle. The yaw moment control system by 4WDIS maintain stability at high speed and increased mobility at low speed in which opposite steering and parallel steering were utilized.

4. The regenerative brake was able to adopt the same control method as anti-lock brake system and was effective as a skid control system.

REFERENCES

Chapter 1 Introduction

[1-1] Anqing Shi, “The impact of population pressure on global cabon dioxide emissions,1975-1996: evidence from pooled cross-country data”, Ecological Economics, Vol.4, Issu 1, Feb 2003, pp29-42

[1-2] S. Solomon, G-K.Plattner, R.Knutti, and P.Friedlingstein,” Irreversible climate change due to carbon dioxide emissions”, P*NAS* 2009 106 (6) 1704-1709; January 28, 2009,doi:10.1073/pnas.0812721106

[1-3] Weiss, M. et al. On the electrification of road transport—Learning rates and price forecasts for hybrid-electric and battery-electric vehicles. Energy Policy 48, 374–393 (2012).

[1-4] Catenacci, M., Verdolini, E., Bosetti, V. & Fiorese, G. Going electric: Expert survey on the future of battery technologies for electric vehicles. Energy Policy 61, 403–413 (2013).

[1-5] P. A Nelson, K. G Gallagher, I.Bloom and D.W. Dees, “Modelling the Performance and Cost of Lithium-Ion Batteries for Electric Drive Vehicles”, Argonne National Laboratory, December 2012. URL: http://www.cse.anl.gov/batpac/files/BatPaC%20ANL-12_55.pdf

[1-6] M.Izhar, H.Ogino, Y.Oshinoya, “Research on Motion Control of 4 Wheel Steering Vehicles (Effect of Regenerative Brake on Vehicle’s Motion)” Proceedings of the School of Engineering, Tokai University, Vol.53, No.2,2013,pp.99-103

[1-7] Y. Hori: “Future vehicle driven by electricity and control—research on four-wheel-motored “UOT Electric March II””, IEEE Trans. Industrial Electronics, Vol. 51, No. 5, pp. 954–962, 2004

[1-8] J. Larminie and J. Lowry: Electric Vehicle Technology Explained, John Wiley and Sons, Ltd., (2003), pp. 23-29.

[1-9] E. Nakamura, M. Soga, A. Sakai, A. Otomo, and T. Kobayashi: Development of Electronically Controlled Brake System for Hybrid Vehicle, SAE Technical Paper, (2002), Paper 2002-01-0300.

[1-10] A.Lorico, J.Taiber and T.Yanni : Effect of Inductive Power Technology Systems on Battery-Electri Vehicle Design, Proceedings of The 37th Annual Conference on IEEE Industrial Electronic Society (IECON), (2011), pp. 4563-4569

[1-11] Mark S. Duvall: Battery Evaluation for Plug-In Hybrid Electric Vehicles, Proceedings of The 2005 IEEE Conference on Vehicle Power and Propulsion (VPCC), (2005), pp. 338-343

[1-12] K.M. Rahman, S. Jurkovic, S.Hawkins, S.Tarnowsky and P.Savagian : Propulsion System Design of a Battery Electric Vehicle, Transaction of the IEEE Electrification Magazine, Vol.2, No.2, (2014), pp. 14-24

[1-13] T.D. Gillespie, "Fundamentals of Vehicle Dynamics", Warrendale: Society of Automotive Engineers, 1992 [CrossRef]

[1-14] J. R. Ellis, "Vehicle Handling Dynamics", Mechanical Engineering Publications

Limited, 1994
[1-15] W.F Milliken and D.W Whitcomb, "General introduction to a programme of dynamic research",Proc. Auto. Div. Instn Mech. Engrs, no. 7, pp. 287-309
[1-16] D. W Whitcomb and W.F Milliken, "Design implications of a general theory of automobile stability and control", Proc, Auto. Div. Instn. Mech. Engrs, no. 7, pp. 367-391
[1-17] L. Segel, "Theoretical prediction and experimental substantiation of the response of the automobile to steering control", Proc. Auto. Div. Instn mech. Engrs, no. 7, pp. 310-330
[1-18] L Segel, "Research in the fundamentals of automobile control and stability", SAE National Summer Meeting
[1-19] J. Hu, D.Yin and Y.Hori : Fault-tolerant Traction Control of Electric Vehicles, Transactions of the Control Engineering Practice, Vol.19, (2011), pp. 204-213
[1-20] Z.Guirong, L.Houyu and H.Fei : Propulsion Control of Fuel Cell Electric Vehicle, Proceedings of the 2011 3rd International Conference on Environmental Cience and Information Application Technology (ESIAT 201), (2011), pp. 439-443
[1-21] S.Caglar Baslamisli, I.E.Koe and G.Alas : Robust Control of Anti-lock Brake System, Transactions of the Vehicle System Dynamics, Vol.45, No.3, (2007), pp. 217-232.
[1-22] J.S.Lin and W.E.Ting : Nonlinear Control Design of Anti-lock Braking Systems with Assistance of Active Suspension, Proceedings of the Fourth International Conference on Fuzzy Systems and Knowledge Discovery, (2007), pp. 343-348
[1-23] M.Corno, M.Gerard, M.Verhaegen and E.Holweg : Hybrid ABS Control using Force Measurement, IEEE Transactions on Control Systems Technology, Vol.20, No.5, (2012), pp. 1223-1235
[1-24] K.Nam, H.Fujimoto and Y.Hori : Advanced Motion Control of Electric Vehicles Based on Robust Lateral Tire Force Control via Active Front Steering, IEEE/ASME Transactions on Mechatronics, Vol.19, No.1, (2014), pp. 289-299
[1-25] Y.Hori : Future Vehicle Driven by Electricity and Control –Research on Four Wheel Motored "UOT Electric March II-, Proceedings of The 7th International Workshop on Advanced Motion Control (AMC), (2002), pp. 1-14
[1-26] L.Feiqiang, W.Jun and L.Zhaodu : Fuzzy-logic-based Controller Design for Four-wheel-drive Electric Vehicle Yaw Stability Enhancement, Proceedings of the 2009 6th International Conference on Fuzzy Systems and Knowledge Discovery (FSKD), (2009), pp. 116-120
[1-27] Nam, H.Fujimoto and Y.Hori : Motion Control of Electric Vehicles Based on Robust Lateral Tire Force Control Using Lateral Tire Force Sensors, Proceedings of The 2012 IEEE/ASME International Conference on Advanced Intelligent Mchatronics, (2012), pp. 526-531
[1-28] Z.Shuai, H.Zhang, J.Wang, J.Liu and M,Quyang : Lateral Motion for Four-wheel-independent-drive electric vehicles using optimal torque allocation and Dynamic

Message Priority Scheduling, Transactions of The Control Engineering Practice, Vol.24, (2014), pp. 55-66
[1-29] K. Kabiraj and A. Bhaumik, "Mathematical modeling for vehicle dynamics, steady state cornering performance prediction using non linear tire data employing a four wheel model," *Current Trends in Engineering and Technology (ICCTET), 2014 2nd International Conference on*, Coimbatore, 2014, pp. 97-102.
[1-30] Tandy, D., Colborn, J., Bae, J., Coleman, C. et al., "The True Definition and Measurement of Oversteer and Understeer," *SAE Int. J. Commer. Veh.*8(1):160-181, 2015
[1-31] Bundorf, R., "The Influence of Vehicle Design Parameters on Characteristic Speed and Understeer," SAE Technical Paper 670078, 1967
[1-32] T. Goggia, A. Sorniotti, L. De Novellis and A. Ferrara, "Torque-vectoring control in fully electric vehicles via integral sliding modes," *2014 American Control Conference*, Portland, OR, 2014, pp. 3918-3923.
[1-33] E. Siampis, E. Velenis and S. Longo, "Predictive rear wheel torque vectoring control with terminal understeer mitigation using nonlinear estimation," *2015 54th IEEE Conference on Decision and Control (CDC)*, Osaka, 2015, pp. 4302-4307.
[1-34] M. I. Ishak, H. Ogino and Y. Oshinoya, "Introduction on dynamic motion of opposite and parallel steering for electric vehicle," *Systems, Process & Control (ICSPC), 2013 IEEE Conference on*, Kuala Lumpur, 2013, pp. 73-78.
[1-35] D. Sawamura and H. Fujimoto, "Minimum collision avoidance distance control for four-wheel-driven electric vehicles with active front and rear steerings," *Mechatronics (ICM), 2015 IEEE International Conference on*, Nagoya, 2015, pp. 341-346.
[1-36] M. Galvani, F. Biral, B. M. Nguyen and H. Fujimoto, "Four wheel optimal autonomous steering for improving safety in emergency collision avoidance manoeuvres," *Advanced Motion Control (AMC),2014 IEEE 13th International Workshop on*, Yokohama, 2014, pp. 362-367.
[1-37] El-Nashar, M., Abdelhady, M., Oraby, W., and El-Sinawy, S., "Enhanced Vehicle Lateral Stability in Crosswind by Limited State Kalman Filter Four Wheel Steering System," SAE Technical Paper 2007-01-0841, 2007
[1-38] A. Hakima and S. Ameli, "Designing a fuzzy logic controller to adjust the angle of tires in four wheel steering vehicles," *Control Automation Robotics & Vision (ICARCV), 2010 11th International Conference on*, Singapore, 2010, pp. 2208-2213.
[1-39] S. Wang and J. Zhang, "The research and application of fuzzy control in four-wheel-steering vehicle," *Fuzzy Systems and Knowledge Discovery (FSKD), 2010 Seventh International Conference on*, Yantai, Shandong, 2010, pp. 1397-1401.
[1-40] J. Zhanga, Y. Zhanga, L. Chena, Jingzhou, "A Fuzzy Control Strategy and Optimization for Four Wheel Steering System," IEEE International Conference on

Vehicular Electronics and Safety, ICVES, 2007.
[1-41] J. Naranjo, C. Gonzalez, R. Garcia, and T. de Pedro, “Lane-change fuzzy control in autonomous vehicles for the overtaking maneuver,” IEEE Transactions on Intelligent Transport Systems, vol. 9, no. 3, pp. 438-450, Sep. 2008
[1-42] J. Tian, N. Chen, J. Yang and L. Wang, "Fractional order sliding model control of active four-wheel steering vehicles," *Fractional Differentiation and Its Applications (ICFDA), 2014 International Conference on*, Catania, 2014, pp. 1-5.
[1-43] M. Amodeo, A. Ferrara, R. Terzaghi, C. Vecchio, “wheel slip control via second-order sliding-mode generation,” IEEE Transactions on Intelligent Transportation Systems, vol. 11, no. 1, pp. 122-131, Mar. 2010.
[1-44] Y. Ikeda, "Active steering control of vehicle by sliding mode control - switching function design using SDRE -," *2010 IEEE International Conference on Control Applications*, Yokohama, 2010, pp. 1660-1665.
[1-45] R. C. B. Sampaio, H. G. Borrero and M. Becker, "Optimal H∞ controller on the adjustment of the steering angles of a two-track 4WD autonomous vehicle,"*Robotics Symposium, 2011 IEEE IX Latin American and IEEE Colombian Conference on Automatic Control and Industry Applications (LARC)*, Bogota, 2011, pp. 1-5.
[1-46] T.P. Newcomb “Energy Dissipated during Braking”, Wear, Vol.59, Issue 2, 15 March 1980, pp. 401-407
[1-47] Lutz, R.A et. Al, “Energy: Ford Energy Report”, Volume 1,
[1-48] K.Barrow, “First DRS class 88 electro-diesel ready for testing”, International Railway Journal, April 15, 2016
[1-49] K.Barrow, “Flexible seating for new Keio railway EMUs”, International Railway Journal, March 17, 2016
[1-50] C. Sankavaram, B. Pattipati, K. R. Pattipati, Y. Zhang and M. Howell, "Fault Diagnosis in Hybrid Electric Vehicle Regenerative Braking System," in *IEEE Access*, vol. 2, pp. 1225-1239, 2014.
[1-51] J. Ko, S. Ko, H. Son, B. Yoo, J. Cheon and H. Kim, "Development of Brake System and Regenerative Braking Cooperative Control Algorithm for Automatic-Transmission-Based Hybrid Electric Vehicles," in *IEEE Transactions on Vehicular Technology*, vol. 64, no. 2, pp. 431-440, Feb. 2015.
[1-52] M.Heerwan, H.Ogino, Y. Oshinoya, “Skid control system of a small electric vehicle with two in-wheel motors: simulation model of ABS and regenerative brake control”, International Journal of Crashworthiness, 23 March, 2016

Chapter 2 Modelling an In-Wheel Small Electric Vehicle with Over Steer Characteristic

[2-1] Oxford Dictionary of English, 3rd Edition, Oxford University Press, 2015
[2-2] Tandy, D., Colborn, J., Bae, J., Coleman, C. et al., "The True Definition and

Measurement of Oversteer and Understeer," *SAE Int. J. Commer. Veh.*8 (1):160-181, 2015, doi: 10.4271/2015-01-1592.
[2-3] M. Abe, “Vehicle Handling Dynamics: Theory and Application. In Vehicle Handling Dynamics: Theory and Application”, First Edition, Butterworth-Heinemann, 2009, pp.72
[2-4] Toyota Auto Body Company Handbook
[2-5] M. Abe, “Vehicle Handling Dynamics: Theory and Application. In Vehicle Handling Dynamics: Theory and Application”, First Edition, Butterworth-Heinemann, 2009, pp.10

Chapter 3 Yaw Moment Control by Four Wheel Drive and Independent Steering

[3-1] S.Murata, “Vehicle Dynamics Innovation with In-Wheel Motor”, SAE International Technical Paper. May 2011, pp.1-6
[3-2] Rojas Rojas, A., Niederkofler, H., and Hirschberg, W., "Mechanical Design of In-Wheel Motor Driven Vehicles with Torque-Vectoring," SAE Technical Paper 2011-36-0132, 2011, doi:10.4271/2011-36-0132.
[3-3] Watts, A., Vallance, A., Fraser, A., Whitehead, A. et al., "Integrating In-Wheel Motors into Vehicles - Real-World Experiences," *SAE Int. J. Alt. Power.* 1(1):289-307, 2012, doi:10.4271/2012-01-1037.
[3-4] M. I. Ishak, H. Ogino and Y. Oshinoya, "Introduction on dynamic motion of opposite and parallel steering for electric vehicle," *Systems, Process & Control (ICSPC), 2013 IEEE Conference on*, Kuala Lumpur, 2013, pp. 73-78.
[3-5] N. Hamzah, M. K. Aripin, Y. M. Sam, H. Selamat and M. F. Ismail, "Yaw stability improvement for four-wheel active steering vehicle using sliding mode control," *Signal Processing and its Applications (CSPA), 2012 IEEE 8th International Colloquium on Signal Processing and its Application*, 2012, pp. 127-132.
[3-6] L. DanYong and S. YongDuan, "Adaptive fault-tolerant tracking control of 4WS4WD road vehicles: A fully model-independent solution," *Control Conference (CCC), 2012*, Hefei, 2012, pp. 485-492.
[3-7] R. Grepl, J. Vejlupek, V. Lambersky, M. Jasansky, F. Vadlejch and P. Coupek, "Development of 4WS/4WD Experimental Vehicle: platform for research and education in mechatronics," *IEEE International Conference on Mechatronic*, Istanbul, 2011, pp. 893-898.
[3-8] M. Abe, “Vehicle Handling Dynamics: Theory and Application. In Vehicle Handling Dynamics: Theory and Application”, First Edition, Butterworth-Heinemann, 2009, pp.50-55
[3-9] C. Chen, Minglei Shu and Ruixia Liu, "Asymptotic tracking control of 4WS

vehicles based on virtual points," *Transportation Electrification Asia-Pacific (ITEC Asia-Pacific), 2014 IEEE Conference and Expo*, Beijing, 2014, pp. 1-6.

Chapter 4 Regenerative Brake as Skid Control System

[4-1] P.Naderi, A.Farhadi, M.Mirsalim and T.Mohammadi : Anti-Lock and Anti-Slip Braking System, Using Fuzzy Logic and Sliding Mode Controllers, Proceedings of the 2010 IEEE Vehicle Power and Propulsion Conference (VPCC), (2010), pp. 1-6

[4-2] W.Wang, M.Chen, Y.Chien and T.Lee : Control of Uncertain Active Suspension System with Anti-lock Braking System using Fuzzy Neural Controller, Proceedings of the 2009 IEEE International Conference on System, and Cybernetics, (2009), pp. 3371-3376

[4-3] W.Wang, K.Hsu, T.Lee and G.Chen : Robust Sliding Mode-Like Fuzzy Logic Control for Anti-lock Braking Systems with Uncertainties and Disturbances, Proceedings of the Second International Conference on Machine Learning and Cybernetics, (2003), pp. 633-638.

[4-4] [1-56] A.Harifi, A.Aghagolzadeh, G.Alizadeh and M.Sadeghi : Designing a Sliding Mode Controller for Slip Control of Antilock Brake Systems, Transactions of the Transportation Research Part C Emerging Technologies, Vol.16, No.6, (2008), pp. 731-741.

[4-5] Z.Junzhi, L.Yutong, L.Chen an Y.Ye : New Regenerative Braking Control Strategy for Rear-Driven Electrified Minivans, Transactions of the Energy Conversion and Management, Vol.82, (2014), pp. 135-145.

[4-6] D.B.Antanaitis : Effect of Regenerative Braking on Foundation Brake Performance, Transaction of the SAE International Journal of Passenger Cars – Mechanical Systems, Vol.3, No.2, (2010), pp. 14-30.

[4-7] M.A.Hannan, F.A.Azidin and A.Mohamed : Multi-Sources Model and Control of an Energy Management System for Light Electric Vehicles, Transactions of the Energy Conversion and Management, Vol.62, (2012), pp.123-130.